Design and Testing of a Complete Heart Soft Robotic Compression Device

Arezoo Abrishami Movahhed

A Thesis

in the Department of

Mechanical, Industrial, and Aerospace Engineering

Presented in Partial Fulfillment

of the Requirements for the Degree of

Master of Applied Science (Mechanical Engineering)

Concordia University

Montreal, Quebec, Canada

May 2023

CONCORDIA UNIVERSITY

SCHOOL OF GRADUATE STUDIES

This is to certify that the thesis prepared:

By: Arezoo Abrishami Movahhed

Entitled: Design and Testing of a Complete Hear Soft Robotic Cardiac
             Compression Device

And submitted in partial fulfillment of the requirements for the degree of

Master of Applied Science (Mechanical Engineering)

complies with the regulations of the University and meets the accepted standards
with respect to originality and quality.

Signed by the final examining committee:

Dr. Hoi Dick Ng	Chair
Dr. Hoi Dick Ng	Examiner
Dr. Rolf Wuthrich	Examiner
Dr. Lyes Kadem	Thesis Supervisor
Dr. Hassan Rivaz	Thesis Supervisor

Approved by

Sivakumar Narayanswamy, MASc. Program Director

April 2023

Dr. Mourad Debbabi, Dean
Gina Cody School of Engineering and Computer Science

Abstract

Design and Testing
of a Complete Heart Soft Robotic Compression Device

By: Arezoo Abrishami Movahhed

Current strategies for cardiac contraction compensation show the potential of soft robotic sleeves as an alternative for cardiac assist devices. Development, testing, and validation of new implantable medical devices always require experiments for approval. The need for clinical trials or *in vivo* tests can be minimized by proposing a new beating heart phantom. The rationale behind this study is the design and fabrication of a soft robotic cardiac compression device, simulation of the heartbeat in a silicone heart phantom, and flow measurement in an aorta model. Here, we create a silicone heart and an aorta phantom based on the MRI data by brushing silicone on their 3D-printed molds. Discovering the best commercially available actuator components is one of the objectives of this work, wherein the most effective combination of the tube and the expandable sleeve is provided in detail. The main parameter for evaluation of cardiac function is fractional shortening, which is higher than 25% in a healthy heart, therefore, we used that as the reference for choosing the best possible actuator elements. Three surgical valves and one lifelike valve are placed in the heart model to mimic realistic flow conditions. Both normal and cardiomyopathy conditions are modeled, and an aortic flow assessment is performed. After optimization of the setup, the direct flow assessment of the aorta represents the peak aortic flow of 20.42 l/min. A stroke volume of more than 65 ml, a cardiac output of 4.05 l/min, and an ejection fraction of 50% can be generated with this model. While, in cardiomyopathy simulation, the missing contraction at the specific regions results in a reduction in aortic flow, ejection fraction, and cardiac output.

Keywords: Cardiac device, soft robot, cardiac flow, fractional shortening, heart failure, 3D-printing, silicone phantom

Acknowledgment

Table of Contents

List of Figures

List of Tables

Acronyms

LV	Left Ventricle
RV	Right Ventricle
PA	Pulmonary Artery
HF	Heart Failure
SV	Stroke Volume
CO	Cardiac Output
HR	Heart Rate
EF	Ejection Fraction
FS	Fractional Shortening
EDV	End-Diastole Volume
ESV	End-Systole Volume
CAD	Cardiac Assist Device
VAD	Ventricular Assist Devices
DCCS	Direct Cardiac Compression Sleeve
PAM	Pneumatic Artificial Muscle
mm	Millimeter
ms	Millisecond
ml	milliliter
g	gram
OD	Outer Diameter
ID	Inner Diameter
l/min	Liter per minute
Hz	Hertz
AV	Aortic Velocity
VTI	Velocity Time Integral
LVOT	Left Ventricular Outflow Tract

Chapter 1

Introduction

1.1 Background

This chapter includes an overview of the clinical significance of the problem dealt with in this thesis, along with an introduction to the research problem. A summary of the advantages of using soft robots in cardiac assist devices is provided, and the objectives of this research work are discussed. Finally, the outline of this thesis is presented in the last section.

Cardiovascular diseases are responsible for 17.9 million deaths per year worldwide, representing 32% of all global deaths (World Health Organization 2022). To restrain the negative impacts of cardiovascular disease on the population and the economy, there is an urgent need to promote innovation in implantable medical devices.

Heart failure is a progressive health burden with consequences for the future health of the population. Any condition characterized by a mismatched relationship between metabolic, exercise, and/or cognitive needs and cardiac performance is recognized as heart failure (Food and Drug Administration 2019; Roche et al. 2017). It is most common among people who are 65 years or older, but practically anyone can be at risk. The causes of heart failure can be coronary artery disease, high blood pressure, congenital heart defects, myocarditis, abnormal heart rhythms, valve disease, diabetes, and obesity (Laing et al. 2018).

Heart transplantation is among the major surgical procedures of organ replacement. Around 60,000 heart transplants are performed each year worldwide. It has been estimated that over 5000 patients in the United States can benefit from heart transplants annually. There are 250,000 deaths reported due to heart failure in the United States, also 900,000 hospitalizations because of this disease (Coles-Black, Bolton, and Chuen 2021).

1.2 Cardiovascular System

The heart lies inside the thoracic cavity, on the diaphragm, surrounded by lungs from the sides, Figure 1.1. Its posterior and anterior border is near the vertebral column and sternum

respectively. The heart is composed of four chambers, superior chambers consist of the left and right atrium, and the inferior chambers are the left and right ventricles (Iaizzo 2005).
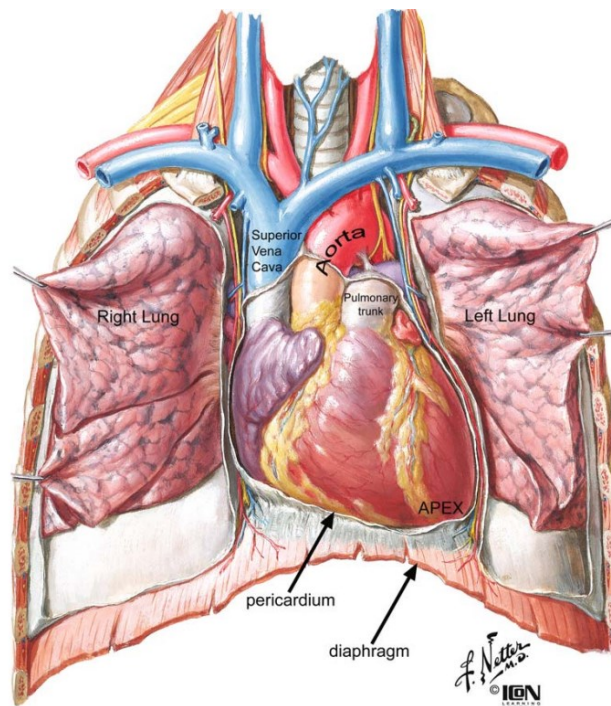
Figure 1.1 The position of the heart in the middle mediastinum (Iaizzo 2005)

There are two closed circuits of vessels divided into two independent networks: the pulmonary and systemic circulations. The pulmonary network is a loop through the lungs, in which deoxygenated blood pumps from the right ventricle (RV) to the pulmonary artery (PA). Then, in systematic blood rich in oxygen goes into the left atrium and then the left ventricle (LV), finally leaving the LV through the aortic valve to supply oxygenated blood for all the organs (Iaizzo 2005).

Blood enters the right atrium from the systemic circulatory system through two veins. The superior vena cava transports oxygen-depleted blood from the upper extremities, head, and neck, and the inferior vena cava transports oxygen-depleted blood from the thorax, abdomen, and lower extremities. Blood exits the right ventricle through the pulmonary artery branches into the left and right pulmonary arteries, which transport blood into the lungs. The left and right pulmonary veins return oxygenated blood from the lungs to the left atrium (Iaizzo 2005).

Four valves maintain the unidirectional flow of blood through the heart. The tricuspid valve (right atrioventricular) controls the blood from the right ventricle to the right atrium. The bicuspid valve is located between the left atrium and the LV. The aortic valve directs the blood from the LV to the aorta to supply oxygenated blood for organs. While through the pulmonary valve, deoxygenated blood from the RV goes into the PA toward the lungs (Iaizzo 2005).
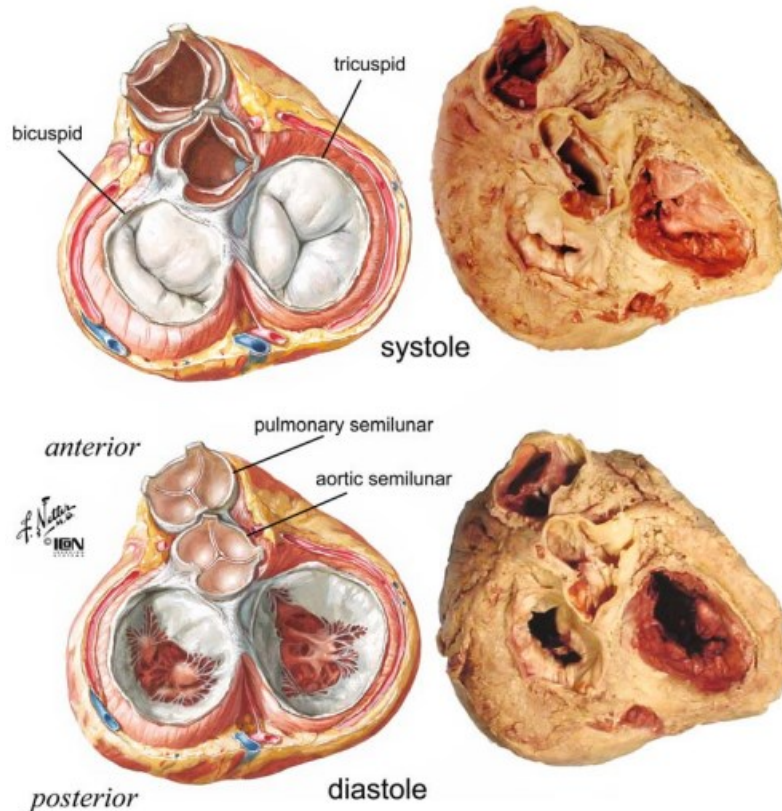
Figure 1.2 Valves of the heart in systole and diastole (Iaizzo 2005)

The cardiac phase is made of systole and diastole, Figure 1.2. Systole represents when the mitral valve is closed and because pressure increases in the left ventricle, the aortic valve opens, and oxygenated blood is pumped into the aorta. The systole concludes with the closure of the aortic valve. In diastole, the heart relaxes and the right side of the heart fills with deoxygenated blood and pumps it through the lungs to get oxygen (Iaizzo 2005).

1.3 Heart Failure

The heart regulates the blood supply based on the needs of the body in both normal and pathological conditions. Many diseases may affect the pumping system, including aging, genetic defects, or environmental stimuli (Voorhees and Han 2015). Heart failure is a complex clinical syndrome in which the heart cannot supply the required blood for organs, and it mainly results from a functional or structural heart disorder (Nadruz et al. 2016). Historically, a majority of the cases ended up heart failure due to coronary artery disease and myocardial infarction. Other structural causes of congestive heart failure are listed as hypertension, valvular heart disease uncontrolled arrhythmia, myocarditis (inflammation of the myocardium), and congenital heart disease (Malik et al. 2023).

Ejection fraction (EF) is defined as the percentage of blood leaving the heart following each contraction. Heart failure causes a reduction in EF, commonly it drops to lower than 40% in patients with HF. It can occur when the heart muscle is weak, "systolic failure", and insufficient blood supply results in the death of the heart muscle; or due to higher stiffness it is unable to relax normally, "diastolic failure". Cardiomyopathy, which means disease of the heart muscle, is one of many causes of heart failure. Patients with end-stage heart failure are often considered for heart transplantation. But, due to a shortage of donors, some patients may die awaiting heart transplantation (Roche et al. 2017).

High-output cardiac failure is a less common form of heart failure. The heart cannot still provide sufficient blood supply, the same as systolic and diastolic failure. The problem lies with an increased demand in the body, even with a normal cardiac function, the heart cannot meet the body's demand. It considers a consequence of the underlying disease process. The causes are mainly either an increase in the body's metabolism, or a bypass of the arteriolar and capillary bed causing an increased flow into venous circulation from a lack of resistance (Voorhees and Han 2015).

1.4 Biomechanics of Cardiovascular Function

Biomechanical principles play a crucial role in governing cardiac function in both normal and diseased hearts (Moreno et al. 2011). The heart, as a multiscale system, functions at the organ, tissue, cellular, and protein levels, and cardiac function can be evaluated at any of

these levels (Voorhees and Han 2015). Mechanical stimuli, for instance, stress or strain, are important epigenetic factors in cardiovascular development, adaptation, and disease. Evidence proves that the local mechanical environment governs remodeling processes. Changes in heart structure and function alter the mechanical forces sensed by the cells, and this results in the biochemical activity of the cells, which in turn stimulates changes in the structure and function of the heart (Moreno et al. 2011).

The complex pumping system of the heart can cause severe disease, for example left ventricular myocardial infarction due to coronary heart disease and diastolic dysfunction due to hypertension and/or left ventricle hypertrophy are two major forms of heart disease. Mechanical stress can result in the development of cardiomyopathy and scar formation. Also, heart valve diseases, either stenosis or insufficiency (regurgitation) have a direct effect on the pumping function of the heart (Voorhees and Han 2015).

However, biomechanics has a part to play in regulating cardiac function in both normal and diseased hearts. Altering the mechanical stress patterns can provide effective approaches for the treatment of myocardial infarction and improving cardiac function (Voorhees and Han 2015).

1.4.1 Quantitative Parameters

Many different parameters are commonly used to quantify the function of the heart. The most useful measures quantify the actual volume of blood being pumped during each cardiac cycle. The stroke volume (SV) is defined as the difference between the LV volume at end-diastole (EDV) and end-systole (ESV), Equation 1.1 (Voorhees and Han 2015). The average SV of a 70 kg male is 70 mL (Bruss and Raja 2023).

$$\textbf{Equation 1.1} \quad \boldsymbol{SV = EDV - ESV}$$

Cardiac output (CO) is defined as the volume of blood a heart pumps per minute (heart rate: HR) (Voorhees and Han 2015). CO in humans is generally 5-6 L/min, but it can increase to more than 35 L/min in athletes during exercise (King and Lowery 2017).

$$\textbf{Equation 1.2} \quad \boldsymbol{CO = SV \times HR}$$

While SV represents how much blood the heart pumps per beat, ejection fraction (EF) is often used to describe heart function, which is the percentage of the total amount of blood

in the heart that is pumped out with each heartbeat, Equation 1.3. In a healthy condition, EF is 50% or higher (Voorhees and Han 2015).

$$\textbf{Equation 1.3} \quad EF = \frac{SV}{EDV} \times 100\%$$

Fractional shortening (FS) is calculated by measuring the percentage change in left ventricular diameter during systole. Echocardiography, motion mode (or M mode), is mainly used for the assessment of FS, in Equation 1.4, LVEDD and LVESD are LV end-diastole diameter and LV end-systole diameter respectively. In a clinical trial, researchers showed in cases of left ventricular dysfunction, FS is less than or equal to 25% (Mosterd et al. 1999). FS normal range is reported to range from 28% to 40% (Huhta 2006). To simulate cardiac contraction at least 25% of LV contraction is then required.

$$\textbf{Equation 1.4} \quad FS = (LVEDD - LVESD) \, / \, LVEDD$$

1.4.2 Cardiac Output in Heart Failure Condition

In a healthy heart considered to be hemodynamically stable, heart performance in terms of providing oxygenated blood supply can meet the oxygen requirement in all organs. A mismatch of oxygen delivery results in hemodynamic instability. In that condition, the CO cannot provide enough blood supply, and low stroke volume occurs (Bruss and Raja 2023).

In a heart failure situation, the heart's goal is compensating to maintain the required CO. As it is stated in equation 1, maintaining CO is possible by increasing the HR, or pumping more blood with each beat (Bruss and Raja 2023). The heart can pump harder by forming a thicker and stronger myocardium, this thickening muscle is called "Hypertrophy". Hypertrophic growth of the heart is a compensatory response to hemodynamic stress. Although it can enhance the CO, over time the blood supply for the myocardium may not be sufficient because a larger heart needs more oxygen and other nutrition (Frey et al. 2004).

1.4.3 Cardiac Function Evaluation

There are invasive and non-invasive techniques (listed in Table 1 in the Appendix) for the evaluation of cardiac function. Clinically, the first choice is echocardiography since it is inexpensive, portable, and there is no ionization radiation. With the help of echocardiography and its latest improvements, this allows us to calculate LV volume, wall

thickness, 3D imaging, pressure, and the velocity of blood in different regions to estimate the performance of the valves (Voorhees and Han 2015).

CT scans have the potential to add higher resolution to the images but at the cost of imposing the patients to X-ray radiation with added expense compared to echocardiography. While MRI provides more geometric details of LV structure, it may not be the best choice for the patients due to its cost and time-consuming process. A Multi Gated Acquisition Scan (MUGA) is a nuclear medicine imaging, in which a radioactive tracer is injected into the bloodstream, then a gamma camera takes images of the gamma particles emitted by the tracer in the heart cavities. MUGA is often reserved for the diagnosed patient with cardiac disease. In invasive cardiac catheterization, a catheter containing a pressure, or a volume sensor is inserted into the heart through the aorta. The guidance of the catheter is aided by a fluoroscope. Any abnormal pressure gradient and pressure-volume loops can be observed with cardiac catheterization (Voorhees and Han 2015).

1.4.4 Diagnosis with Doppler Ultrasound

Doppler ultrasound is a medical imaging technique that uses sound waves to measure blood flow. The pulsed wave (PW) Doppler can analyze sound waves reflected from a specific location. The user can simply specify the location of measurements with the help of the Doppler line, then the probe sends short pulses, and the ultrasound machine is programmed to ignore all signals, except those reflected from the sample volume the certain depth specified by the doppler line (Rawshani 2018).

The main parameters in PW Doppler measurement are:

- Aortic valve maximal velocity: AV V_{max} [m/s]
- Aortic valve mean velocity: AV V_{mean} [m/s]
- Aortic valve maximal pressure gradient: AV PG_{max} [mmHg]
- Aortic valve mean pressure gradient: AV PG_{mean} [mmHg]
- Velocity time integral: VTI [cm]

Stroke volume is not one of the aforementioned parameters, but it can be calculated by measuring the flow in the aortic valve by Doppler ultrasound. Firstly, the diameter of the aortic annulus should be measured in systole when the diameter is maximum. Then in the

left ventricular outflow tract (LVOT), VTI can simply be measured by PW Doppler. Stroke volume is the product of VTI, and the area of the LVOT. The cardiac output is the product of stroke volume and heart rate (Eq 1.2) (Rawshani 2018).

1.5 Cardiac Assist Devices

Cardiac assist devices (CADs) are widely used to provide circulatory support to patients dealing with heart failure and waiting for heart transplantation (Han 2020). To assist the failing heart mechanically, ventricular assist devices (VADs) are used as a life-prolonging therapy, either as a bridge to transplant or, in some cases, as a "destination therapy" for patients with end-stage heart failure. With the help of the VADs, the function of one or both ventricles of the heart can be evaluated (Roche et al. 2017). VADs reported to date use electric, pneumatic, hydraulic, electromagnetic, and electro-hydraulic systems (Kongahage, Ruhparwar, and Foroughi 2021).

There have been three generations of VADs, first-generation pumps were pulsatile, contained artificial heart valves, and ejected blood at normal heart rates between 80 and 100 beats per minute with the use of either forced air or electricity. Second-generation pumps blood in a continuous fashion without valve (Givertz 2011), see Figure 1.3. The third generation of VADs works with continuous-flow pumps that use contactless bearing and magnetic levitation (Kari 2018). Components of a typical VAD are a continuous flow of a pump connected to the heart and aorta via an inflow and outflow cannula, a driveline that exits the skin on the right, and a system controller that is typically worn on a belt. Power to the controller and pump is provided by external batteries or a power-based unit (Givertz 2011). The three different VAD generations can be seen in Figure 1.4.
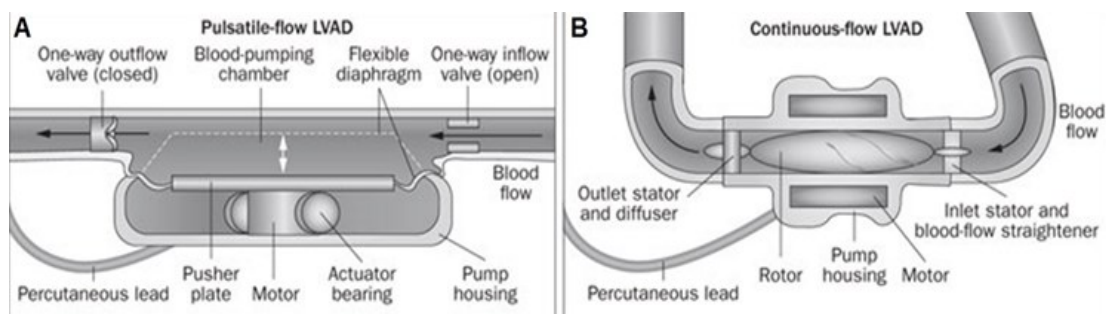
Figure 1.3 (A) The first generation pulsatile-flow pumps, a replica of the native cardiac cycle using a diaphragm and unidirectional artificial heart valves, (B)The second generation continuous-flow pumps integrated a valveless axial pump designed to rapidly spin a single impeller (Han and Trumble 2019)
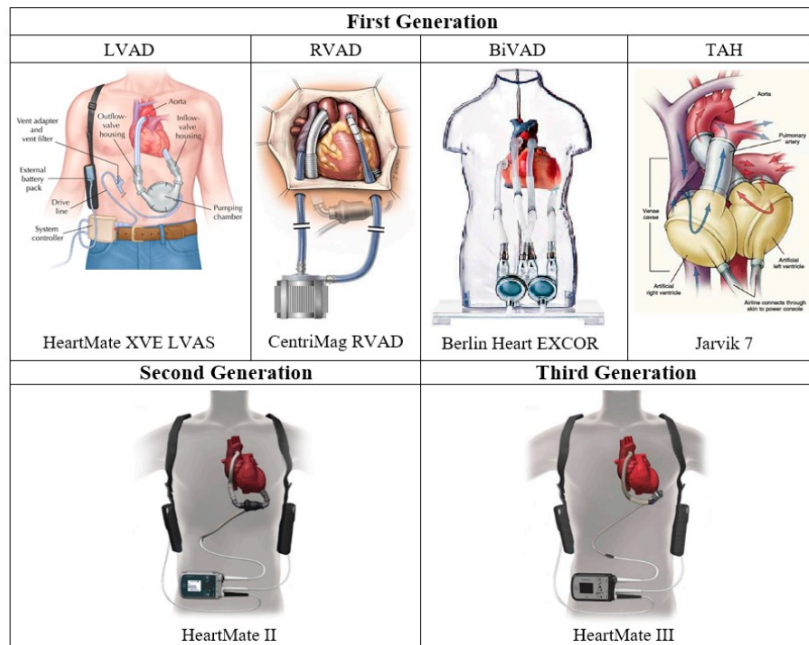
Figure 1.4 Examples of first, second, and third-generation cardiac assist devices (Han and Trumble 2019)

1.6   Direct Cardiac Compression Sleeve (DCCS)

The biventricular compression device was introduced as Anstadt Assistor Cup for the first time in 1991 (Lowe et al. 1991). Recently, researchers introduced soft robotic technologies to improve the functionality of DCCSs. They mainly use contractile elements and wrap them around a heart model, then compress the actuators to replicate the heartbeat in real conditions. These sleeves have not become a viable method of long-term support since they are associated with thromboembolism with extended use due to their direct interaction with the blood stream. In Figure 1.5 schematic of some cup-shaped sleeves is shown (Han and Trumble 2019).
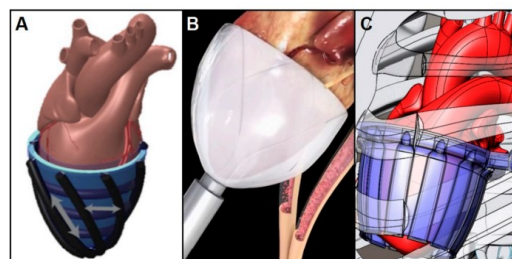
Figure 1.5 Biomimetic (A) Minimally invasive, (B) Muscle-powered, (C) Soft robotic direct cardiac compressive sleeves (Han and Trumble 2019)

9

1.7   Soft Robots

Soft robotics provides a huge opportunity to think about problems in new ways and make it feasible to manufacture machines that fit us by design, at a reasonable price. In addition, they are easily customizable, safe to use, or even adjustable to fit anybody. Soft robots can also be inexpensive compared to traditional ones, so there is a great opportunity to develop new disruptive machines (Payne et al. 2017).

Soft robotic mechanisms address issues critical to how people's bodies interfere with the material world. With soft robotics, one can design mechanisms that can easily be integrated with the human body (Payne et al. 2017). The necessity of integrating different components with different physical, biological, and mechanical properties into one system makes the fabrication of soft robots challenging and complicated (Chang et al. 2015). The power source for the actuation of soft robots must be stretchable and portable, and this can be challenging. For pneumatic actuators, existing fluidic power sources are not soft and are usually big and bulky. Current sources are generally limited to compressors or pumps, and compressed air cylinders (Borzikova, Balara, and Pitel 2007).

It is well established that with the emergence of soft robotic technologies mimicking the motion of human tissue has been possible, wearable assistive devices have become widely available. In addition to devices that can be worn outside the body, implantable soft robotic CADs have recently been proposed (Kari 2018).

The advantages of using soft robotic techniques for direct cardiac compression devices are, firstly, the anatomy of the heart is not a problem and a sleeve that fully conforms to it can be fabricated. Secondly, multiple actuators can be embedded or oriented in a sleeve to achieve complex three-dimensional motion that can mimic the architecture and motion of heart muscle. Thirdly, the precise timing of individual actuators relative to the native heartbeat and to other actuators can be finetuned to optimize cardiac output and, finally, as the actuators can extend with vacuum, the device has the potential to augment diastolic function as well as systolic function (Obiajulu et al. 2013).

1.7.1 Flexible Fluids Actuators

A flexible fluidic actuator generally consists of a flexible shell that transmits potential energy, delivered by the pressurized fluid, into a mechanical force, which then can be used to create a motion. They are mainly classified based on the type of force they can create. Different designs may use expansion, contraction, or bending directions to drive a system (Gaiser et al. 2012).

1.7.2 Flexible Fluidic "Contraction" Actuators

Contraction actuators generate a tensile force when pressure is applied. They can be sorted into two groups "Anisotropic Membrane Stiffness" and "Vectored Structural Degrees of Freedom" (Berselli, Giovanni, Rocco Vertechy, and Gabriele Vassura. 2012; Gaiser et al. 2012).

Anisotropic membrane stiffness actuators increase in surface area when pressurized. The axial contraction is coupled to a radial expansion in which some of the energy is used for membrane deformation. The radial expansion causes a shortening in the length of the actuator, and eventually contraction (Gaiser et al. 2012).

Vectored structural degrees of freedom designs try to raise efficiency and minimize the hysteresis compared to the first group of actuators. Ideally, there is no strain on one membrane and almost no internal friction. Once pressure is applied to these actuators, they increase in volume while maintaining the same surface area (Gaiser et al. 2012).

In this research project, the first type of actuator, anisotropic membrane stiffness, is used.

1.7.3 Pneumatic Artificial Muscles (PAMs)

PAMs are contractile and linear motion engines operated by gas pressure that are widely used as contractile elements. They are also known as McKibben-based actuators, "Fluidic Muscles", "Biomimetic Actuators" (Andrikopoulos et al. 2011), or "Braided Muscles" (Daerden and Lefeber 2002). The structure is composed of an inflatable bladder placed within a mesh so that when the bladder is pressurized, the mesh contracts linearly and expands radially (Payn et al. 2017). This type shows similar behavior to biological muscle properties. The magnitude of contraction depends on the air pressure and the time of air

flowing into the muscle or deflating artificial muscle. When a load of muscle is increased, its pull force rises while the lift of a muscle decreases (Borzikova, Balara, and Pitel 2007).

In Figure 1.6 different types of PAMs can be seen. PAMs have been used as a pneumatic actuator in different studies (Mirvakili, Sim, and Langer 2021; Liu et al. 2013; Skorina et al. 2018; Greer et al. 2017; Borzikova, Balara, and Pitel 2007; Obiajulu et al. 2013).
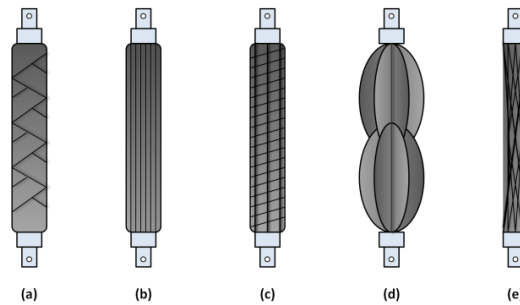
Figure 1.6 Various types of PAMs (a) McKibben Muscle/Braided, Muscle, (b) Pleated Muscle, (c) Yarlott Netted Muscle, (d) ROMAC, Muscle, and (e) Paynter Hyperboloid Muscle (Andrikopoulos 2011)

1.8 Research Problem

Developing safer class III medical devices and promoting innovation plays a crucial role in this field. To this end, a beating heart phantom is required to simulate different cardiac surgery for a variety of disorders. In addition, as it is mentioned in Section 1.5, mechanical assist devices can improve cardiac function and they can be considered as a treatment for end-stage patients.

1.9 Rationale

Implantable medical devices are required to undergo an extensive series of bench testing (Lipshultz et al. 1994). However, current heart simulators are not optimized for such tests, so they provide very limited information regarding the expected performance of the device and its delivery system. Therefore, there is a significant missing block in bench testing and the development of implantable medical devices consisting of a close-to-real bench test. The next generation of heart simulators would be fruitful in terms of the development, testing, and validation of new implantable medical devices.

An artificial cardiac model, powered by a soft robotic sleeve can reduce potential risks in human clinical trials. In addition, we will be able to reproduce various pathological conditions at different degrees of severity simulating a wide spectrum of patients that can be found in a real population based on their medical images. Heart phantoms can be used to simulate a cardiac procedure for planning the operation and measuring the size of required instruments, especially in pediatric surgeries (Laing et al. 2018).

Some challenges persist in terms of the activation of the 3D-printed hearts models. Mechanical activation has proven to be bulky and limited in its ability to reproduce physiologically realistic heart contractions and flow rates. Soft actuators, inspired by nature, have been shown to enable smooth and complex motions while maintaining a low weight and reducing energy consumption (Kari 2018; Borzikova, Balara, and Pitel 2007; Obiajulu et al. 2013).

1.10 Thesis Outline

The current thesis is structured as follows. Throughout Chapter 2, a literature review of related works is provided to familiarize the reader with the concept. Chapter 3 is dedicated to the methodology of experiments, and it follows the results in Chapter 4 regarding the flow assessment. Subsequently, in Chapter 5, the essential findings, and a quick note regarding the limitations of the work are described. In the hope of extending the work to an upper level, we already started improving the model and performing measurements with Doppler ultrasound, the preliminary results are reported in the Appendix, in addition, complete exported data are outlined wishing their fruitfulness in future studies.

Chapter 2

Literature Review

This chapter reviews and discusses the existing research in cardiac assist devices and implantable soft actuators and highlights the currently existing knowledge gaps.

2.1 Relevant Works

Here we offer a review of relevant research studies in a chronological order.

In 2011, Moreno et al. managed to create a minimally invasive direct cardiac contact device capable of providing not only adjustable cardiac support to modulate cardiac size but also synchronous active assistance to modulate cardiac output. A cup-shaped device composed of two inner and outer nylon chambers was constructed, deployed on an ovine heart, and activated with air in the outer chamber, then device pressure LV volume and pressure were measured. Their nonblood contacting device could apply uniform compression and provide active support (Moreno et al. 2011).

In 2013, Obiajulu et al. developed a custom-made McKibben PAM actuator to investigate the effect of mesh geometry and elastomer material on the force and contraction of the actuator. The materials were silicone elastomer tubes with low stiffness (Shore OO-30, Ecoflex 00-30, Smooth-on, Inc.) and higher stiffness elastomer (Shore A-28, Elastosil M4601, Wacker Chemie AG) with outer diameters of 8 to 14 cm and thickness of 1 mm to 2 mm with the length of 14 cm. The experimental results show that elastomeric material and initial mean braid angle can greatly affect the performance of the actuators. A softer elastomer enabled greater contraction and a much faster response time, while a lower initial mean braid angle increased force output and maximum contraction (Obiajulu et al. 2013).

In 2013, Liu et al. created a dynamic cardiac simulator utilizing pneumatic artificial muscle made of thermoplastic elastomers (TPE) to simulate a heartbeat. The air pressure in the pericardial cavity started to make the left ventricular systole and diastole like a real human heart. They showed that the model could eject liquid (water used as blood) out of the left

ventricular without obvious backflow. It proves that the artificial pneumatic muscle could perform as designed and the valve was functional during the systole (Liu et al. 2013).

In 2014, Roche et al. conducted experiments on custom-made McKibben PAM actuators, made of silicone elastomer (Ecoflex 00-30, Smooth-on Inc.), with a 3D-printed mold. Also, they used an expandable mesh (Techflex, Inc.) to constrain the radial expansion. A layer of elastomer is used to bond the mesh and tube together. The results show more contraction/expansion occurs at lower pressures due to the low durometer of the inner elastomeric tube. In addition, finite element analysis of displacement on a simplified version of the LV 3D model was observed because LV twist is a useful index of cardiac performance and myocardial mechanics and can be affected by a range of diseases (Roche et al. 2014).

In 2015, Roche et al. worked on four different custom-made sleeves for the McKibben PAM. Silicone, Polyester Terephthalate (PET), Nylon medical balloon, and Thermoplastic Urethane (TPU) were used to manufacture the bladder. Axial contraction of each of the four types of PAMs was measured by dynamically actuating each at 1 Hz for 200 ms and 400ms actuation (to represent different clinical scenarios) at a pressure of 80 kPa and 145 kPa, using a custom-designed control box and Labview interface (National instruments). The PAM with a TPU internal bladder was capable of the highest force generation and was selected as the actuator for device development. They compared all sleeve designs on the in vitro model. In the standard configuration (helical outside) the thin silicone sleeve had the best performance with a volumetric output from the simulator of 60 ml of saline for each contraction. The thin silicone sleeve indicated superior performance giving a volumetric output of 92 ml per cycle, the result shows a maximum flow of 7 l/min (Roche et al. 2015).

In 2017, Roche et al. mimicked the motion of the mammalian heart by biologically inspired design for actuators in a layered helical and circumferential fashion. Two types of McKibben PAM actuators were made as the contractile elements, one with a custom-made silicone tube with a low durometer, and another one made of Thermoplastic Urethane (TPU). The outer diameter of the bladders, the thickness, and the length were 8 mm, 2 mm, and 80 mm respectively. The authors demonstrated the feasibility of in vivo cardiac output recovery

from a failing heart in a pig model of acute heart failure and enhanced the maximum flow from 7 l/min to almost 20 l/min with the designed cardiac sleeve (Roche et al. 2017).

In 2017, Payne et al. used a thermoplastic elastomer (Stretchlon 200; Airtech International) to make a bladder for a McKibben actuator. They performed an in vivo test and wrapped the soft robot around a porcine heart programmed to contract and relax in synchrony with the beating heart. The outcomes are, firstly, designing recoiling ability to refill the heart, secondly, introducing a method of device adhesion to the ventricles to enable diastolic assistance, and finally, programming a control system based on real-time hemodynamics for synchronization with the native heart. The authors reported the aorta flow rate, the pulmonary flow rate, and LV pressure, the maximum aortic flow is reported around 10 l/min (Payne et al. 2017).

In 2017, Payne et al. constructed a VAD with a combination of soft actuators and bracing assembly. The device anchors to the interventricular septum and applies forces to the free wall of the ventricle to cause an approximation of the septum and free wall in systole and assist with recoil in diastole. The concept on both the right and the left ventricles was demonstrated through in vivo studies in a porcine model. Finally, the results represent that the VAD provides rhythmic loading and can increase the flow in heart failure from 5 to 15 l/min (Payne et al. 2017).

In 2018, Horvath et al. compared various strategies for the direct fixation of cardiac compression sleeves on the heart. They tested four fixation methods including patches of gripping material (3M) assembled in silicone band, medical mesh (FixPro, Bandage plus) TG fix, Silicone in combination with cyano-acrylate adhesive, and Velcro/suture combination. The results show that a Velcro/suture combination is the most effective way. For the first sleeve design, two methods were applied. Firstly, they used a gel interface layer to deliberately decouple the dynamic parts of the sleeve and the myocardium to reduce friction at the interface. Secondly, in the coupling method, they substituted the gel liner with spots of cyano-acrylate adhesive at the device-heart interface to represent myocardial coupling between the medical mesh layer of the sleeve and the surface of the heart. Cardiac output of the cases in the in-vivo study shows the coupled actuator was able to increase

cardiac output above baseline, also having the potential to increase diastolic function (Horvath et al. 2018).

In 2020, Salinas et al. worked on the same device as their previous work (Payne et al., 2017), and designed a signal acquisition system to obtain an electrogram signal through two pacing wires on the right ventricle. Then, the delay between the R-wave slope of the electrogram signal and the beginning of the pressure signal was detected to be able to synchronize the VAD with the patient's heart rate. Eventually, in vivo experiments on two pigs were conducted. The authors reported the pulmonary artery (PA) flow in two experiments and finally concluded that characterization of the delay provides a safe region where the device can start working so that the cardiac output increases (Salinas et al. 2020).

In 2021, Kongahage et al. fabricated a custom-made electrothermal silicone-coated actuator as a new type of sleeve. By increasing the temperature of the actuator with a fixed length around a silicone-coated artificial heart structure a force was generated. The objective of this study was the evaluation of the pressure generated by the artificial heart muscle (AHM) on the temperature of the actuator. By wrapping the actuator around a lamb's heart, they could push the liquid into a tube around 1.5cm. The authors concluded these electrically contractile polymer-based actuators can be a decent alternative to support patients with other weak heart muscles (Kongahage, Ruhparwar, and Foroughi 2021).

In 2022, Wamala et al. mimicked RV heart failure in nine swine by a pulmonary artery band, and maintained it to make an ongoing afterload in RV. A cotton umbilical tape was placed around the proximal main pulmonary artery to simulate the RV failure. A soft robotic right ventricle assist device was actuated in synchrony with the heartbeat to enhance the cardiac output for up to an hour. They proved the feasibility of short-term augmentation of the RV by employing this RV assist device (Wamala et al. 2022).

Recently a team used medical imaging to create a 3D model of the heart and the aorta, then 3D printed the phantoms with a polymer-based 3D printer. To replicate the heart's pumping action, the model is wrapped in a sleeve connected to a pneumatic system, by which the sleeve can be filled with air and make a contraction similar to a human heartbeat. Also, with

other sleeves around the aorta to act as the aortic valve, they mimicked the stenosis in the aortic valve (MIT News 2023).

2.2 Thesis Objectives

Patient-specific heart simulators have the potential to facilitate the device design and preparation for surgery in rare cardiovascular diseases and complicated pediatric cases. Also, women and especially racial and ethnic minority populations remain underrepresented in cardiovascular trials. By performing *in vitro* experiments on their 3D-printed heart models and simulation of the heartbeat a great burden on clinical trials can be lifted when it comes to the evaluation of new devices' performance.

The emerging field of soft robots develops the feasibility of new cardiac assist device fabrication, by which the cardiac output can be increased in cardiomyopathy or heart failure patients. The main concepts of the previous studies are proposed:

- An innovative design and/or material for soft robot fabrication
- An installation method on an animal heart
- Comparison of a variable, for instance, flow, displacement, or pressure, before and after using the actuator(s)

Given these challenges and opportunities, the objectives of this research are:

- Introducing contractile actuators made of commercially available products
- Creating a 3D printed heart and aorta models based on MRI raw data
- Developing a method for making silicone heart and aorta phantoms
- Assembly of the soft robot and the heart phantom
- Maximizing the flow through the aorta to augment the cardiac output
- Mimicking cardiomyopathy conditions by deactivating different actuators

Chapter 3

Materials and Methods

The study aims to create LV and RV phantoms, then generate the maximum possible cardiac contraction to simulate real conditions in terms of aortic flow.

3.1   Pump Characteristics

Experiments are conducted with a 1750 rpm direct current permanent magnet motor manufactured by LEESON Electric Corporation. The variable in the pump is the voltage, by changing it, different amounts of water are injected into the connected actuator. In Table 3.1, the volume of water versus voltage is reported. In this project, for all the experiments, a sinusoidal waveform with 1Hz frequency is used to simulate the human cardiac cycle.

Table 3.1 Fluid volume injection in each voltage applied to the pump

Voltage (V)	Volume (mL)
1	10
2	20
3	35
4	65
5	85

3.2   Tube and Mesh Selection

To reach the maximum contraction, a minimum durometer should be considered in tube selection. Of all commercially available products, McMaster-Carr company provides a variety of expandable sleeves and tubes made of different materials. Due to the higher durometer of latex tubes, 40A, and 50A, they are excluded from this study. 35A is the minimum available durometer at McMaster-Carr and it only comes with silicone-made tubes. Based on the previous studies, the diameter of the actuator should be between 8 and 14 mm, with 1 to 2 mm thickness (Obiajulu et al. 2013; Roche et al. 2017; 2014; 2015). The

selected tubes in Table 3.2 and the selected meshes (expandable sleeves) in Table 3.3 are outlined.

Table 3.2 Selected tubes for the experiments

Tube Number	Material	Outer Diameter (mm)	Thickness (mm)	Durometer
I	Silicone	6.35	1.58	35A
II	Silicone	9.52	1.58	35A
III	Silicone	8.00	1.00	35A
IV	Silicone	11.00	1.00	35A

Table 3.3 Selected meshes for the experiments

Mesh Number	Material	Diameter (mm)	Thickness (mm)	Expandable ID[1] (mm)
1	Polyester	6.3	0.08	1.1
2	Polyester	9.5	0.08	1.3
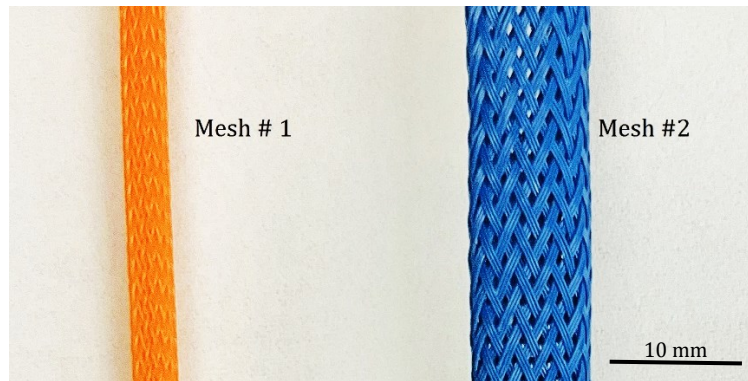
Figure 3.1 Polyester meshes with different textures, sizes, and expandable inner diameters

3.2.1 Preliminary Tests

To choose the best combination of mesh and tube, all eight combinations, four tubes with two meshes, need to be examined. Other than the outer diameter and the thickness of the tube, the length of the actuator can influence the contraction. Therefore, the testing variables are the actuator length and the pump voltage.

---

[1] ID: Inner Diameter

The principal control system used for the testing trials is the custom-made in-house STITCH software (Simulation Through In-Vitro Testing on the Complete Heart). STITCH is a Labview-based software designed for the study of cardiac phenomena in cardiovascular fluid dynamics experiments. Regarding the test protocol, firstly, actuators with three different lengths of 15, 25, and 30 cm are made of mesh #2 and tube #III. Secondly, in each of them, one end is closed by a medical valve, and the other end is connected to the motor by a tube. Finally, by placing a ruler next to the tube, the contraction for each voltage is measured. It should be mentioned that to minimize the error of reading the contraction amount based on the ruler placed next to the actuator, we record all the tests and extract the amounts after a careful review of the videos, Figure 3.2.

In Figure 3.3 to Figure 3.8, all the results of the test can be seen. By comparison of meshes, mesh #2 shows higher contraction, as it was expected, since it has a higher expandable diameter, also its thicker texture helps to prevent any rupture while it is expanding radially. Therefore, mesh number two is finally selected. Of all four tubes, tube #III shows the maximum contraction for almost all the voltages, especially for voltages higher than 3V. Thus, these results can guide the conception of an optimized soft robot made of tube #III and mesh #2 that can contract more than 20%. As it is stated in section 1.3.1, the normal fractional contraction range is 25% to 40%.
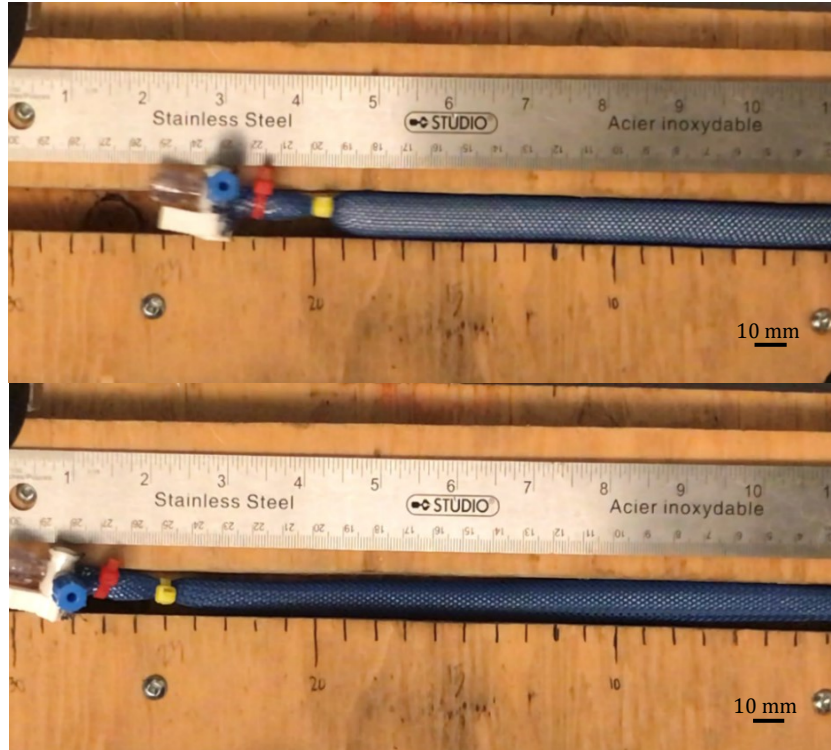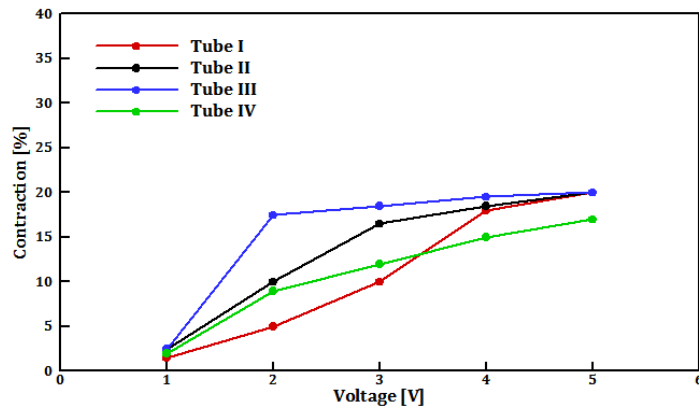
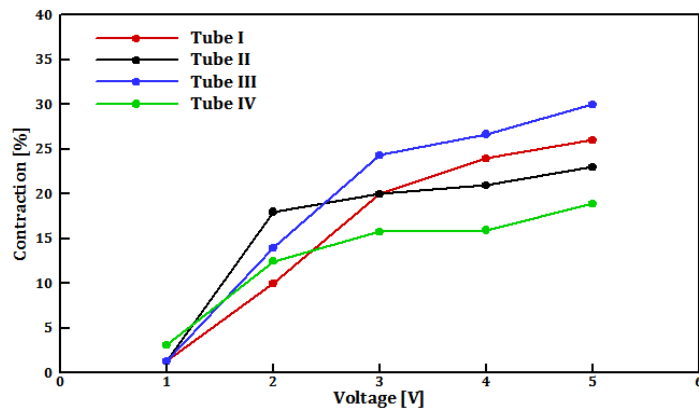**Figure 3.2** Experiment setup for contraction assessment
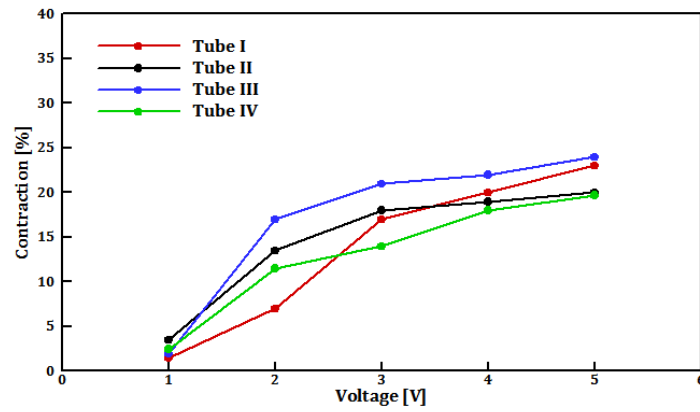
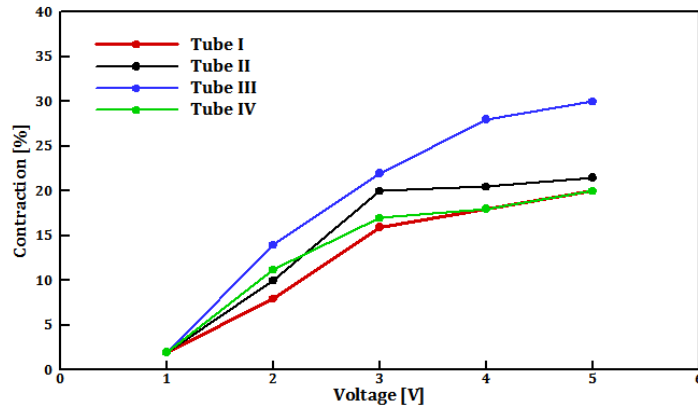**Figure 3.3** Actuator length: 15 cm, mesh #1
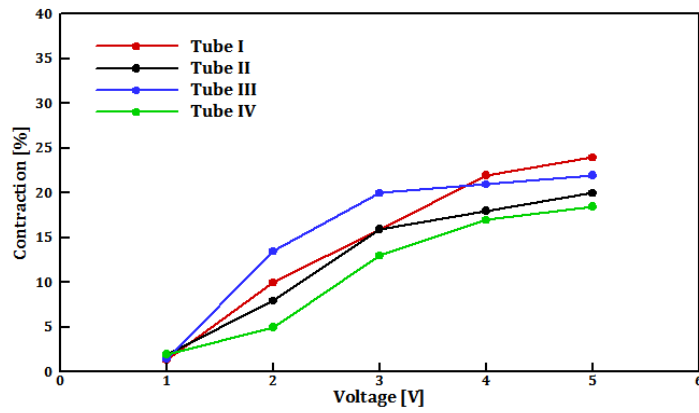
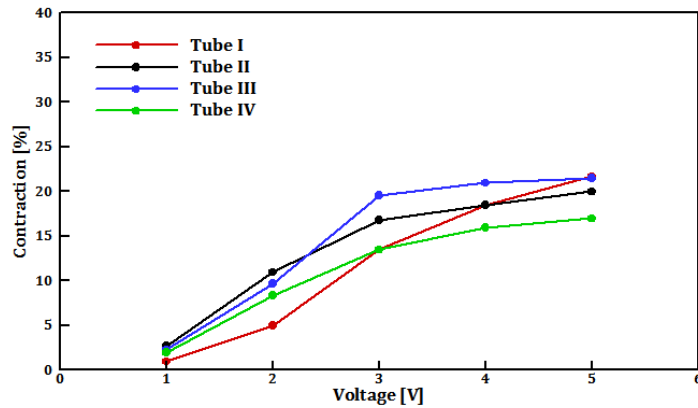**Figure 3.4** Actuator length: 25 cm, mesh #1

Figure 3.5 Actuator length: 30 cm, mesh #1

Figure 3.6 Actuator length: 15 cm, mesh #2

Figure 3.7 Actuator length: 25 cm, mesh #2

Figure 3.8 Actuator length: 30 cm, mesh #2

3.2.2 Repeatability Tests

When it comes to cardiac cycle simulation, the design should be able to work continuously to make the evaluation or any measurement process possible. To test the feasibility of our proposed strategy, we evaluate the efficacy of the actuator by repeatability tests. We have applied voltage ranging from 3 to 5 volts for each length because 1 V and 2V do not show promising results and barely can contraction be seen. Frequency is set to 1 Hz for sinusoidal waves in all the tests for sixty cycles. As it is reported in Table 3.4, minor changes happen in all the test configurations in sixty seconds.

Due to cavitation, the motor created bubbles after one minute, so the compressive air bubbles could act as a source of error and cause a decrease in contraction. Before each test, all the bubbles were removed from the system through the medical valves, and we performed the repeatability test for one minute to prevent errors.

25

Table 3.4 Repeatability test results for tube #III and mesh #2

L (cm)	Voltage (V)	Tube OD: 8 mm, Thickness: 1 mm, Mesh #2: 9.5 mm						
		Normalized Contraction (%)						
		1 (s)	10 (s)	20 (s)	30 (s)	40 (s)	50 (s)	60 (s)
15	4	0.3	0.3	0.3	0.3	0.3	0.3	0.3
15	4	0.27	0.27	0.27	0.27	0.27	0.27	0.27
15	4	0.27	0.27	0.27	0.27	0.27	0.27	0.27
15	4	0.27	0.27	0.27	0.27	0.27	0.27	0.25
15	4	0.29	0.29	0.27	0.27	0.27	0.27	0.27
25	4	0.24	0.24	0.24	0.24	0.24	0.24	0.24
25	4	0.24	0.24	0.24	0.24	0.24	0.24	0.24
25	4	0.24	0.23	0.23	0.23	0.22	0.22	0.22
25	4	0.24	0.24	0.24	0.24	0.24	0.24	0.24
25	4	0.24	0.24	0.24	0.24	0.24	0.24	0.24
25	4	0.24	0.24	0.23	0.23	0.23	0.23	0.23
25	4	0.24	0.24	0.24	0.24	0.24	0.24	0.24
25	4	0.24	0.24	0.24	0.24	0.24	0.24	0.24
30	4	0.22	0.22	0.22	0.22	0.21	0.21	0.21
30	4	0.25	0.24	0.23	0.23	0.23	0.23	0.23
30	4	0.23	0.23	0.22	0.22	0.21	0.21	0.21
30	4	0.22	0.22	0.22	0.22	0.22	0.22	0.22

In some relevant works, the researchers suggest coating the actuator with an elastomer or a low-durometer silicone material (Obiajulu et al. 2013; Roche et al. 2014; 2015; 2017; Kongahage, Ruhparwar, and Foroughi 2021). Before advancing the experiments, we examined the same actuators in terms of the length, the tube, and the mesh, with and without silicone coating. The material used for coating was an Ecoflex 00-30 silicone kit, with a durometer of 30. The results show higher contraction compared to the non-coated actuator in only 1 V and 2 V. The focus of our work is on maximizing the contraction by applying higher voltages to the pump; thus, we continued the experiments without coating the actuators.

3.3 Heart Phantom

As mentioned, the objective of this study is flow assessment in a heart phantom. In this section, the process of creating the phantom is explained.

3.3.1 3D-Printing

With the help of imaging systems, we can create a seemingly similar 3D model to the human heart. Currently, there is no gold standard for validating the accuracy of patient-specific

anatomical models produced by 3D printing. However, early work from multiple groups suggests the accuracy of 3D-printed models is within acceptable limits for presurgical planning (Coles-Black, Bolton, and Chuen 2021). In this study, Computed Tomography (CT) and Magnetic Resonance Imaging (MRI) data (Solid Heart Gen 2, Zygote; American Fork, UT, U.S.A.) are used to construct the 3D models of right and left ventricles and the aorta. Then, a stereolithographic (STL) format of each part, LV, RV, and aorta was extracted to print it by a 3D-printer system.

The CURA (Ultimaker, Utrecht, Netherlands) slicing program is compatible with the available 3D printer Lulzbot Taz 6 (Aleph Objects, Loveland, CO, U.S.A.) at LCFD laboratory at Concordia University. The STL file is viewed, sliced, and prepared for 3D printing. The STL files of the ventricles do not include valves which are key components in this project.

Anatomically speaking, the reconstructed geometry replicates some of the essential features of the human ventricles in terms of size, curvature, and the place of the four valves. The molds are made of PLA filament in two parts, as depicted in Figure 3.9 and Figure 3.10, small magnets are placed in them, Figure 3.11 since the next step is brushing silicone on the surface of the molds, and we need to take the mold out of the silicone phantom. In addition, based on the same imaging data, we create an aorta model with sinuses, but instead of arch-shape, we make it straight to be able to perform Doppler measurement under optimal conditions, Figure 3.12.
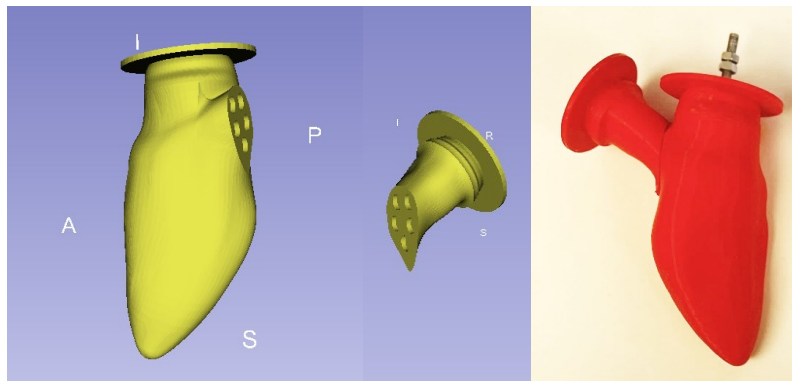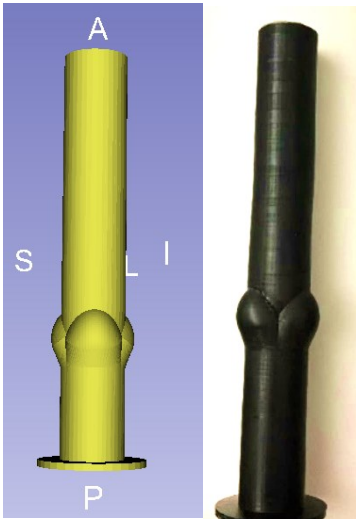

Figure 3.9 Left: LV STL file, Right: 3D printed model of LV with PLA
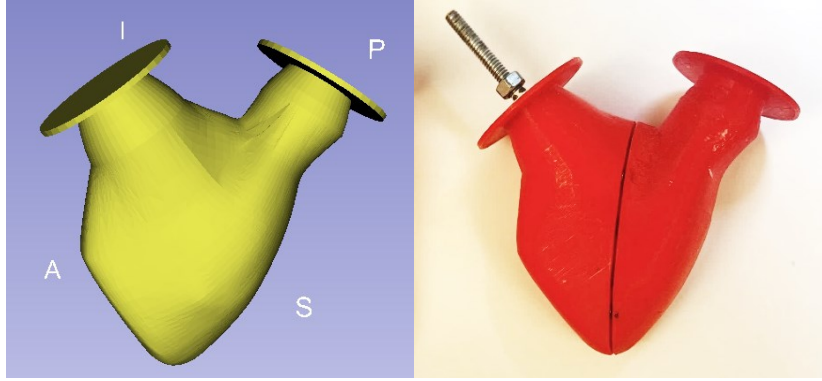
Figure 3.10 Left: RV STL file, Right: 3D printed model of RV with PLA

Figure 3.11 LV and RV molds with the placed magnets

Figure 3.12 Left: aorta STL file, Right: 3D printed model of the aorta with PLA

3.3.2 Silicone Model

The aforementioned left ventricle, right ventricle, and aorta molds are used to make the phantom by painting 40A hardness silicone (MB Fiberglass, Polycraft Silastic T4) with a 10:1 ratio by weight of the base material and the curing agent, Figure 3.13. Overall, five to six layers, made of 10 g to 12 g of silicone for each ventricle are needed to coat the transparent model. The volume of LV is 135 ml which is equal to the end-diastole LV volume.

Figure 3.13 Silicone ventricles and aorta

3.3.3 Heart Valve Placement

To simulate what is happening in the human heart, we place four valves in the model to make the flow comparison with the human heart possible. Three surgical valves named Perimount Theon RSR valve (Edwards Lifescience; Irvine, CA, US) are mounted for mitral (ID[1]: 26 mm, OD[2]: 29 mm), aorta (ID: 22 mm, OD: 25 mm), and pulmonary (OD: 25 mm, ID: 22 mm) valves, also a lifelike valve (LifeLike BioTissue, Ontario, Canada) is used for tricuspid valve (OD: 29 mm, ID: 26 mm). All valves are sutured with nylon thread to the phantoms and then glued with marine silicone.

---

[1] Inner Diameter
[2] Outer Diameter

Figure 3.14 Aortic valve sutured to the silicone aorta

3.4 Experimental Setup Optimization

The main purpose of this study is to create a heart phantom, make it beat, maximize the contraction, measure the flow, and compare the flow with human aortic flow. The soft robotic sleeves we create took inspiration from the native heart muscle and are designed to augment cardiac function by closely replicating it.

The actuators surround the heart phantom and contact the epicardial surface of the heart on the RV side, so that they act on the heart directly, while the LV side is laying at a plexiglass plate. Knowing the fact that actuator length has an adverse effect on its contraction, the actuators' length should be minimized. The phantom heart size allows us to wrap it with a maximum of three actuators of 16, 22, and 23cm lengths are made, and connected to a custom-made 3-way connector. Since there is a 7cm distance in the design, the effective length of actuators is 9 cm near the apex, 16cm in the middle, and 15cm near the base of the phantom. A custom-made three-way connector is employed to connect the actuators to the pump's tube.

By using a 3D-printed holder based on the outer surface of the RV, Figure 3.15, the pressure made by the actuators can be spread on a bigger surface. We use this optimized setup for the following measurements. The phantom and the whole experiment setup are submerged in a container filled with water.

Figure 3.15 Left: holder, Right: holder placed on the phantom

3.5 Flow Assessment

The input variable in all experiments is the voltage of the pump, which has a direct relation with the amount of water we put in the system, Table 3.1. For flow measurements, Transonic Systems INC T206 Small Animal Blood Flow Meter is used to extract flow and time, Figure 3.16. We place the probe on the aorta and run the experiments, Figure 3.17. On STITCH software, a sinusoidal wave with a 1 Hz frequency is selected to replicate a heartbeat of 60 beats per minute. The voltage range is 1 V to 3.5 V, the higher voltages result in failure of the tests.

Two conditions with or without a holder are considered for the experiments to prove the flow fluctuation and the effectiveness of spreading the pressure by the holder. In addition, different combinations of actuators are examined to demonstrate the role of each one on the flow, so that by deactivating one or two actuators, the contraction of that specific part of the model will be canceled. The purpose of this part of the experiment is to provide a setup to replicate cardiomyopathy. In Figure 3.18, the radial expansion of all three rows of actuators and the contraction of the phantom can be seen clearly.
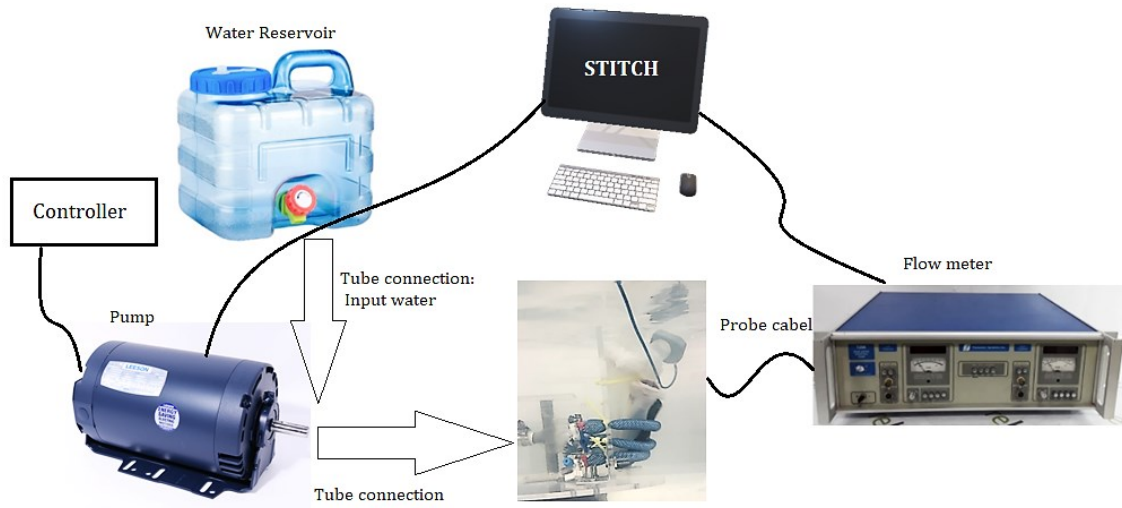
Figure 3.16 Experiment setup and connections for flow assessment
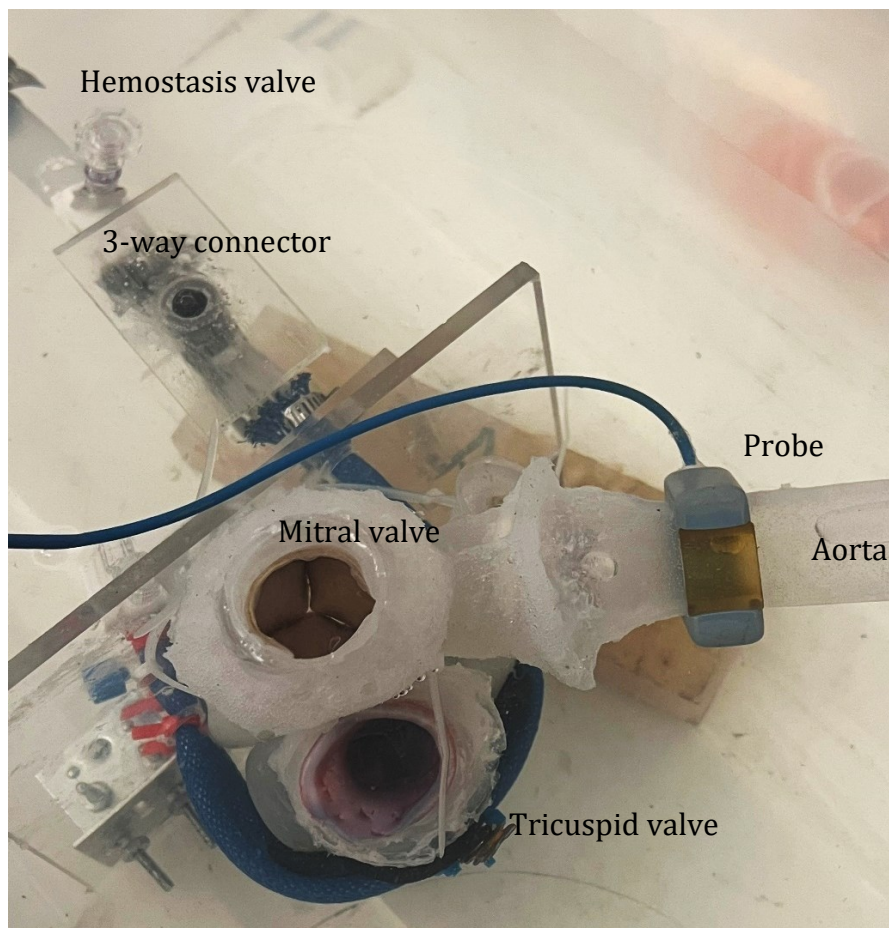
Figure 3.17 Model setup and flow meter probe
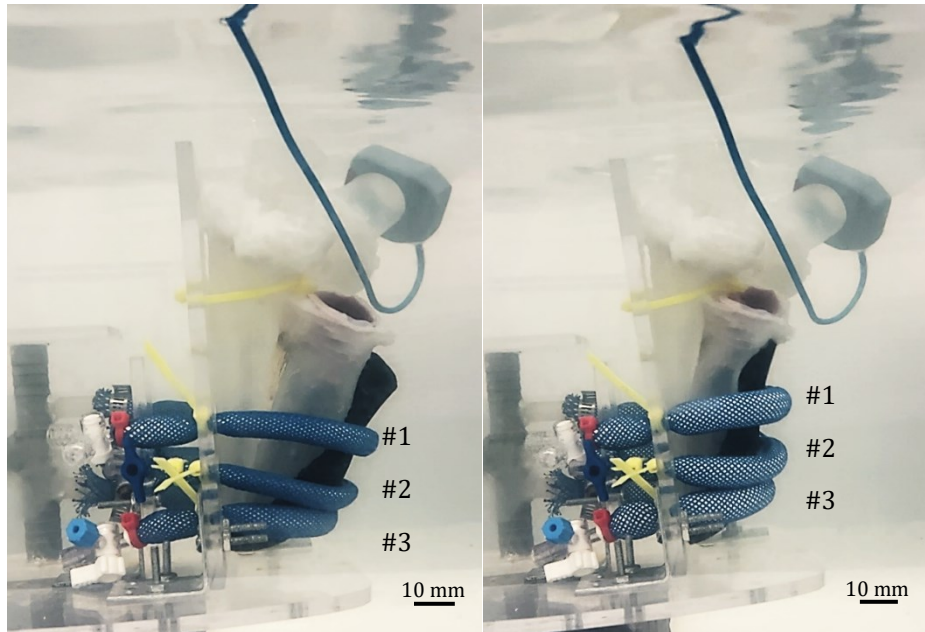
Figure 3.18 Experimental setup at diastole (left) and systole (right)

Chapter 4

Results

In this chapter different heart conditions including normal and heart failure are simulated to study the flow in the aorta. Firstly, all three actuators are activated, and all the measurements are performed with and without the holder. Subsequently, by deactivating each actuator, different heart failure conditions are reproduced, in these tests, two active actuators contract the heart model. Finally, only one actuator is responsible for the contraction to simulate severe heart failure in the three different regions of the heart, near the base, in the middle, and near the apex. The effective role of the holder on the aortic flow is indicated. Cardiomyopathy, one of the main causes of heart failure, can be simulated and studied by the proposed model, and the effect of each region's deactivation is discussed.

4.1   Simulation of Normal Heart Conditions

By activating all three actuators and using the holder, the maximum flow can be generated. The design does not allow increasing the pump voltage to more than 3.5 V, which is equal to ejecting 50 mL per beat. The backflow is negligible as can be seen in Figure 4.1. The peak and mean aortic flow reached 20.42 L/min and 4.05 L/min respectively.

To show the effect of the holder on the flow rate, we test the setup without the holder and with the same maximum voltage of 3.5 V. The maximum aortic flow drops then to 13.60 L/min as can be seen in Figure 4.2. The voltage range of 1 V to 3.5 V with a 0.5 V increment is considered for the experiments, and all the waveforms for each voltage are reported in the appendix. Figure 4.3 represents the mean flow versus voltage in both configurations with/without the holder. The comparison of maximum flow in both with/without holder setups is shown in Figure 4.4. In both cases, the flow rate displays a linear relationship with the voltage applied to the pump. To conclude, the role of the holder in spreading the pressure is crystal clear, by removing the holder the mean and the peak flow drop to 2.74 L/min and 13.61 L/min respectively.
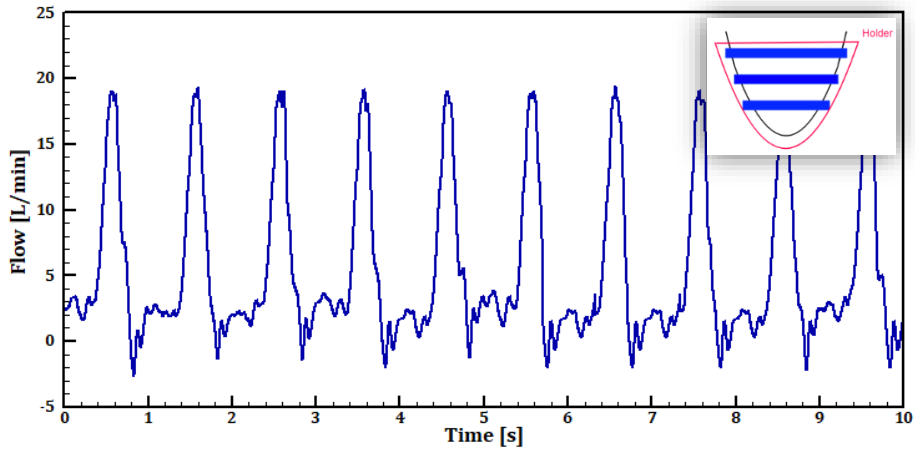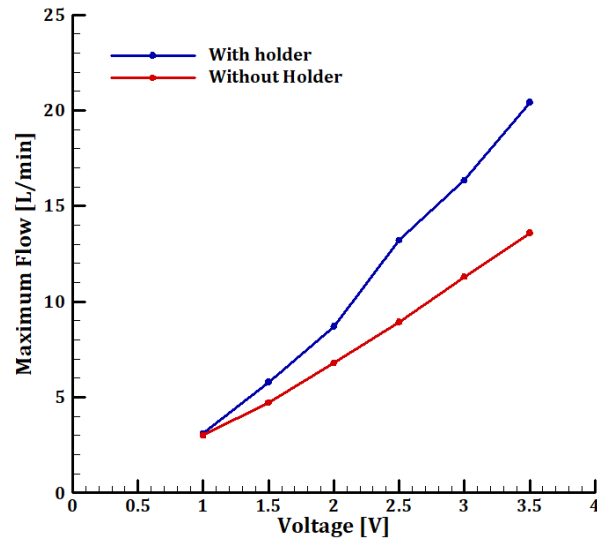
Figure 4.1 Flow waveform with three active actuators and the holder, Voltage: 3.5 V
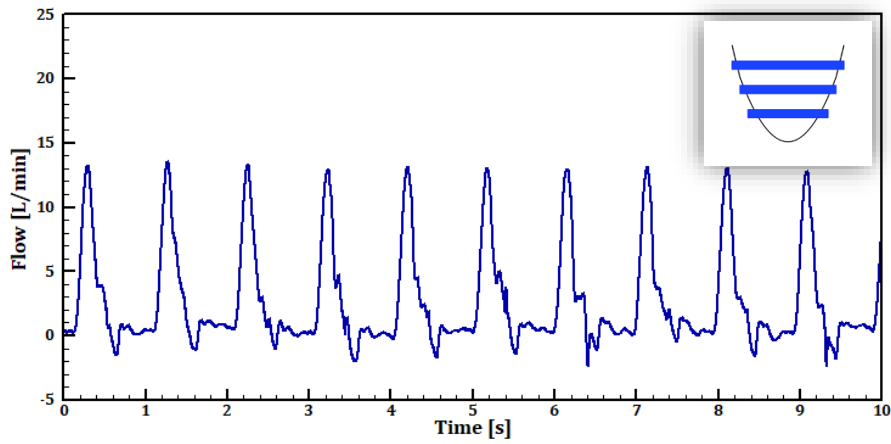
Figure 4.2 Flow waveform with three active actuators (without holder), Voltage: 3.5 V
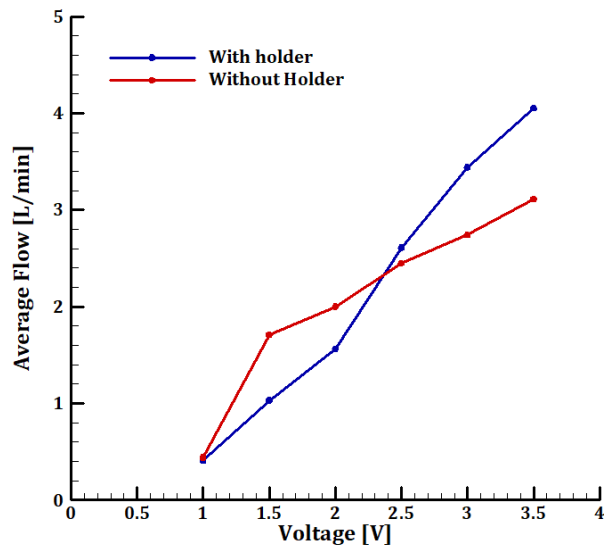
Figure 4.3 Average flow as a function of the input voltage with and without holder

**Figure 4.4** Peak flow rates as a function of the input voltage with and without holder

4.2 Simulation of Heart Failure

Heart failure might cause the heart to become bigger and/or stiffer since it tries to compensate for the required blood for all organs and needs to pump harder to generate higher flow. Also, it may result in cardiomyopathy due to insufficient blood supply in the coronary arteries. In this part of the experiments, we simulated cardiomyopathy by deactivating one actuator, then two to replicate severe heart failure conditions. Besides, by discovering the effect of each actuator on the flow and testing different combinations, we can propose the most effective region for actuation so that in a smaller model, for example, pediatric phantoms, by wrapping only one actuator on the optimized region, the best possible results in terms of mean and peak flow can be achieved.
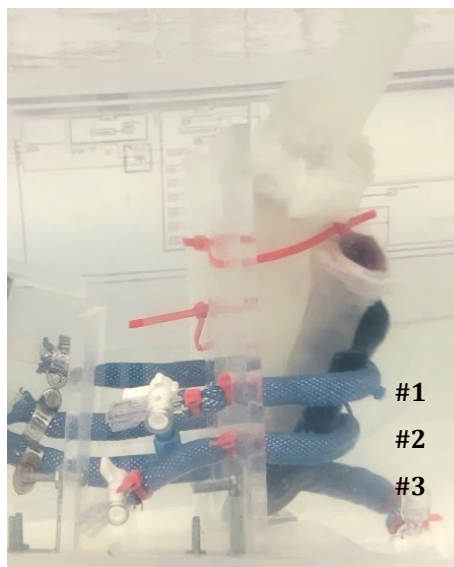
4.2.1 Two Active Actuators

There are three actuators wrapped around the ventricles' phantom, near the base, in the middle, and near the apex numbered #1, #2, and #3 respectively, see Figure 4.5. To simulate different stages of heart failure, when the heart does not pump blood correctly, we have performed experiments while systematically disconnecting one actuator and then a second actuator. In order to maintain the same flow to the actuators, when compared to the healthy case, the same total input flow is provided, and the actuators are simply disconnected (not

wrapped around the heart model). For example, Figure 4.6 illustrates how the apex is not activated by disconnecting actuator #3. For each combination, we measured the flow waveform for voltages ranging between 1, 2, 3, and 3.5 V with the holder. All the waveforms are provided in the Appendix. The combination of #1 and #2 results in the peak aortic flow of 15.5 L/min, Figure 4.7. However, the other combinations cannot exceed 12 L/min (#1 and #3), and 9 L/min (#2 and #3), shown in Figure 4.8 and Figure 4.9 respectively.
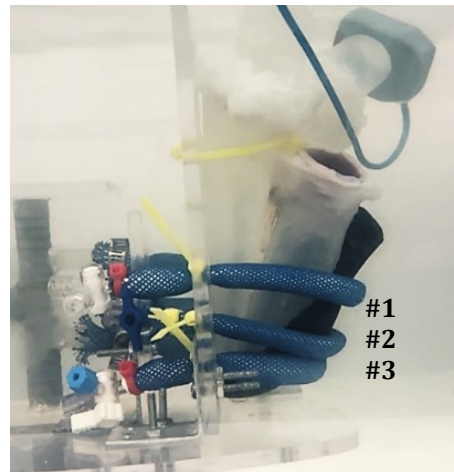
Figure 4.5 Numbering of the actuators from the base of the model to the apex: #1, #2, #3

Figure 4.6 Configuration where actuators #1 & #2 are activated while #3 is disconnected
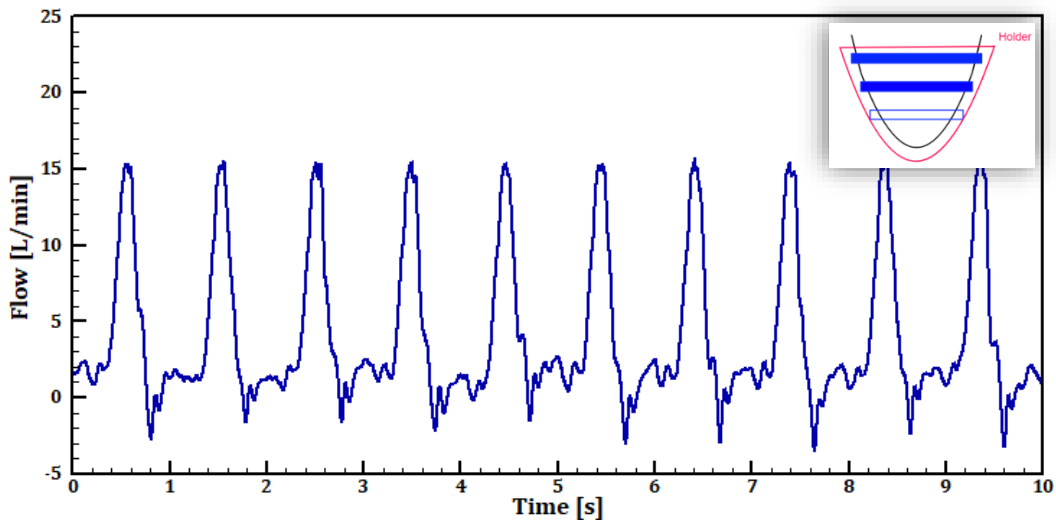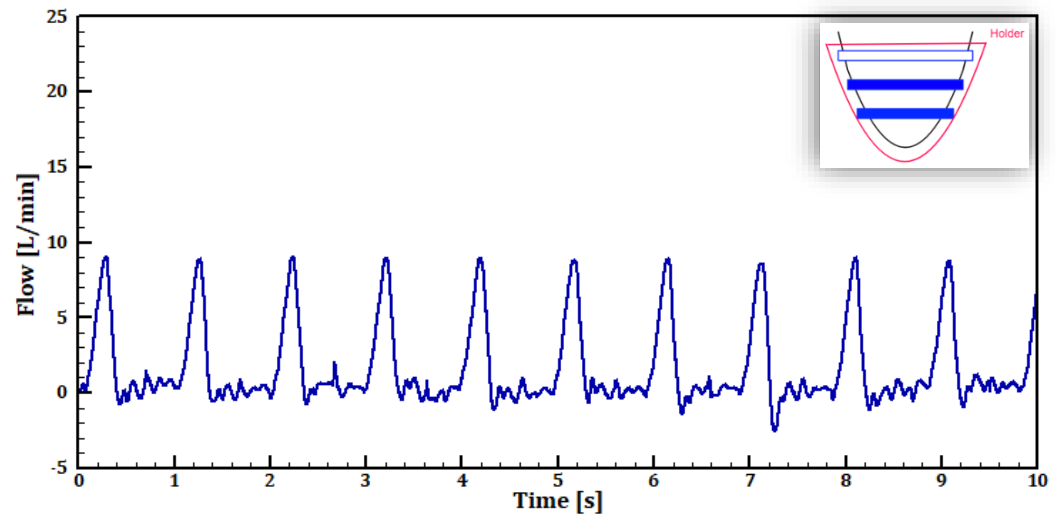
Figure 4.7 Flow waveform with active actuators: #1, #2, Voltage: 3.5 V, with holder
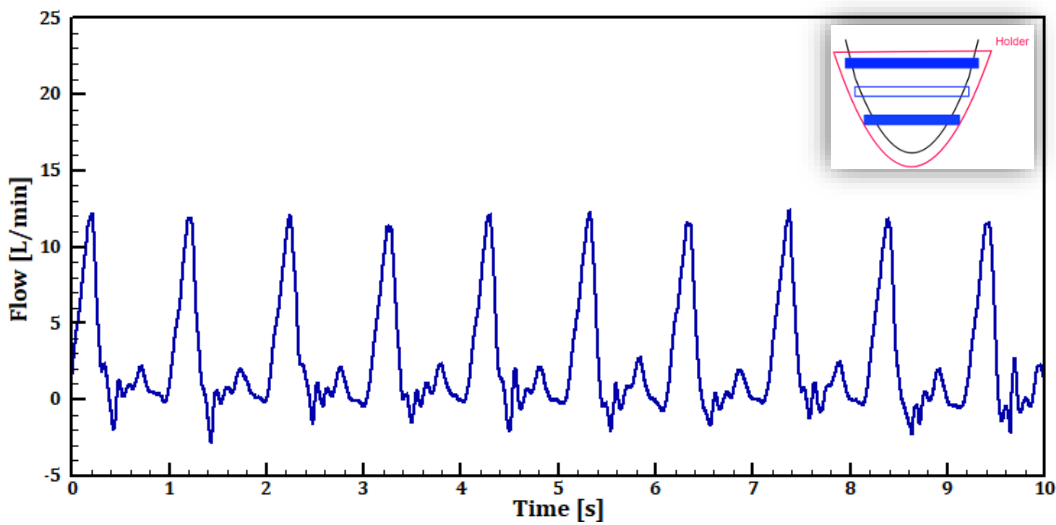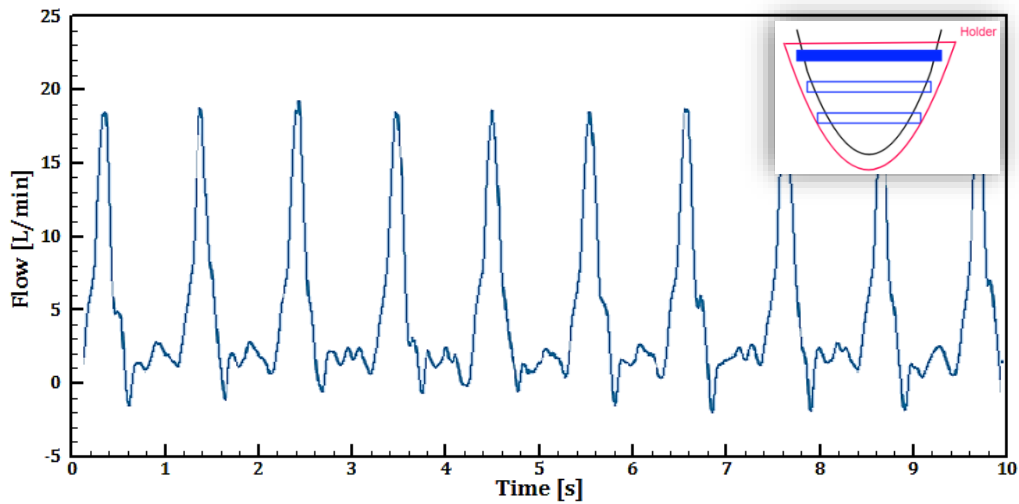

Figure 4.8 Flow waveform with active actuators: #1 and #3, Voltage: 3.5V, with holder
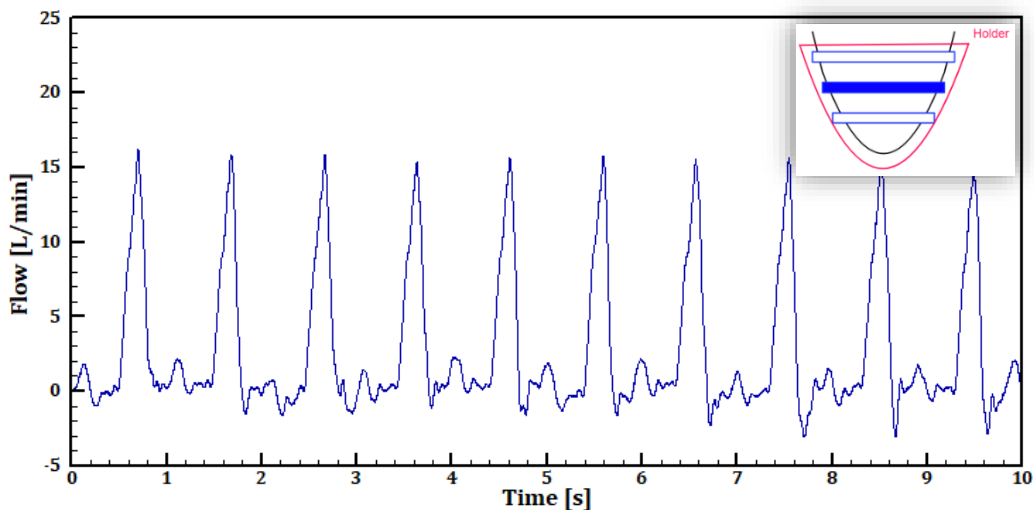

Figure 4.9 Flow waveform with active actuators: #2 and #3, Voltage: 3.5V, with holder
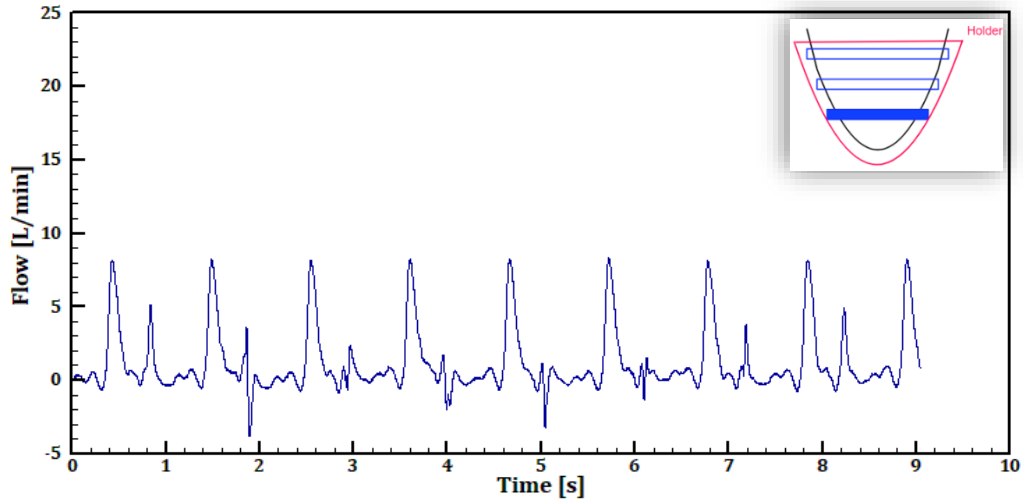
4.2.2 One Active Actuator

One of the objectives of this study is to simulate heart failure in which the ejection fraction declines to 40% or lower. The same condition as previous experiments were provided, but only one actuator was kept activated in the voltage range of 1 to 3.5V with the holder (All graphs are available in the appendix). Aortic flow is measured when each actuator works as a single contractile element in the maximum feasible voltage of 3.5V, Figure 4.10 to Figure 4.12.

Figure 4.10 Flow waveform with active actuator: #1, Voltage: 3.5 V, with holder

Figure 4.11 Flow waveform with active actuator: #2, Voltage: 3.5 V, with holder

Figure 4.12 Flow waveform with active actuator: #3, Voltage: 3.5 V, with holder

## 4.3 Effect of Active Actuators on the Average Flow Rate

The results of the investigation of the flow in different setup configurations are presented in this section. The peak and mean flows of different configurations at the maximum possible voltage of 3.5 V are reported in Table 4.1. Based on the definition given in Chapter 1.4.1, the mean flow replicates the cardiac output. Then, the stroke volume and the ejection fraction can be calculated based on the cardiac output data.

A summary of all mean flows in each configuration is shown in Figure 4.13. Regarding the results of one active actuator experiment, when the contraction is made near the base a higher mean flow can be created in the aorta. The mean flow of actuator #1, when it works solely, equals 3.08 L/min, and actuators #2 and #3 could generate 2.68 and 1.15 L/min respectively. Therefore, we can report actuator #3 as the least effective actuator in the proposed model.

The optimized model is composed of three actuators and the holder, by which mean and peak aortic flow of 4.05 L/min and 20.42 L/min can be produced. The second-best mean aortic flow is 3.98 L/min, and it can be generated when the actuator near the apex (#3) is deactivated.

Table 4.1 Cardiac assessments in the different configurations, Voltage: 3.5 V

Configuration	Peak Flow [L/min]	Cardiac Output [L/min]	Stroke Volume (ml)	Ejection Fraction (%)
S1 with Holder	18.87	3.08	51.33	38.02
S2 with Holder	16.19	2.68	44.50	33.96
S3 with Holder	8.33	1.15	19.17	14.20
S1, S2 with Holder	16.52	3.98	66.33	49.13
S1, S3 with Holder	12.45	2.47	41.17	30.49
S2, S3 with Holder	9.11	1.65	27.50	20.37
S1, S2, S3	13.61	2.74	45.66	33.82
S1, S2, S3 with Holder	20.42	4.05	67.50	50.00
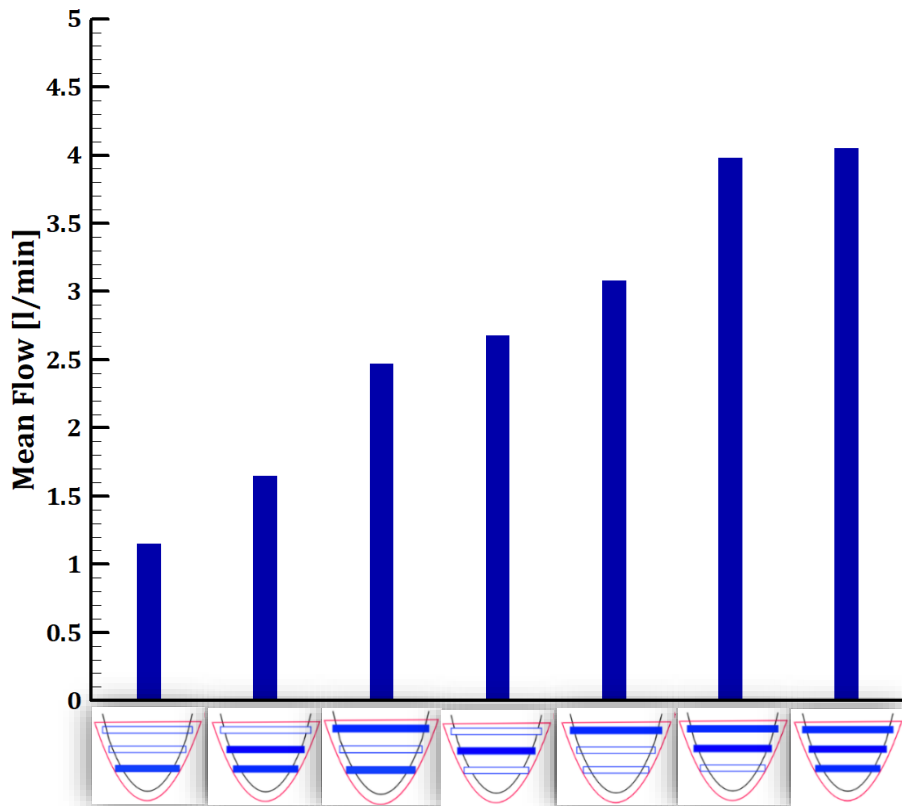
Figure 4.13 Comparison of the mean flow values in the different configurations, Voltage: 3.5 V

41
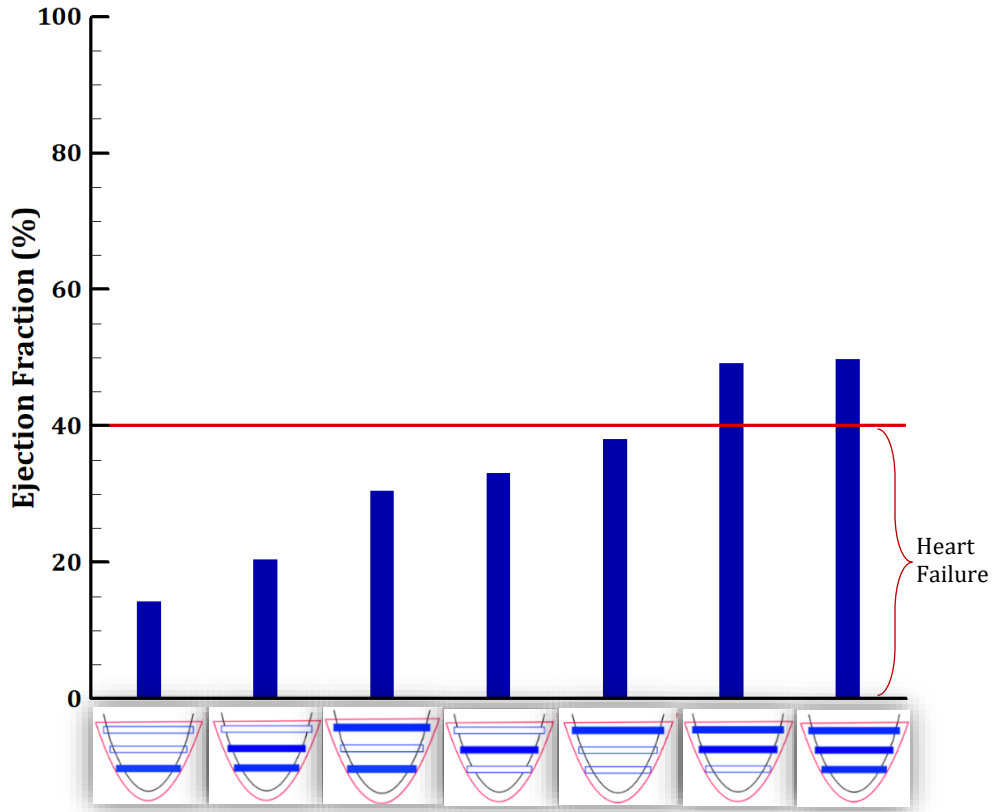
Figure 4.14 Ejection fraction of each configuration, the lines show the normal range

Chapter 5

Conclusion

The objectives of this work were creating a new custom-made heart phantom, simulating the heartbeat by using soft robotic actuators and measuring the flow in the aortic valve. Firstly, the fabrication of the silicone phantoms was described in detail, by which any complex anatomical structure can be 3D-modeled and fabricated by brushing silicone on the 3D-printed molds. Secondly, for the simulation of the heartbeat, we employed the novel method of soft robotic sleeves to produce heart contraction. From a cardiovascular biomechanics' perspective, mimicking realistic conditions and values was one of the crucial objectives. Therefore, we chose one of the main diagnostic parameters, "Fractional Shortening", which is at least 25% in a healthy heart. Then, we fabricated the actuators composed of commercially available elements that can contract more than 25%. The proposed mesh-based soft robot made of three actuators was fabricated to investigate the possibility of making heart contraction. By inducing over 25% ventricular contraction, we managed to generate an aortic flow of 4.05 l/min to replicate the normal conditions by contracting all regions of the heart phantom.

As already stated in Chapter 4, to prove the possibility of mimicking cardiomyopathy, we deactivated different actuators and measured the aortic flow to observe the effect of losing contraction in different regions on the flow. By activating the actuators closer to the base, a higher flow can be generated, therefore, in case of having a limited area for smaller cardiac sizes, for instance in female or pediatric models, the basal contraction can compensate the aortic flow to some extent. To clarify each actuator's role in the aortic flow, the basal actuator (#1) generates the maximum flow when it works solely, and the apex actuator (#3) has the least role in the flow generation.

To conclude, the results show that our custom-made silicone heart phantom can be a realistic substitute for early-phase *in vivo* studies since we were able to create realistic aortic velocities and cardiac output. Using such a multidisciplinary approach in the design of heart models can be of help in clinical pre-procedural care for patients with congenital heart disease, especially in pediatric surgeries and medical device selection.

The proposed model is Doppler ultrasound-compatible and the opening and closing valves can be observed in motion mode. The preliminary results of the mean flow, peak flow, velocity time integral (VTI) at left ventricular outflow tract (LVOT) are measured and reported in the Appendix, then cardiac output and fractional shortening are calculated. Since the quantitative preliminary results, including the continuous and pulsed wave Doppler ultrasound measurements for both aortic and mitral valves, are beyond the objectives of this study, we provided them in the Appendix.

The comparisons of the two data assessment methods, direct flow measurement and Doppler ultrasound, are promising since a great compatibility can be seen in the results of the second-best configuration. However, there are differences between the data of the optimized method with three active actuators. The reason might lie in the movement of the model because actuator #3 contracts the apex and pushes the phantom upward. The whole setup is submerged into the water and the model is dealing with the lift force as well, it can be a source of error during the measurement process.

There is always room for improvement, a few suggestions are proposed in this section as stepping stones for future studies. Firstly, making a complete heart phantom instead of only the ventricles can make the simulation and measurements more realistic. To this end, a 52-year-old female Computed Tomography Angiography (CTA) data were used for the 3D modeling with open-source software, "3D Slicer". The "Grow from Seed" segment editor was employed for the modeling of the blood and the myocardium. Then, by employing Gaussian smoothing, the rough parts of the surface and edges were corrected. Finally, in some slices, manual corrections were applied.

We printed the blood part with the available 3D printer Lulzbot Taz 6 (Aleph Objects, Loveland, CO, U.S.A.) at the LCFD laboratory at Concordia University. Creating a silicone model of the complete heart myocardium by brushing silicone on the blood part was challenging. In addition, placing the valves in a closed model was complicated, therefore, we observed the concept of using a soft robot in a simplified model as is already shown in this thesis. We highly recommend 3D-printing a flexible myocardium model and trying the same experiments to observe the aortic flow and the contraction. Using a 3D printer with silicone

filament would make way more accurate models, by which the accuracy of the measurement methods would be improved.

The best commercially available mesh and tube have been introduced in this work, unlike the proposed custom-made sleeves, the same actuators can be used for heartbeat simulation in future studies. The setup should be optimized, we submerged the model under the water, because an inflow needed to be generated through the mitral valve. Finding a new way to create the flow can be a new challenge the future researchers.

Regarding the setup's design, there are other possible arrangements for the actuators, for instance, placing them in a cross order, or from the base to the apex (quite the opposite of how they are placed in this study). The asynchrony of actuators' contraction will also affect the flow. Here, all of them are contraction synchronized, we suggest creating the contraction with a delay, firstly in the apex, then in the middle region, and finally near the base; so that a higher flow can be produced in the aorta.

In terms of the limitations of this study, the echo machine provided by Concordia University was not in its best condition and the presets for the cardiac measurement were not set properly and the images were noisy.

References

Andrikopoulos, Georgios, Nikolakopoulos, George, and Manesis Stamatis. 2011. "A Survey on Applications of Pneumatic Artificial Muscles." In *19th Mediterranean Conference on Control and Automation*, 1439–46.

Berselli, Giovanni, Rocco Vertechy, and Gabriele Vassura. 2012. *Smart Actuation and Sensing Systems Recent Advances and Future Challenges.* InTech.

Bautista-Salinas, Daniel, Peter E. Hammer, Christopher J. Payne, Isaac Wamala, Mossab Saeed, Thomas Thalhofer, Pedro J. Del Nido, Conor J. Walsh, and Nikolay V. Vasilyev. 2020. "Synchronization of a Soft Robotic Ventricular Assist Device to the Native Cardiac Rhythm Using an Epicardial Electrogram." *Journal of Medical Devices, Transactions of the ASME* 14, no. 3: 1–8.

Borzikova, Jana, Milan Balara, and Ján Pitel. 2007. "The Mathematical Model of Contraction Characteristic k = (F, p) of the Pneumatic Artificial Muscle." In *Instruments and Control*. VŠB - Technická univerzita Ostrava.

Bruss, Zachary S., and Avais Raja. 2023. *Physiology, Stroke Volume*. StatPearls Publishing.

Chang, L., S. S. Dhruva, J. Chu, L. A. Bero, and R. F. Redberg. 2015. "Selective Reporting in Trials of High Risk Cardiovascular Devices: Cross Sectional Comparison between Premarket Approval Summaries and Published Reports." *BMJ* 350, no. may27 7 (June): h2613–h2613.

Coles-Black, Jasamine, Damien Bolton, and Jason Chuen. 2021. "Accessing 3D Printed Vascular Phantoms for Procedural Simulation." *Frontiers in Surgery* 7, no. Article 626212 (January).

Daerden, Frank, and Dirk Lefeber. 2001. "The Concept and Design of Pleated Pneumatic Artificial Muscles." *International Journal of Fluid Power* 2, no. 3: 41–50.

Daerden, Frank, and Dirk Lefeber. 2002. "Pneumatic Artificial Muscles: Actuators for Robotics and Automation." *Article in European Journal of Mechanical and Environmental Engineering*.

Frey, Norbert, Hugo A. Katus, Eric N. Olson, and Joseph A. Hill. 2004. "Hypertrophy of the Heart." *Circulation* 109, no. 13 (April): 1580–89.

Gaiser, I., R. Wiegand, O. Ivlev, A. Andres, H. Breitwieser, S. Schulz, and G. Bretthauer. 2012. "Compliant Robotics and Automation with Flexible Fluidic Actuators and Inflatable Structures." *InTech*, 22:567–608. https://doi.org/10.5772/51866.

Givertz, Michael M. 2011. "Ventricular Assist Devices: Important Information for Patients and Families." *Circulation* 124, no. 12 (September).

Greer, Joseph D., Tania K. Morimoto, Allison M. Okamura, and Elliot W. Hawkes. 2017. "Series Pneumatic Artificial Muscles (SPAMs) and Application to a Soft Continuum Robot." In *Proceedings - IEEE International Conference on Robotics and Automation*, 5503–10. Institute of Electrical and Electronics Engineers Inc.

Han, Jooli. 2020. Muscle-Powered Soft Robotic Ventricular Assist Devices. Ph.D. diss., University of Carnegie Mellon. Pittsburgh, PA.

Han, Jooli, and Dennis R. Trumble. 2019. "Cardiac Assist Devices: Early Concepts, Current Technologies, and Future Innovations." *Bioengineering* 6, no. 1.

Horvath, Markus A., Claudia E. Varela, Eimear B. Dolan, William Whyte, David S. Monahan, Christopher J. Payne, Isaac A. Wamala, et al. 2018. "Towards Alternative Approaches for Coupling of a Soft Robotic Sleeve to the Heart." *Annals of Biomedical Engineering* 46, no. 10 (October): 1534–47.

Huhta, James C. 2006. "Echocardiography and Noninvasive Diagnosis." In *Pediatric Critical Care*, 273–84. Elsevier. https://doi.org/10.1016/B978-032301808-1.50024-9.

Iaizzo, Paul A. 2005. *Handbook of Cardiac Anatomy, Physiology, and Devices: Second Edition*.

Institute of Medicine (U.S.). Committee on Social Security Cardiovascular Disability Criteria., and Institute of Medicine (U.S.). Board on the Health of Select Populations. 2010. *Cardiovascular Disability: Updating the Social Security Listings*. National Academies Press.

King, Jordan, and David R. Lowery. 2017. *Physiology, Cardiac Output*. StatPearls Publishing, Treasure Island (FL).

Kongahage, Dharshika, Arjang Ruhparwar, and Javad Foroughi. 2021. "High Performance Artificial Muscles to Engineer a Ventricular Cardiac Assist Device and Future Perspectives of a Cardiac Sleeve." *Advanced Materials Technologies* 6, no. 5 (May).

Justin Laing, John Moore, Reid Vassallo, Daniel Bainbridge, Maria Drangova, and Terry Peters. 2018. "Patient-Specific Cardiac Phantom for Clinical Training and Preprocedure Surgical Planning." *Journal of Medical Imaging* 5, no. 02 (March): 1.

Lipshultz, Steven E., E.John Orav, Stephen P. Sanders, Kenneth McIntosh, and Steven D. Colan. 1994. "Limitations of Fractional Shortening as an Index of Contractility in Pediatric Patients Infected with Human Immunodeficiency Virus." *The Journal of Pediatrics* 125, no. 4 (October): 563–70.

Liu, Hao, Jie Yan, Yuanyuan Zhou, Hongyi Li, and Changji Li. 2013. "A Novel Dynamic Cardiac Simulator Utilizing Pneumatic Artificial Muscle." In *Proceedings of the Annual International Conference of the IEEE Engineering in Medicine and Biology Society, EMBS*, 715–18.

Kari, Love. 2018. *Soft Robotics: A DIY Introduction to Squishy, Stretchy, and Flexible Robots*. Maker Media, Inc.

Lowe, James E., Mark P. Anstadt, Peter Van Trigt, Peter K. Smith, Paul J. Hendry, Mark D. Plunkett, and George L. Anstadt. 1991. "First Successful Bridge to Cardiac Transplantation Using Direct Mechanical Ventricular Actuation." *The Annals of Thoracic Surgery* 52, no. 6 (December): 1237–45.

Malik, Ahmad, Daniel Brito, Sarosh Vaqar, Lovely Chhabra, and Chaddie Doerr. 2023. *Congestive Heart Failure (Nursing)*. StatPearls Publishing, Treasure Island (FL).

Mirvakili, Seyed M., Douglas Sim, and Robert Langer. 2021. "Inverse Pneumatic Artificial Muscles for Application in Low-Cost Ventilators." *Advanced Intelligent Systems* 3, no. 1 (January): 2000200.

Moreno, Michael R., Saurabh Biswas, Lewis D. Harrison, Guilluame Pernelle, Matthew W. Miller, Theresa W. Fossum, David A. Nelson, and John C. Criscione. 2011. "Assessment of Minimally Invasive Device That Provides Simultaneous Adjustable Cardiac Support and Active Synchronous Assist in an Acute Heart Failure Model." *Journal of Medical Devices* 5, no. 4 (December).

Mosterd, A, A W Hoes, M C de Bruyne, J W Deckers, D T Linker, A Hofman, and D E Grobbee. 1999. "Prevalence of Heart Failure and Left Ventricular Dysfunction in the General Population." *European Heart Journal* 20: 447–55.

Nadruz, Wilson, Erin West, Mário Santos, Hicham Skali, John D. Groarke, Daniel E. Forman, and Amil M. Shah. 2016. "Heart Failure and Midrange Ejection Fraction." *Circulation: Heart Failure* 9, no. 4 (April).

Obiajulu, Steven C, Ellen T Roche, Frank A Pigula, and Conor J Walsh. 2013a. "Soft Pneumatic Artificial Muscles with Low Threshold Pressures for a Cardiac Compression Device." *International Design Engineering Technical Conferences & Computers and Information in Engineering Conference*, August (August), 1–8.

Payne, Christopher J., Isaac Wamala, Colette Abah, Thomas Thalhofer, Mossab Saeed, Daniel Bautista-Salinas, Markus A. Horvath, et al. 2017. "An Implantable Extracardiac Soft Robotic Device for the Failing Heart: Mechanical Coupling and Synchronization." *Soft Robotics* 4, no. 3 (September): 241–50.

Payne, Christopher J., Isaac Wamala, Daniel Bautista-Salinas, Mossab Saeed, David Van Story, Thomas Thalhofer, Markus A. Horvath, et al. 2017. "Soft Robotic Ventricular Assist Device with Septal Bracing for Therapy of Heart Failure." *Science Robotics* 2, no. 12: 1–12. https://doi.org/10.1126/scirobotics.aan6736.

Rawshani, Araz. 2018. *Clinical Echocardiography*. Elsevier.

https://ecgwaves.com/topic/fractional-shortening-for-estimation-of-ejection-fraction/

Roche, Ellen T, Markus A Horvath, Ali Alazmani, Kevin C Galloway, Nikolay V Vasilyev, David J Mooney, Frank A Pigula, and Conor J Walsh. 2015. "Design and Fabrication of a Soft Robotic Direct Cardiac Compression Device." *International Design Engineering Technical Conferences & Computers and Information in Engineering Conference.*

Roche, Ellen T, Markus A Horvath, Isaac Wamala, Ali Alazmani, Sang-Eun Song, William Whyte, Zurab Machaidze, et al. 2017. "Soft Robotic Sleeve Supports Heart Function." *Science Translational Medicine* 9, no. eaaf3925: 1–11.

Roche, Ellen T., Robert Wohlfarth, Johannes T.B. Overvelde, Nikolay V. Vasilyev, Frank A. Pigula, David J. Mooney, Katia Bertoldi, and Conor J. Walsh. 2014. "A Bioinspired Soft Actuated Material." *Advanced Materials* 26, no. 8 (February): 1200–1206. https://doi.org/10.1002/adma.201304018.

Skorina, Erik H., Ming Luo, Wut Yee Oo, Weijia Tao, Fuchen Chen, Sina Youssefian, Nima Rahbar, and Cagdas D. Onal. 2018. "Reverse Pneumatic Artificial Muscles (RPAMs): Modeling, Integration, and Control." *PLoS ONE* 13, no. 10 (October). https://doi.org/10.1371/journal.pone.0204637.

Takosoglu, Jakub Emanuel, Pawel Andrzej Laski, Slawomir Blasiak, Gabriel Bracha, and Dawid Pietrala. 2016. "Determining the Static Characteristics of Pneumatic Muscles." *Measurement and Control (United Kingdom)* 49, no. 2 (March): 62–71. https://doi.org/10.1177/0020294016629176.

US Food and Drug Administration Guidance Document. 2019. "Recommended Content and Format of Non-Clinical Bench Performance Testing Information in Premarket Submissions, Guidance for Industry and Food and Drug Administration Staff", (accessed December 2019)"

https://www.fda.gov/regulatory-information/search-fda-guidance-documents/recommended-content-and-format-non-clinical-bench-performance-testing-information-premarket

Voorhees, Andrew P., and Hai Chao Han. 2015. "Biomechanics of Cardiac Function." *Comprehensive Physiology* 5, no. 4 (October): 1623–44.

Wamala, Isaac, Christopher J. Payne, Mossab Y. Saeed, Daniel Bautista-Salinas, David Van Story, Thomas Thalhofer, Steven J. Staffa, et al. 2022. "Importance of Preserved Tricuspid Valve Function for Effective Soft Robotic Augmentation of the Right Ventricle in Cases of Elevated Pulmonary Artery Pressure." *Cardiovascular Engineering and Technology* 13, no. 1: 120–28.

World Health Organization, Cardiovascular Diseases, 2022
https://www.who.int/health-topics/cardiovascular-diseases#tab=tab_1

Appendix

Table 1 Clinical methods for evaluation of cardiac function (Voorhees and Han 2015)

Measurement	Methods
Dimensions and Geometry	Echocardiography, MRI, CT, SPECT, PET, MUGA
Contractile Function and Strain	Tagged MRI, Tissue Doppler Echocardiography, Speckle-Tracking Echocardiography
Pressure-Volume Relationship	Cardiac Catheterization

Table 2 Selected tubes for the experiments

Outer Diameter (mm)	Thickness (mm)	Durometer	Material	Code on McMaster
6.35	1.58	35A	Silicone	5236K506
9.52	1.58	35A	Silicone	5236K512
8.00	1.00	35A	Silicone	5054K812
11.00	1.00	35A	Silicone	5054K826

Table 3 Selected meshes for the experiments

Diameter (mm)	Thickness (mm)	Expandable ID (mm)	Material	Code on Techflex	Code on McMaster
6.3	0.08	1.1	Polyester	PTN0.38OR	9284K612
9.5	0.08	1.3	Polyester	PTN0.38BL	9284K613

Note: All the aortic flow waveforms with different configurations are given in color codes.
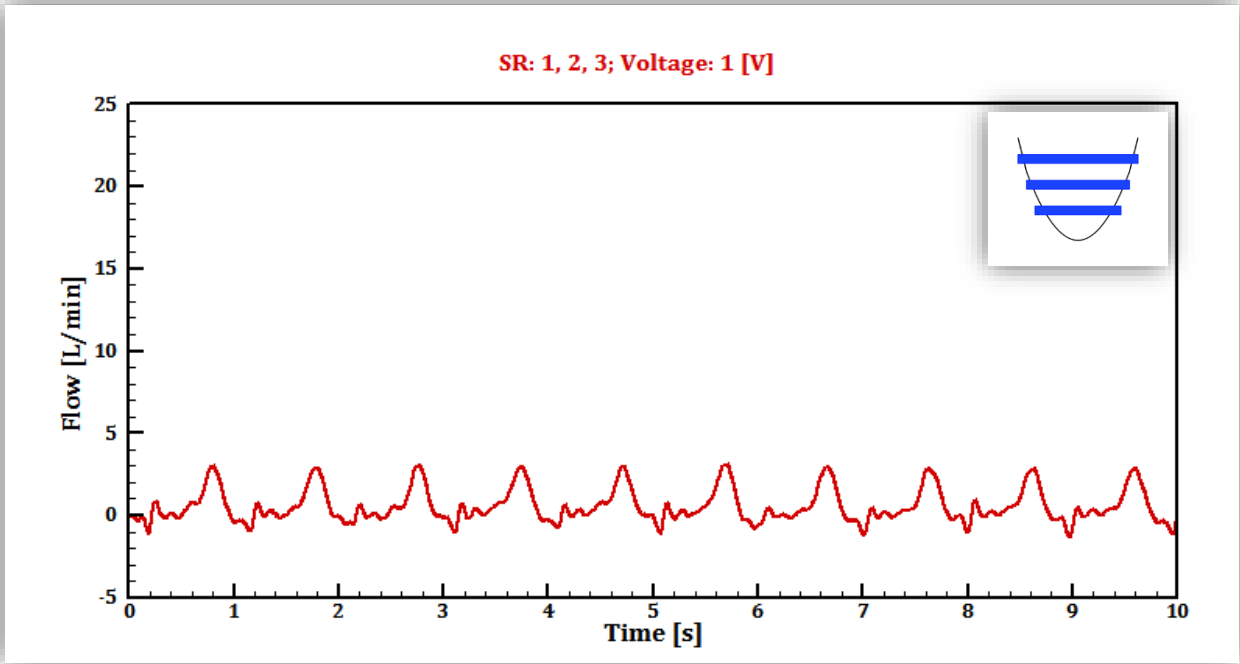
Figure 1 Flow waveform with active actuators: #1, #2, #3, Voltage: 1V, without holder
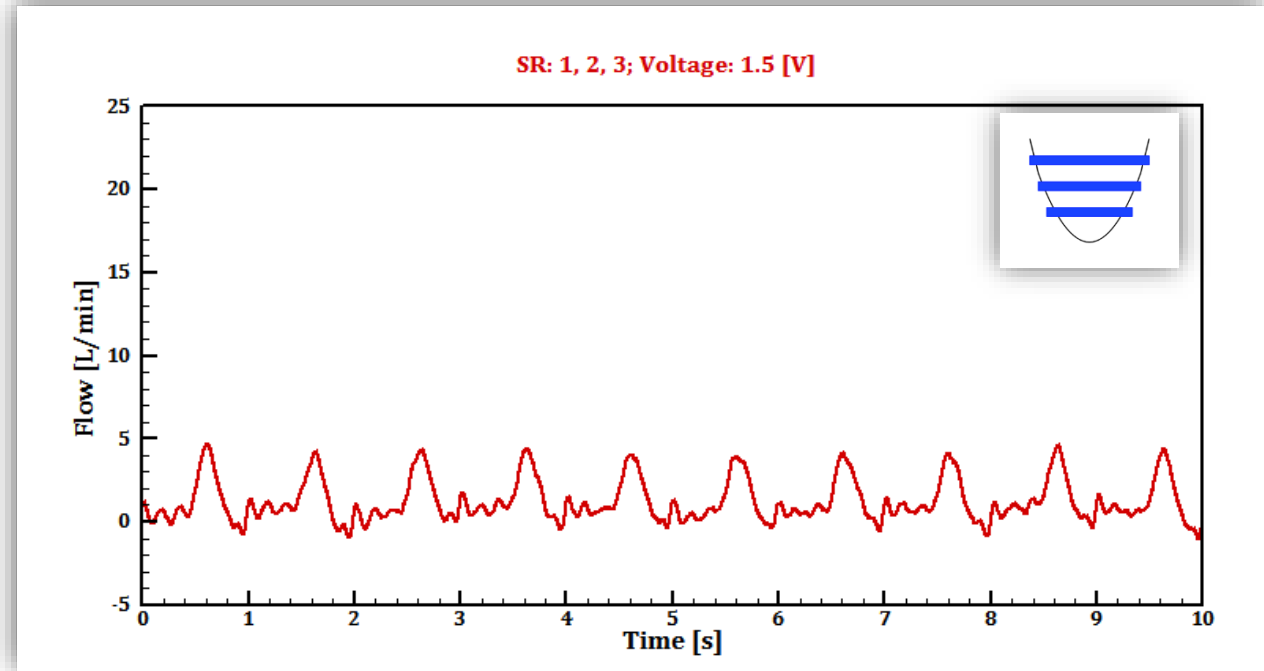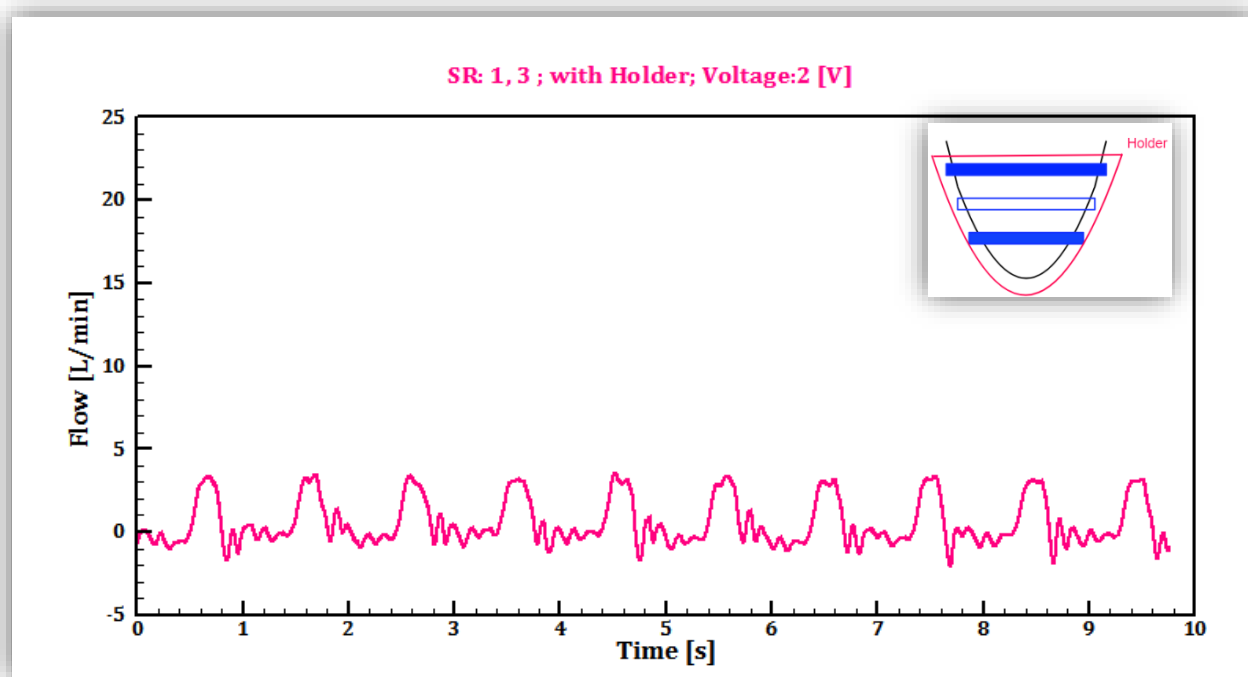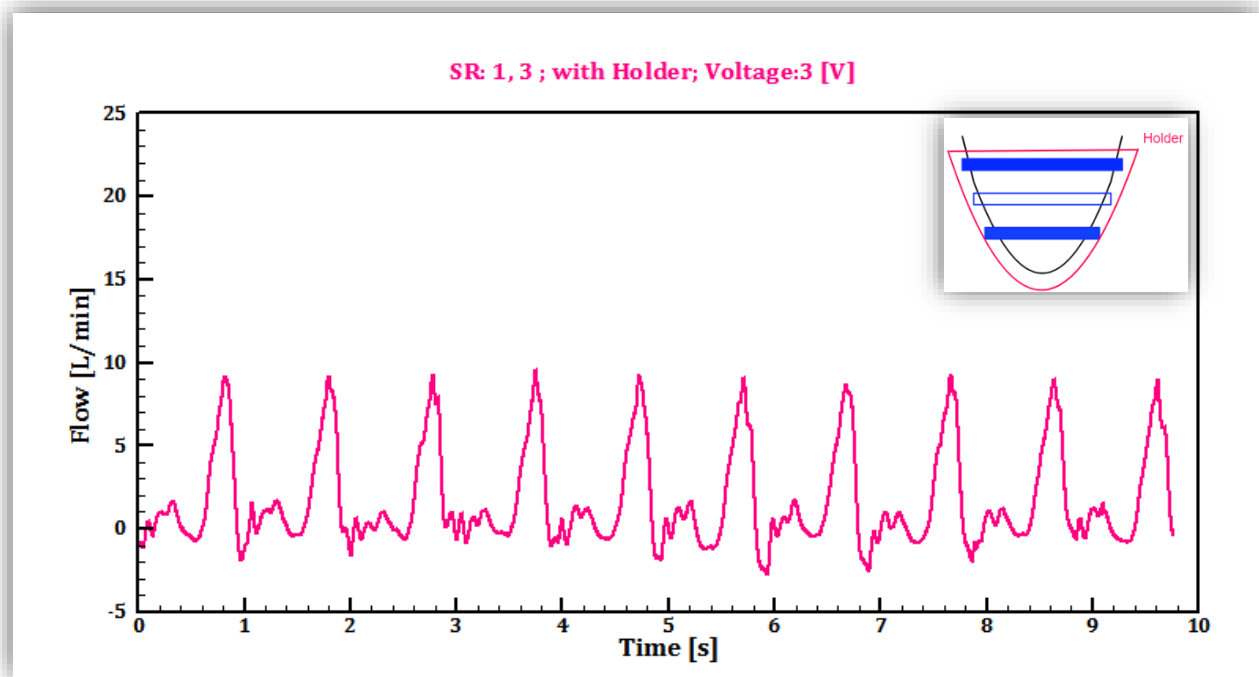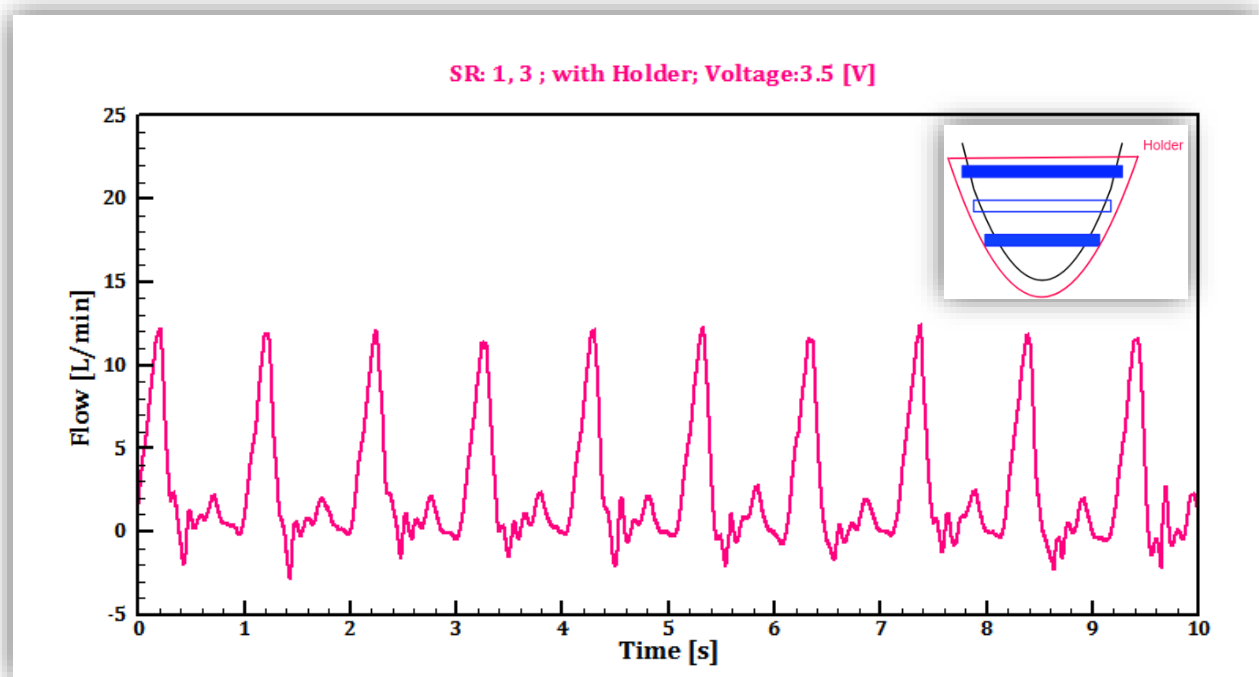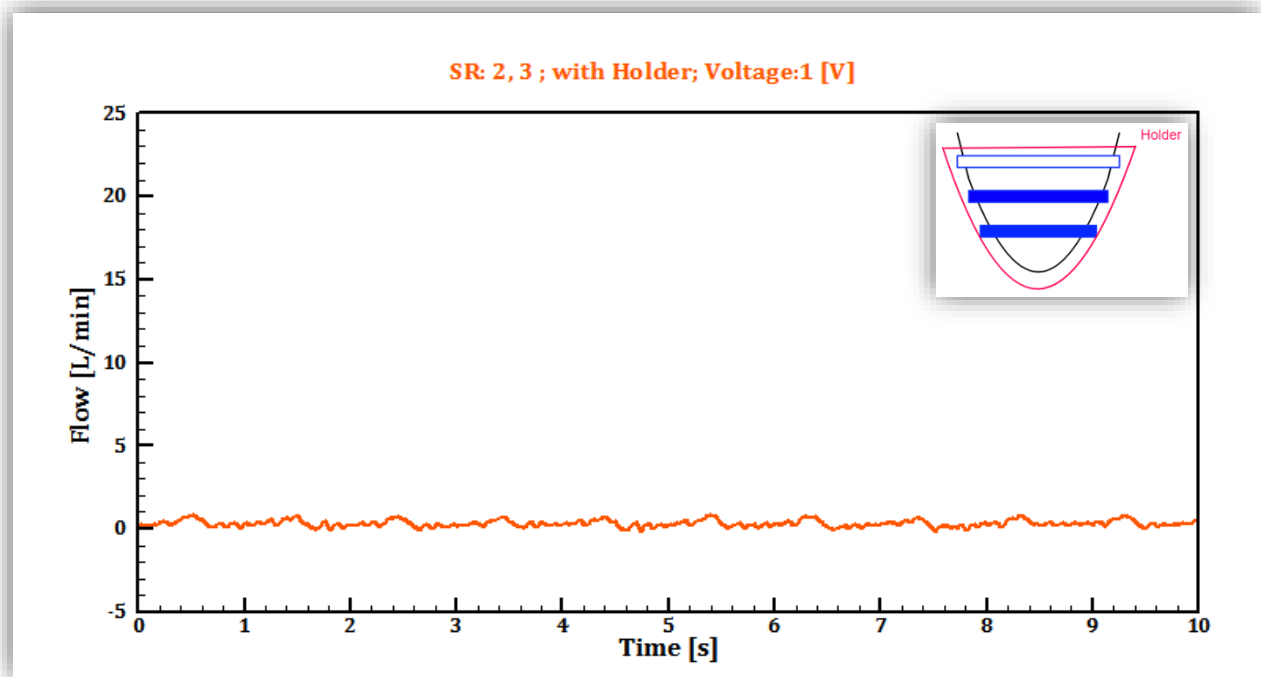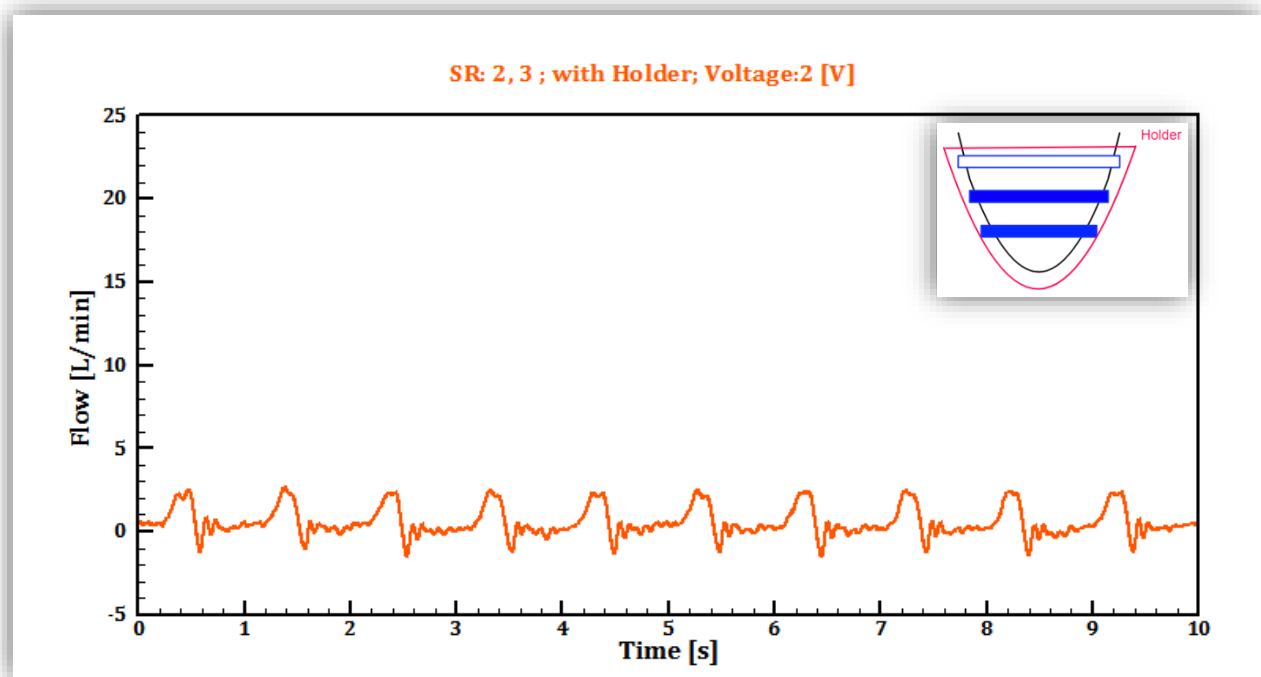

Figure 2 Flow waveform with active actuators: #1, #2, #3, Voltage: 1.5 V, without holder
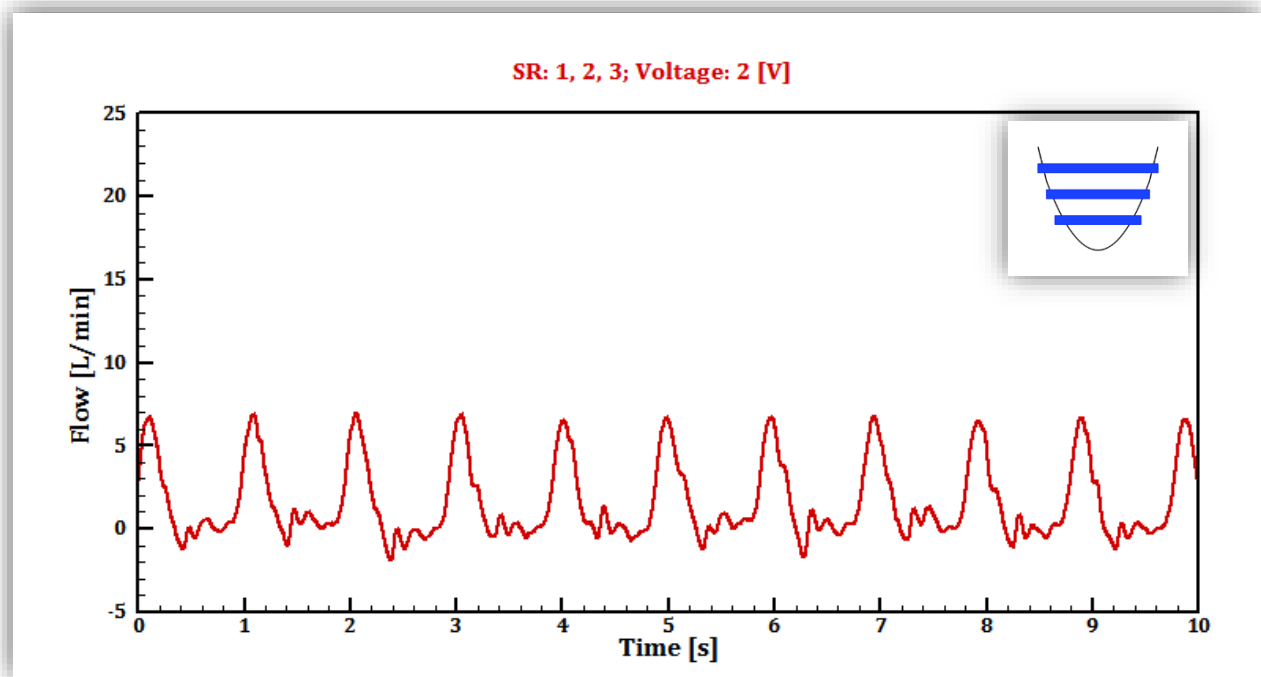
Figure 3 Flow waveform with active actuators: #1, #2, #3, Voltage: 2 V, without holder
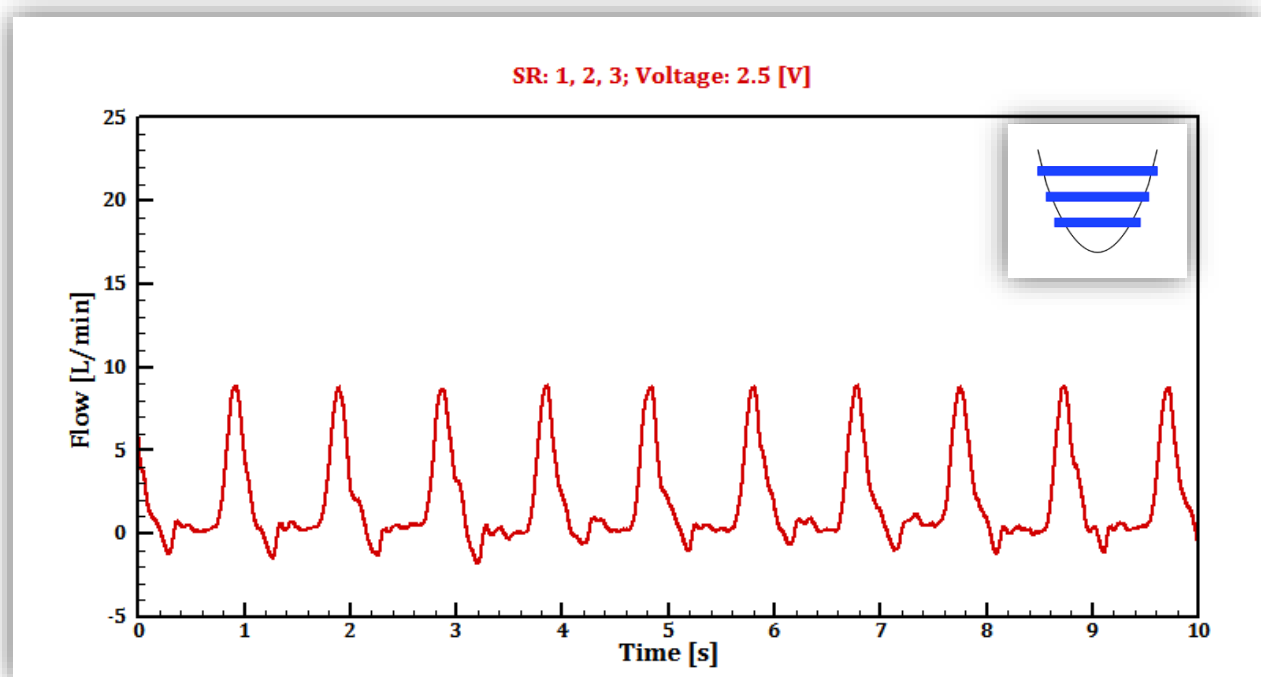
Figure 4 Flow waveform with active actuators: #1, #2, #3, Voltage: 2.5 V, without holder
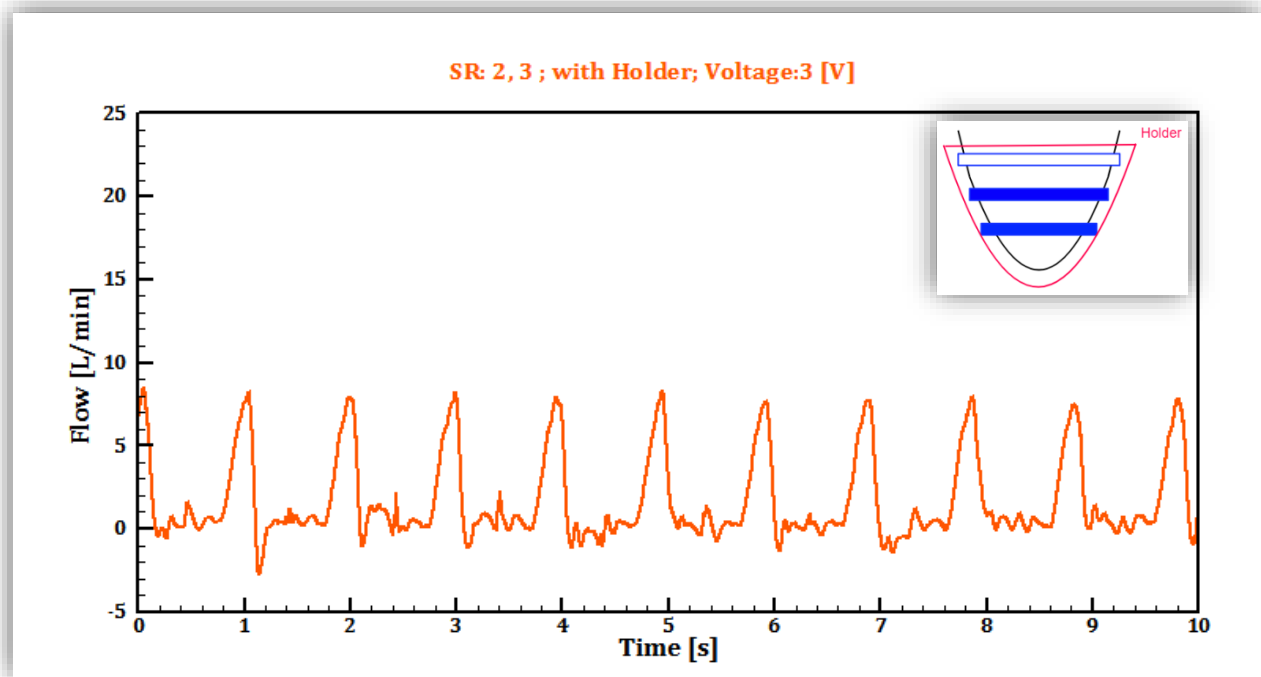
55
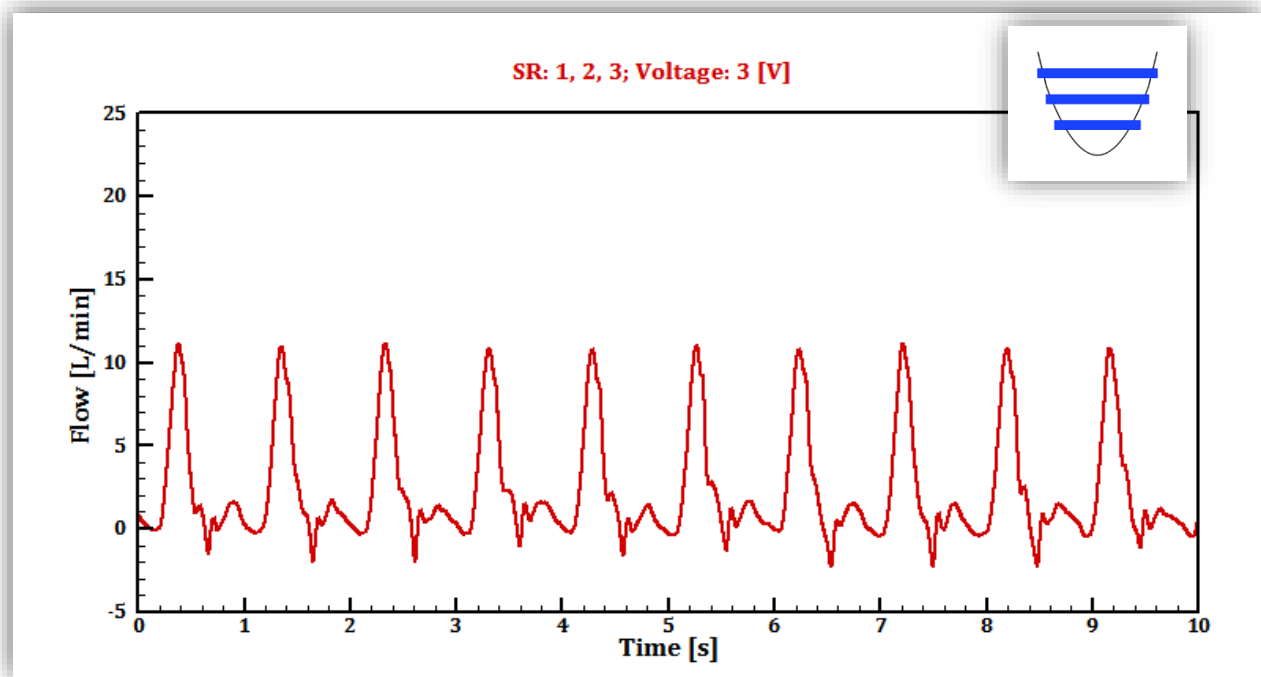
Figure 5 Flow waveform with active actuators: #1, #2, #3, Voltage: 3 V, without holder
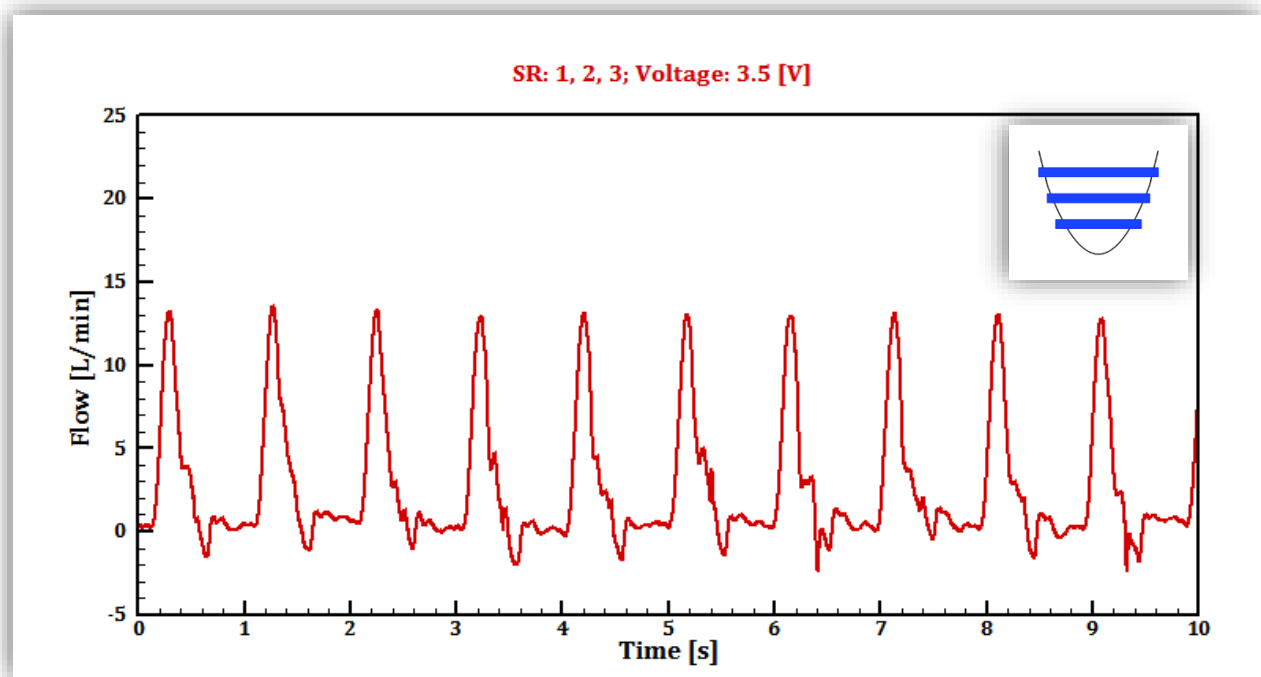
Figure 6 Flow waveform with active actuators: #1, #2, #3, Voltage: 3.5 V, without holder
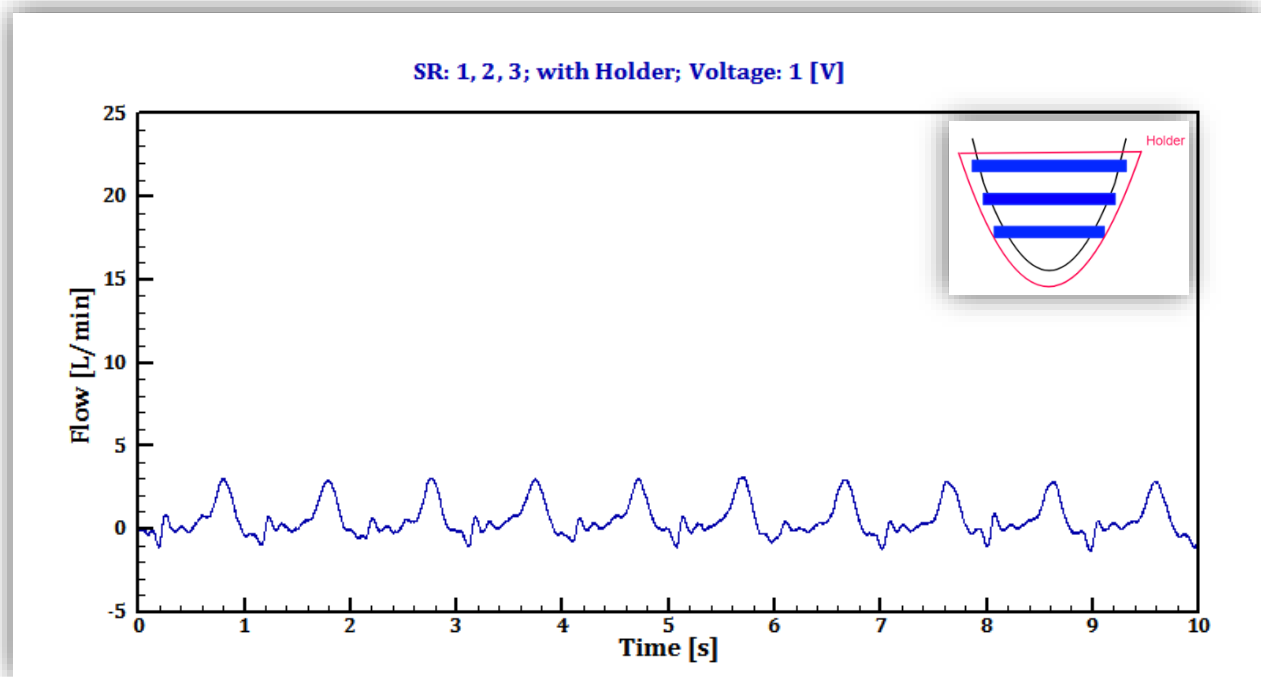
Figure 7 Flow waveform of the optimized setup with active actuators: #1, #2, #3, Voltage: 1 V, with holder
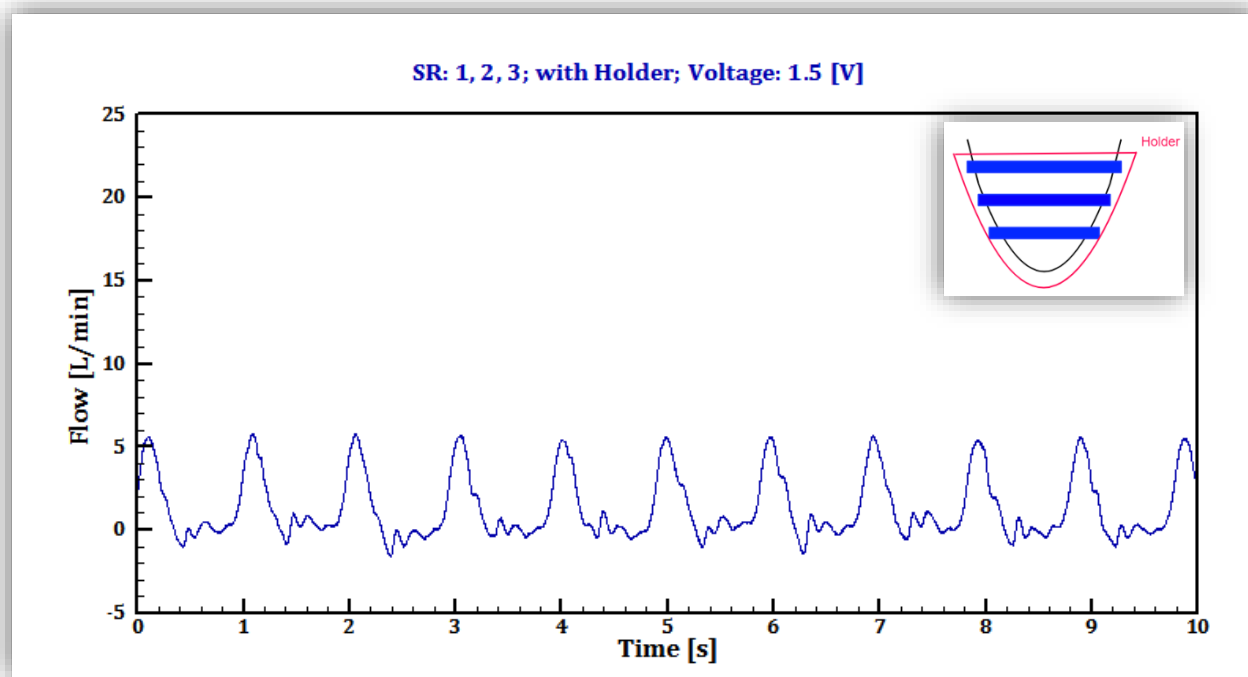
Figure 8 Flow waveform of the optimized setup with active actuators: #1, #2, #3, Voltage: 1.5 V, with holder
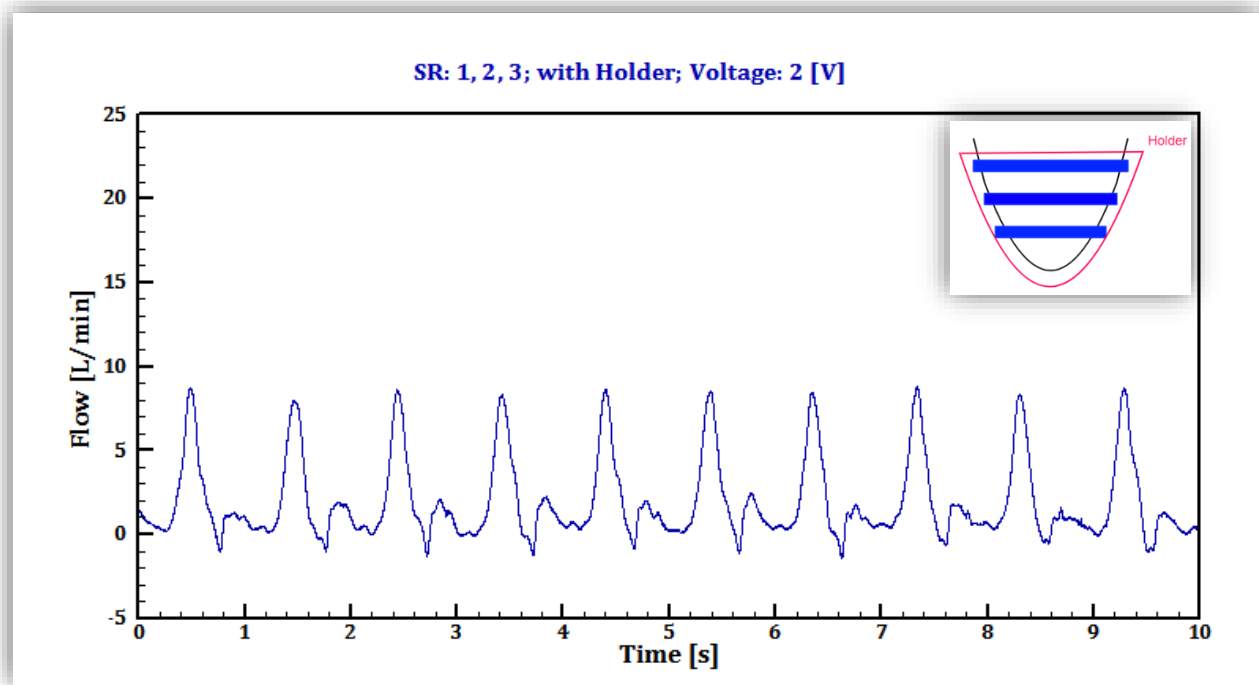
Figure 9 Flow waveform of the optimized setup with active actuators: #1, #2, #3, Voltage: 2 V, with holder
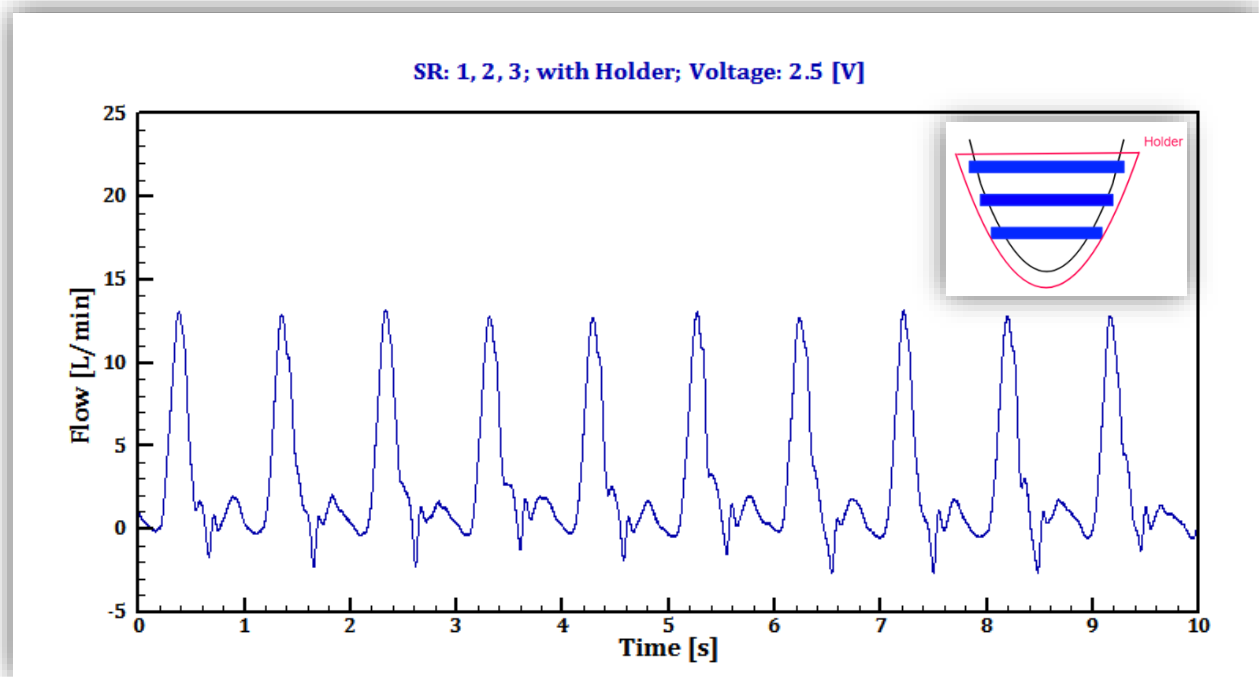
Figure 10 Flow waveform of the optimized setup with active actuators: #1, #2, #3, Voltage: 2.5 V, with holder
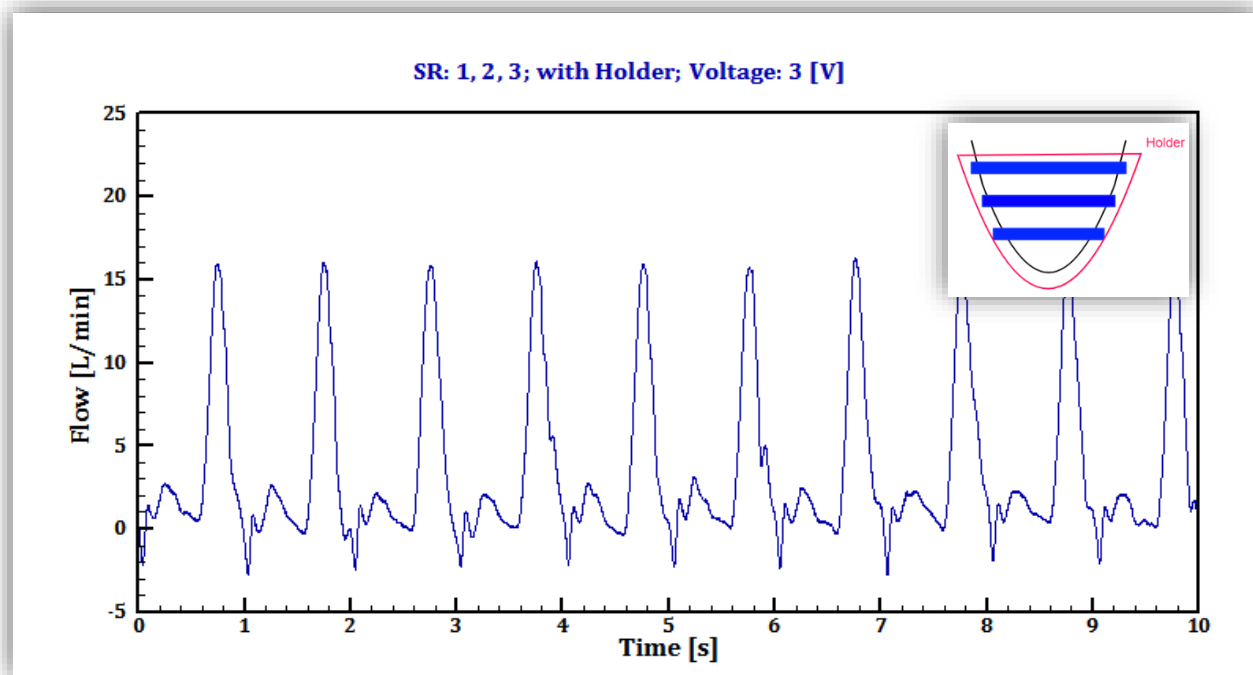
Figure 11 Flow waveform of the optimized setup with active actuators: #1, #2, #3, Voltage: 3 V, with holder
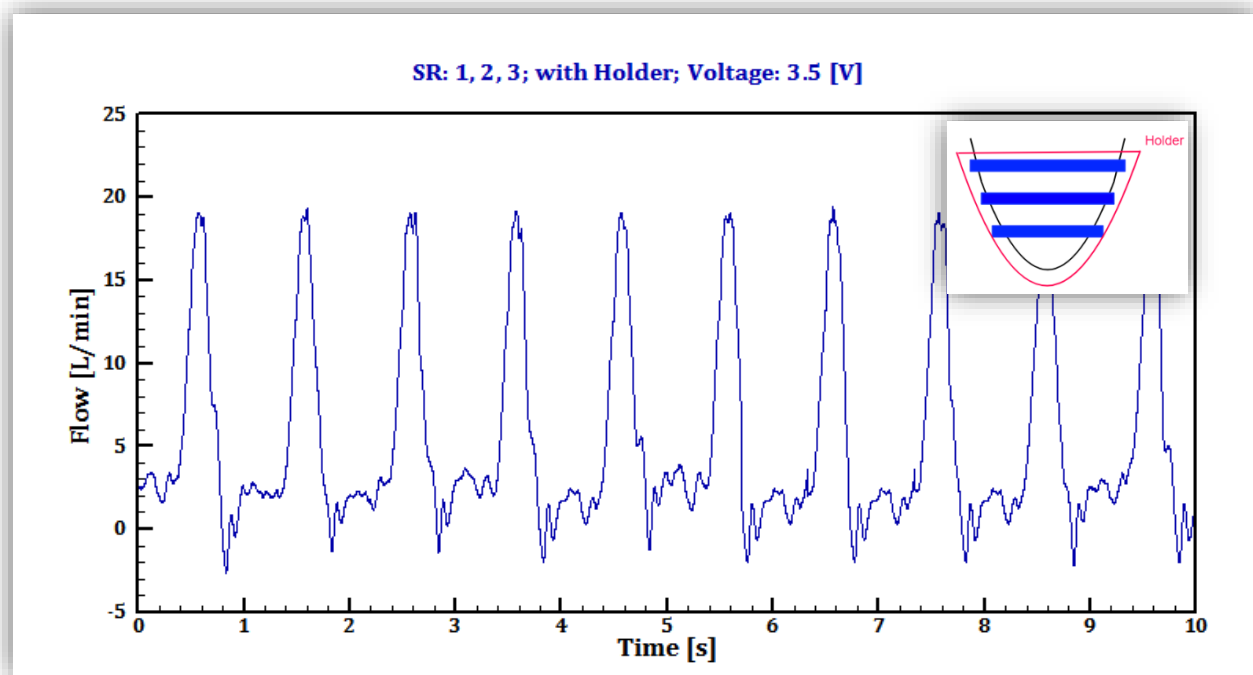
Figure 12 Flow waveform of the optimized setup with active actuators: #1, #2, #3, Voltage: 3.5 V, with holder
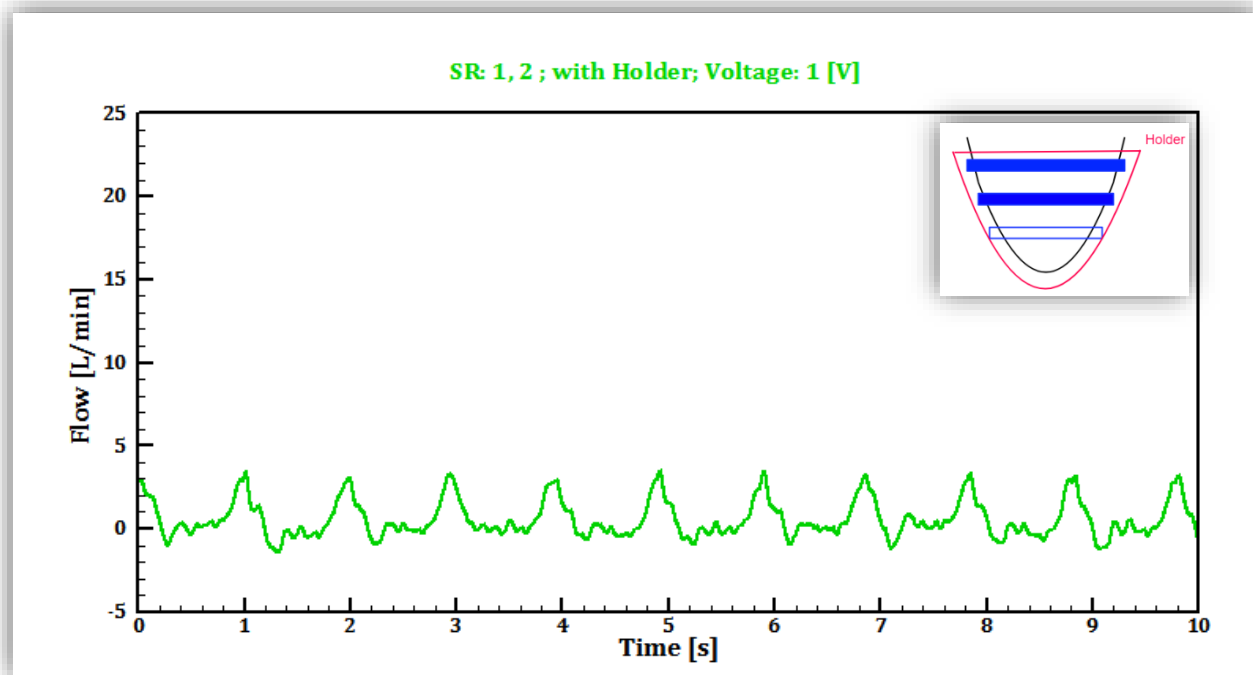
Figure 13 Flow waveform with active actuators: #1, #2, Voltage: 1 V, with holder
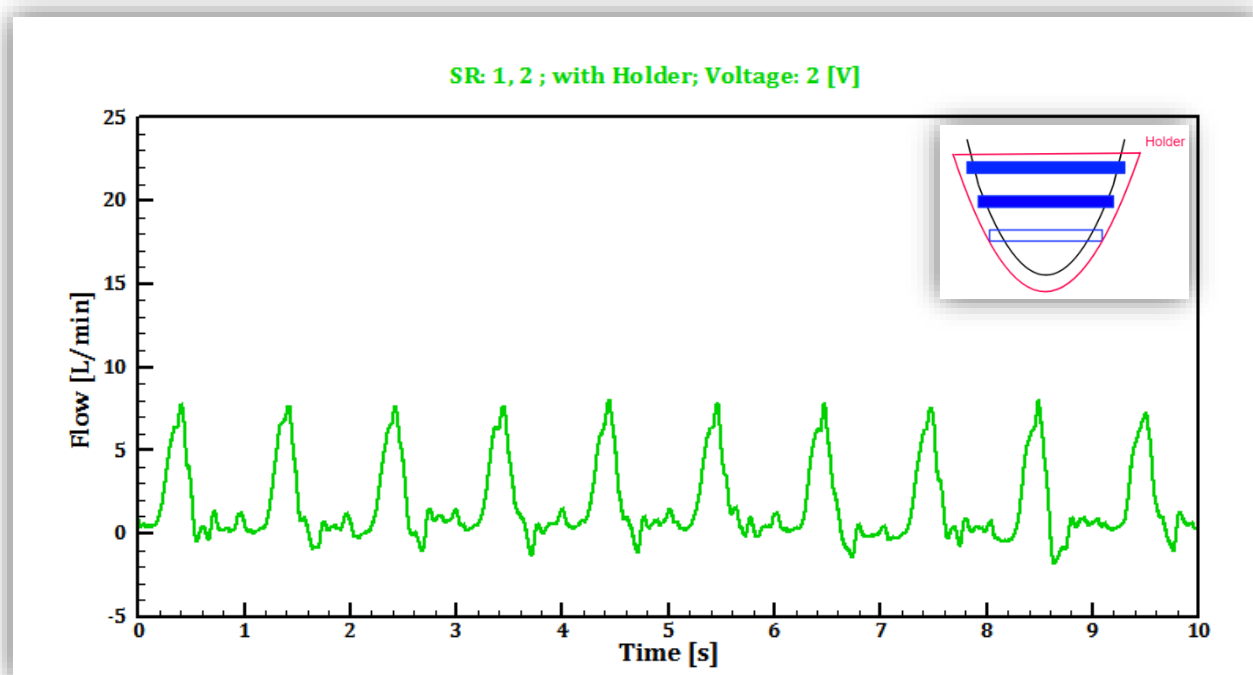
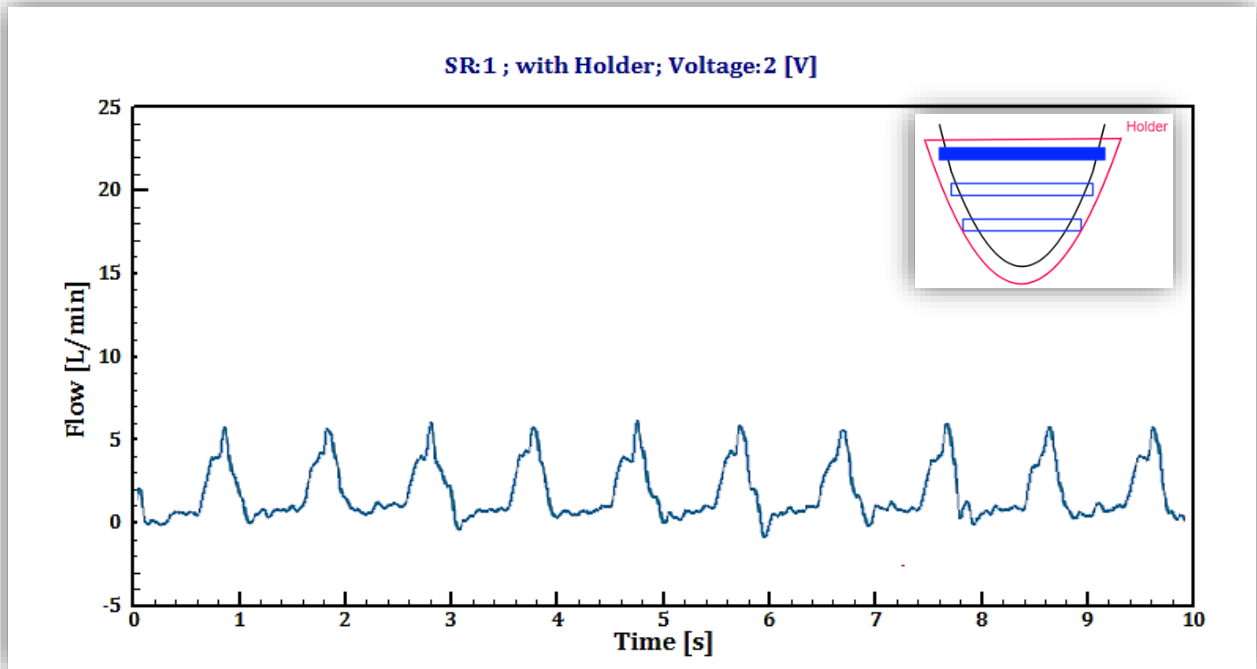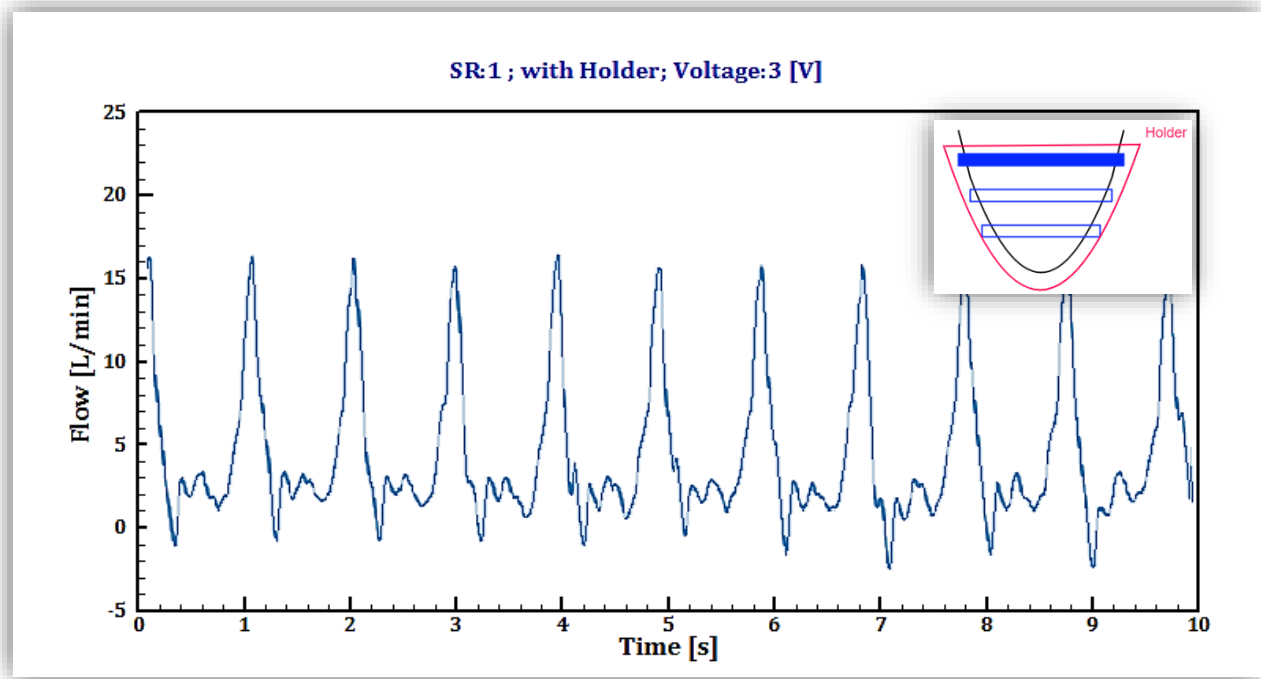**Figure14 Flow waveform with active actuators: #1, #2, Voltage: 2 V, with holder**
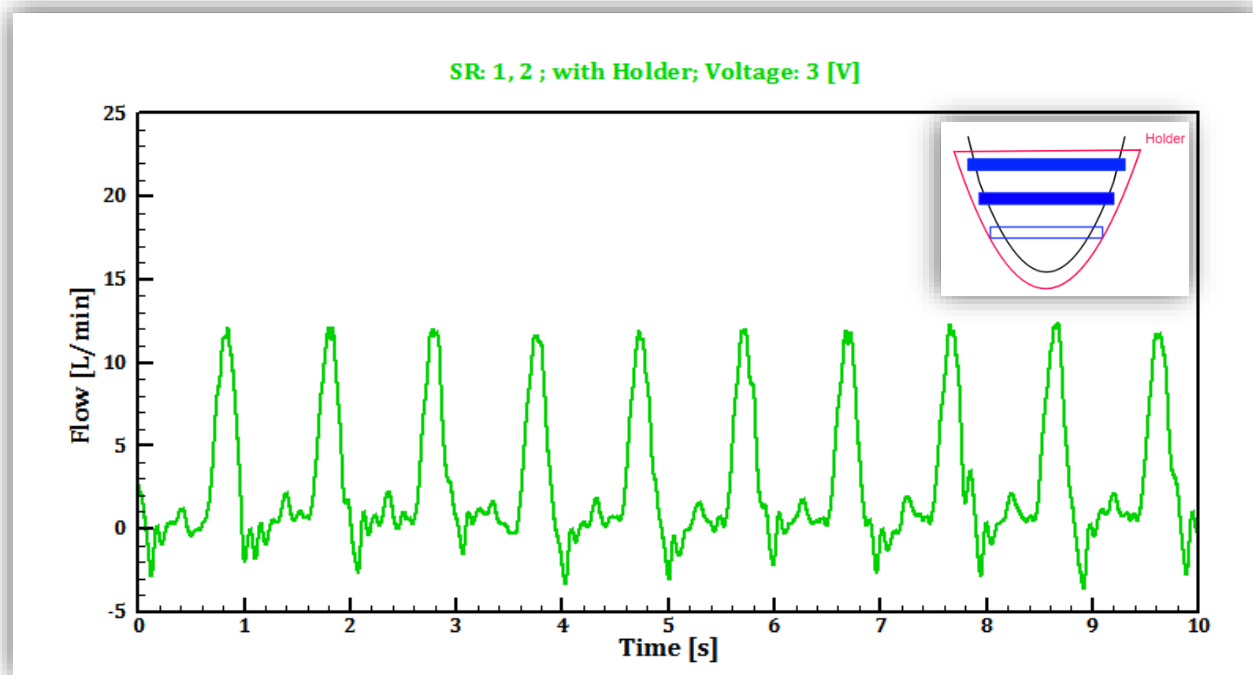
Figure 15 Flow waveform with active actuators: #1, #2, Voltage: 3 V, with holder
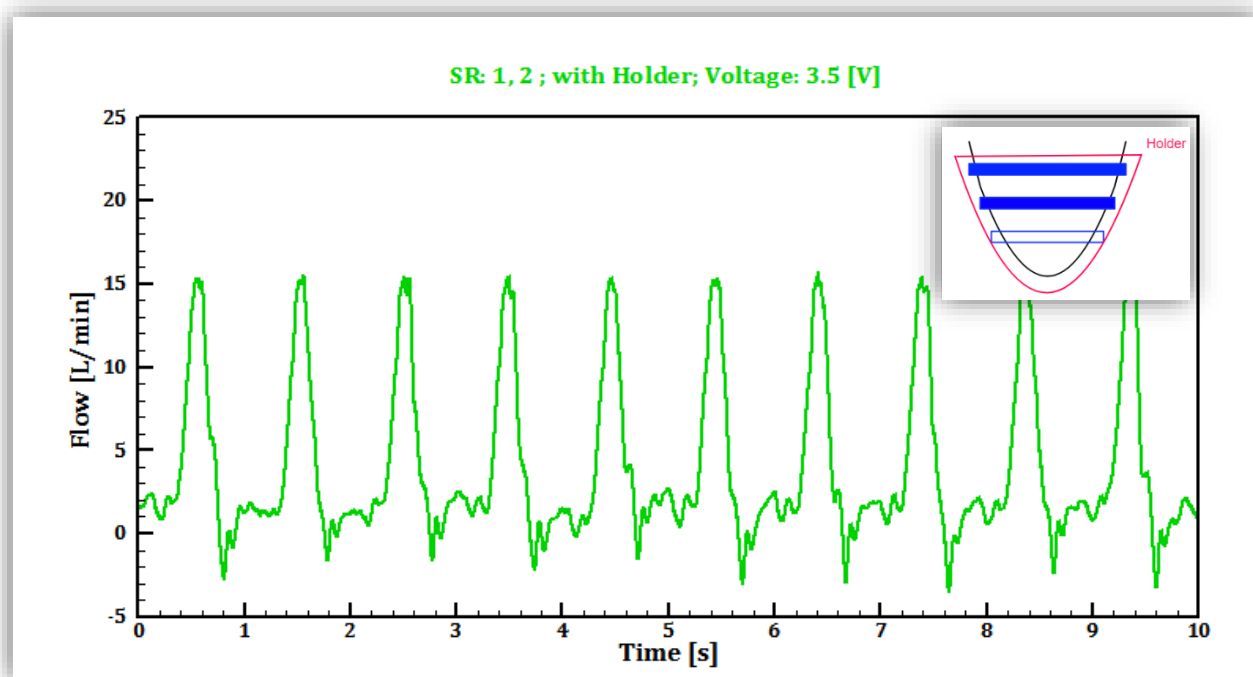
Figure 16 Flow waveform with active actuators: #1, #2, Voltage: 3.5 V, with holder

61
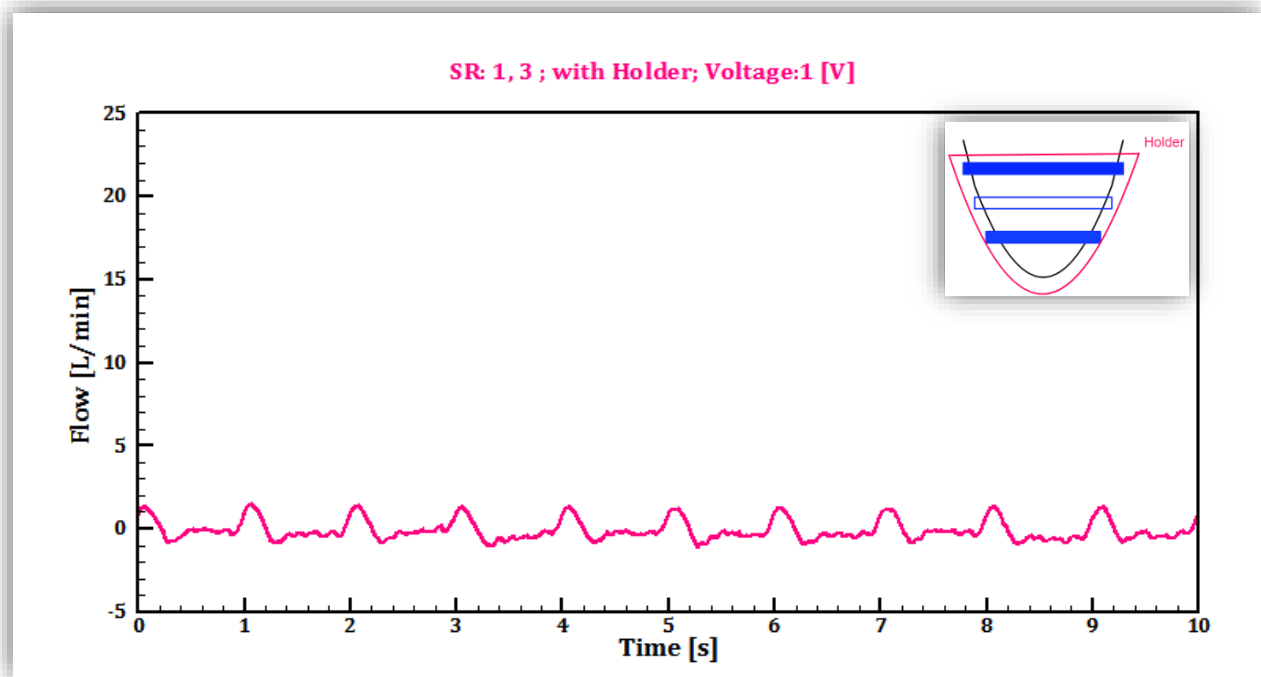
Figure 17 Flow waveform with active actuators: #1, #3, Voltage: 1 V, with holder

Figure 18 Flow waveform with active actuators: #1, #3, Voltage: 2 V, with holder

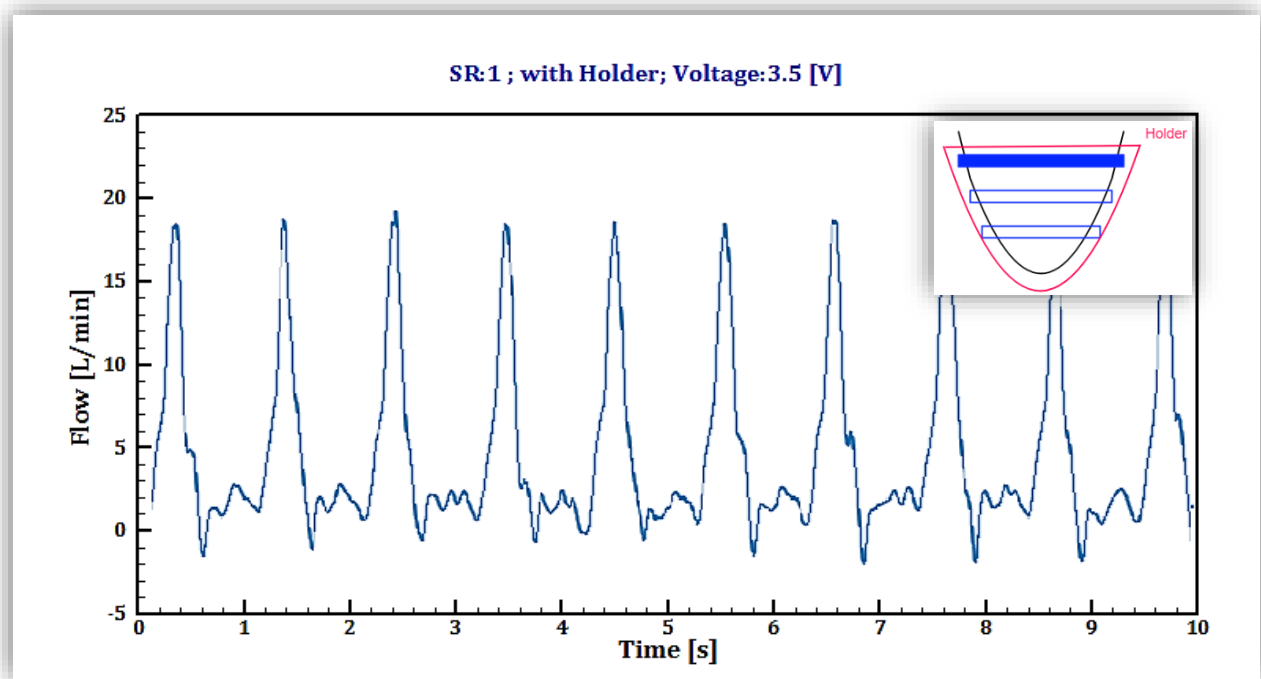**Figure 19 Flow waveform with active actuators: #1, #3, Voltage: 3 V, with holder**
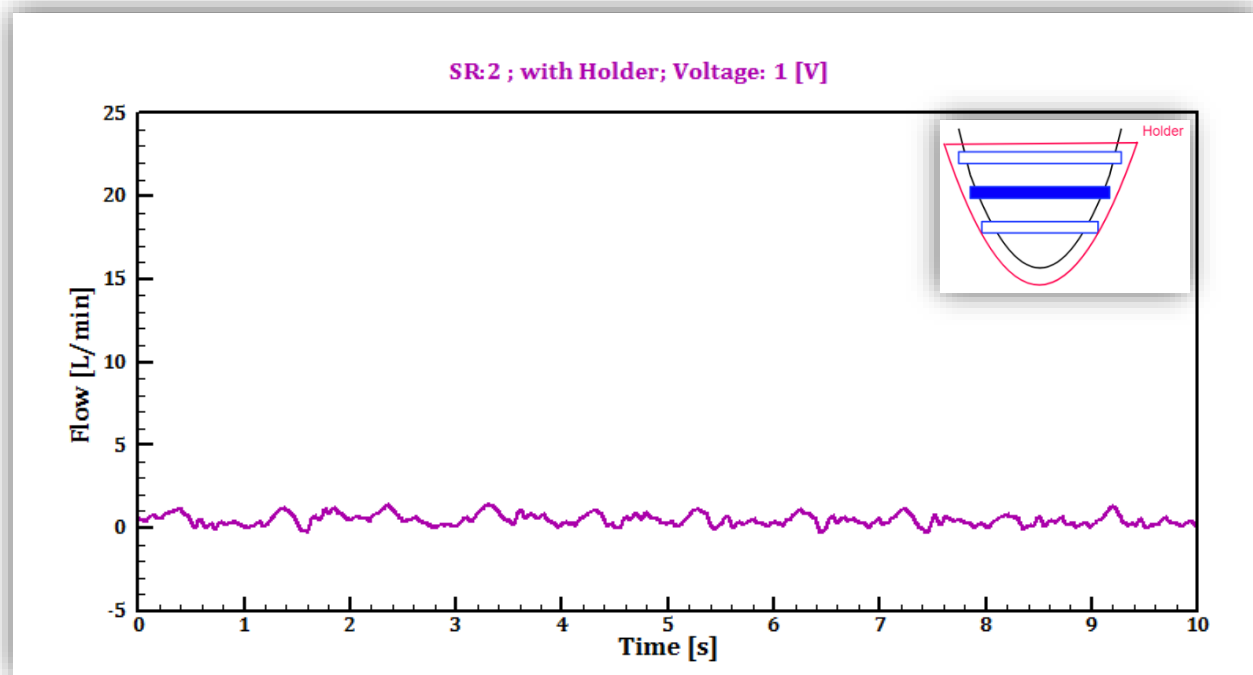

Figure 20 Flow waveform with active actuators: #1, #3, Voltage: 3.5 V, with holder
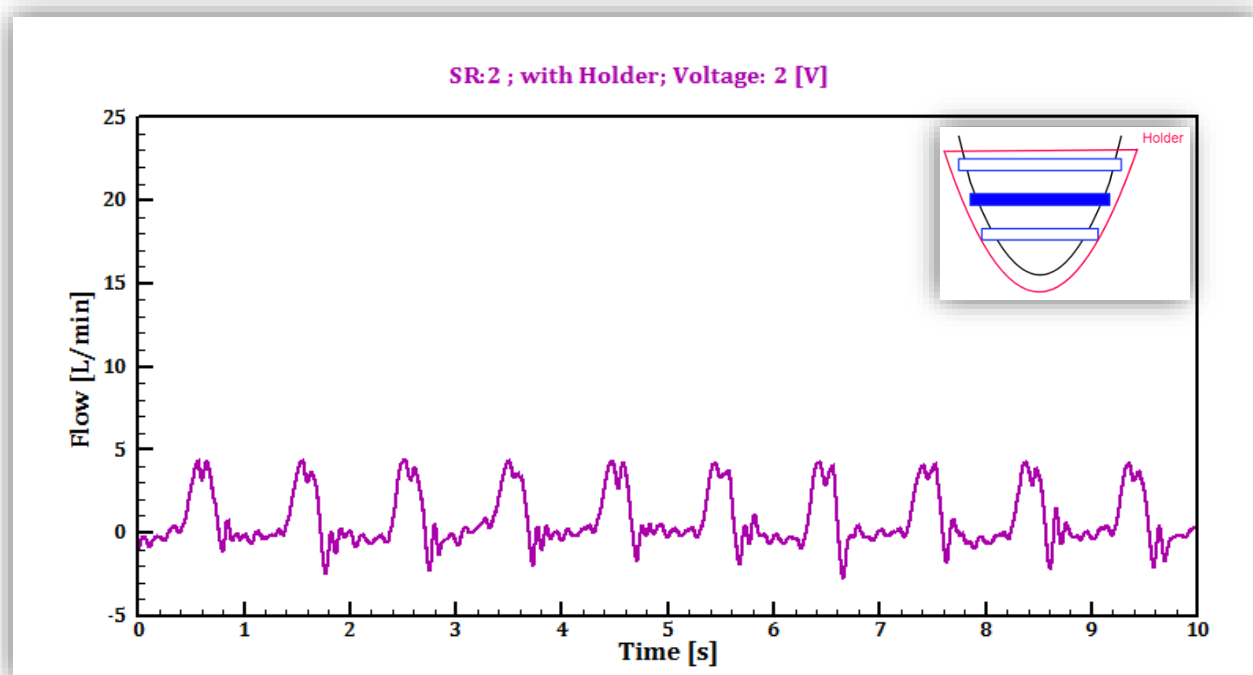
63

Figure 21 Flow waveform with active actuators: #2, #3, Voltage: 1 V, with holder

Figure 22 Flow waveform with active actuators: #2, #3, Voltage: 2 V, with holder

64

Figure 23 Flow waveform with active actuators: #2, #3, Voltage: 3 V, with holder
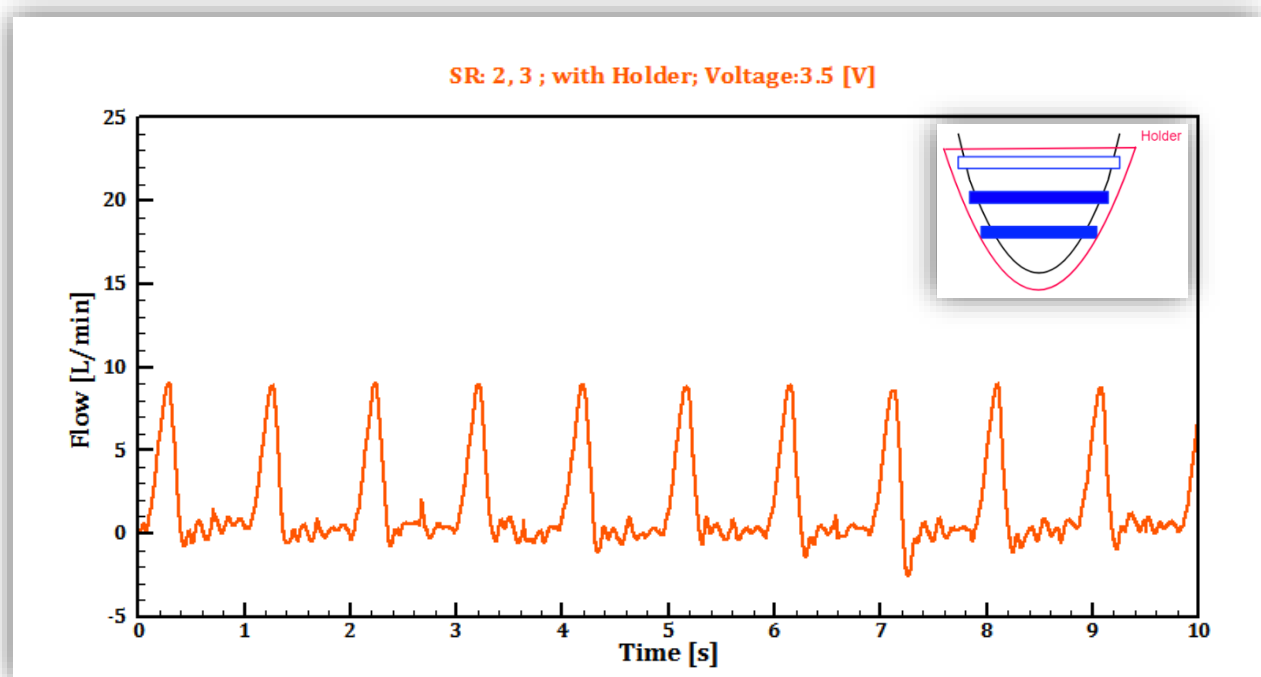
Figure 24 Flow waveform with active actuators: #2, #3, Voltage: 3.5 V, with holder
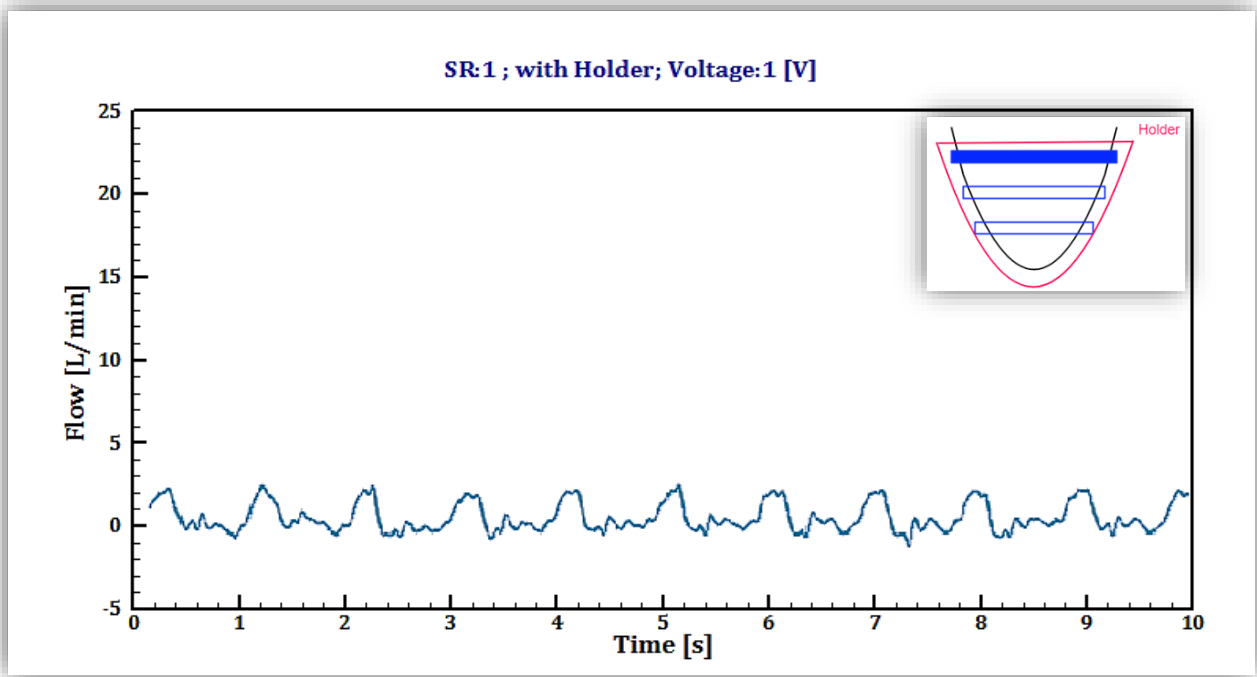
Figure 25 Flow waveform with active actuator: #1, Voltage: 1 V, with holder

Figure 26 Flow waveform with active actuator: #1, Voltage: 2 V, with holder

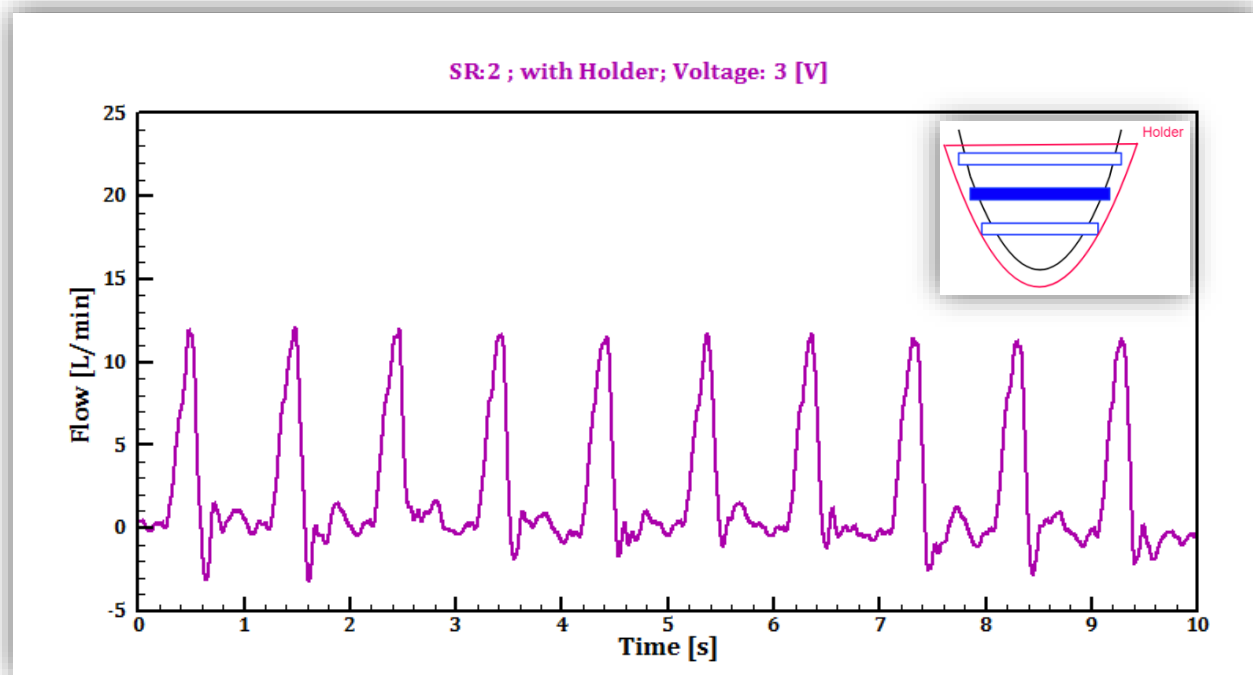**Figure 27 Flow waveform with active actuator: #1, Voltage: 3 V, with holder**

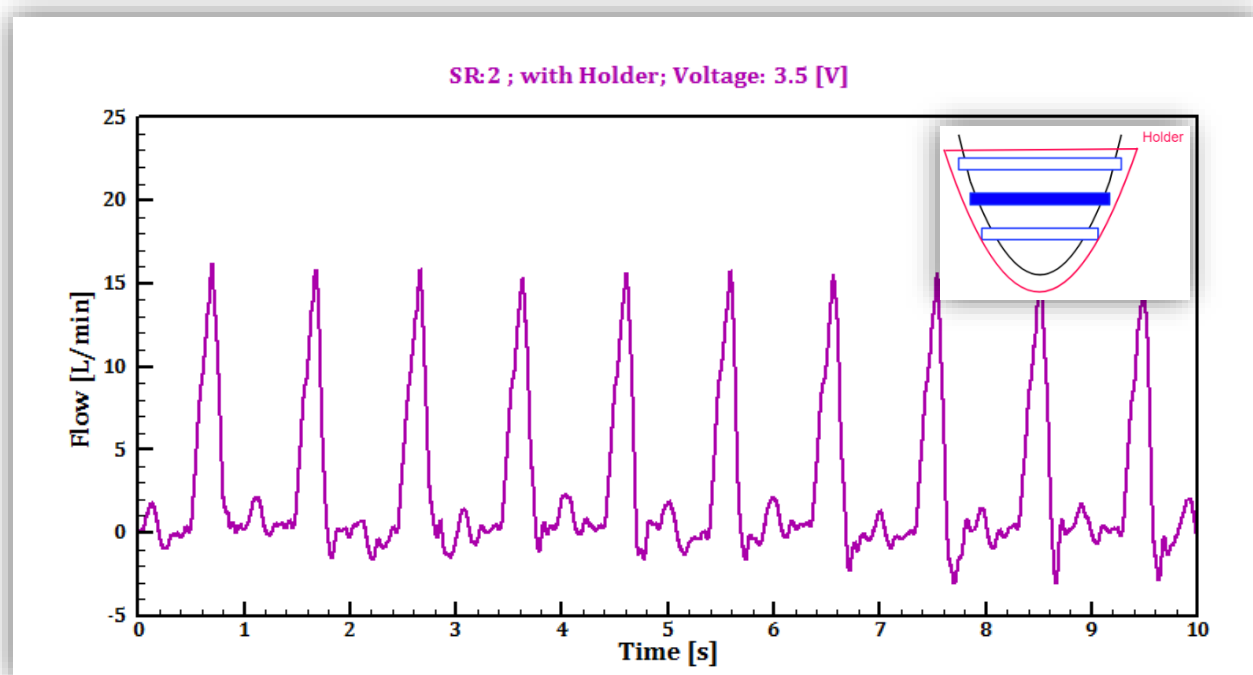**Figure 28 Flow waveform with active actuator: #1, Voltage: 3.5 V, with holder**

Figure 29 Flow waveform with active actuator: #2, Voltage: 1 V, with holder

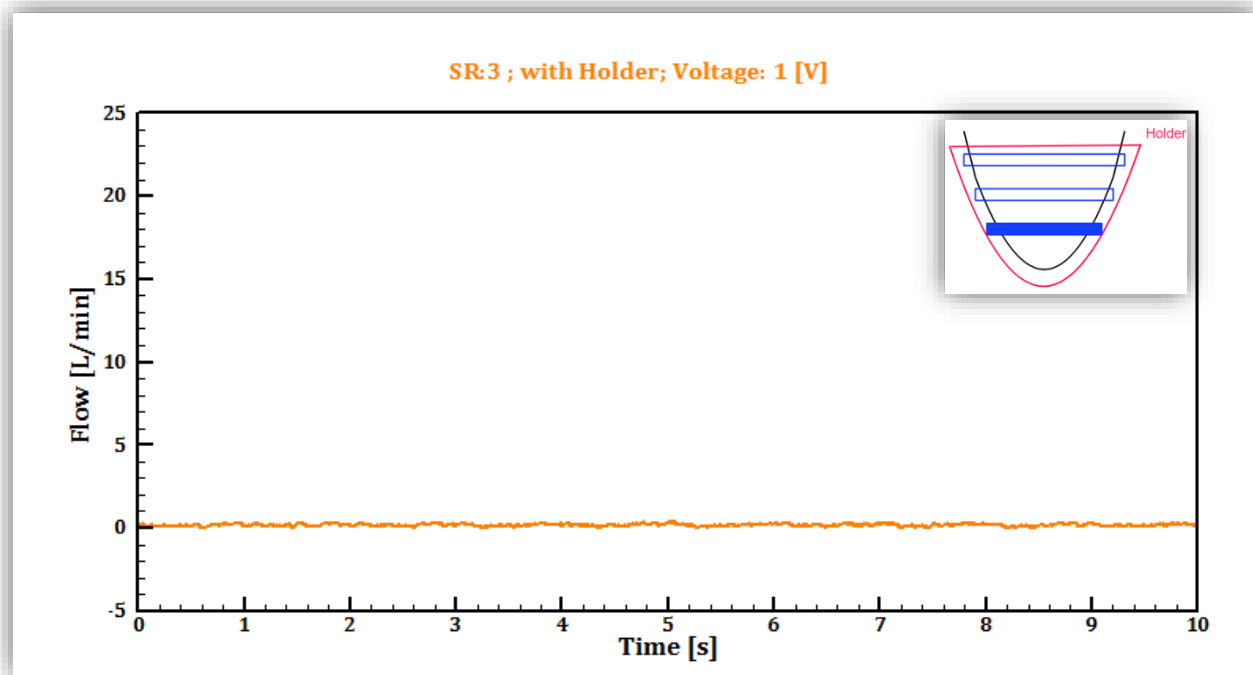**Figure 30 Flow waveform with active actuator: #2, Voltage: 2 V, with holder**

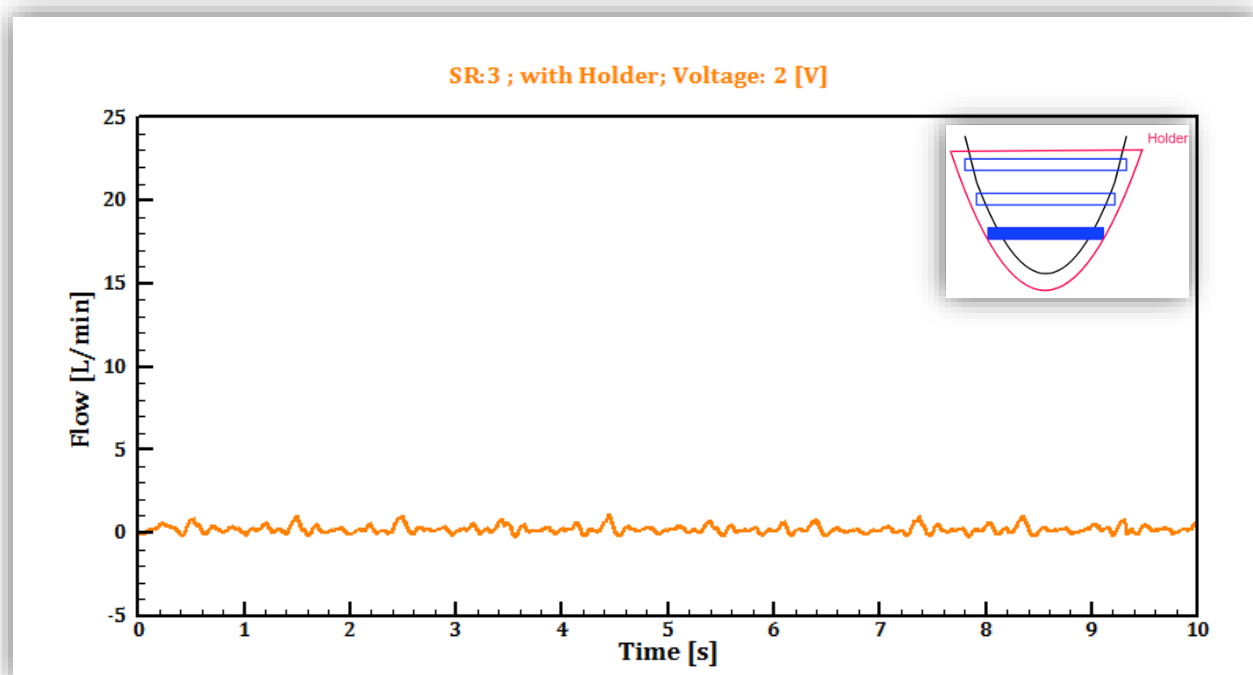**Figure 31 Flow waveform with active actuator: #2, Voltage: 3 V, with holder**

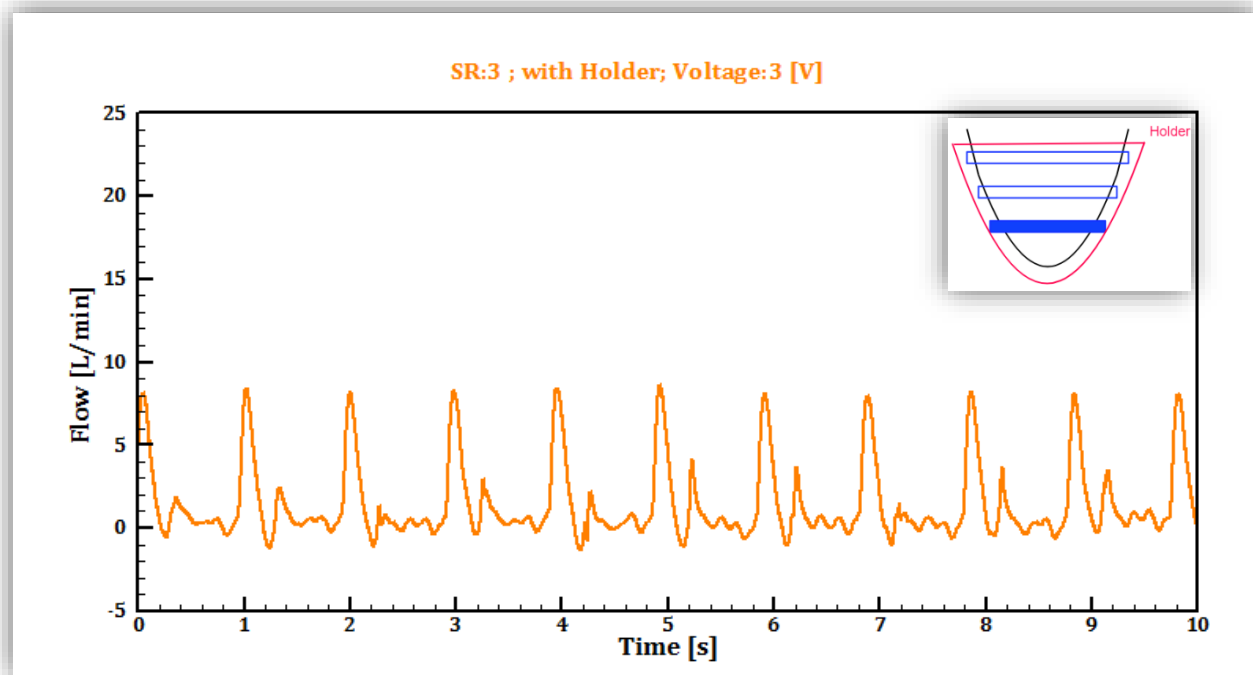**Figure 32 Flow waveform with active actuator: #2, Voltage: 3.5 V, with holder**
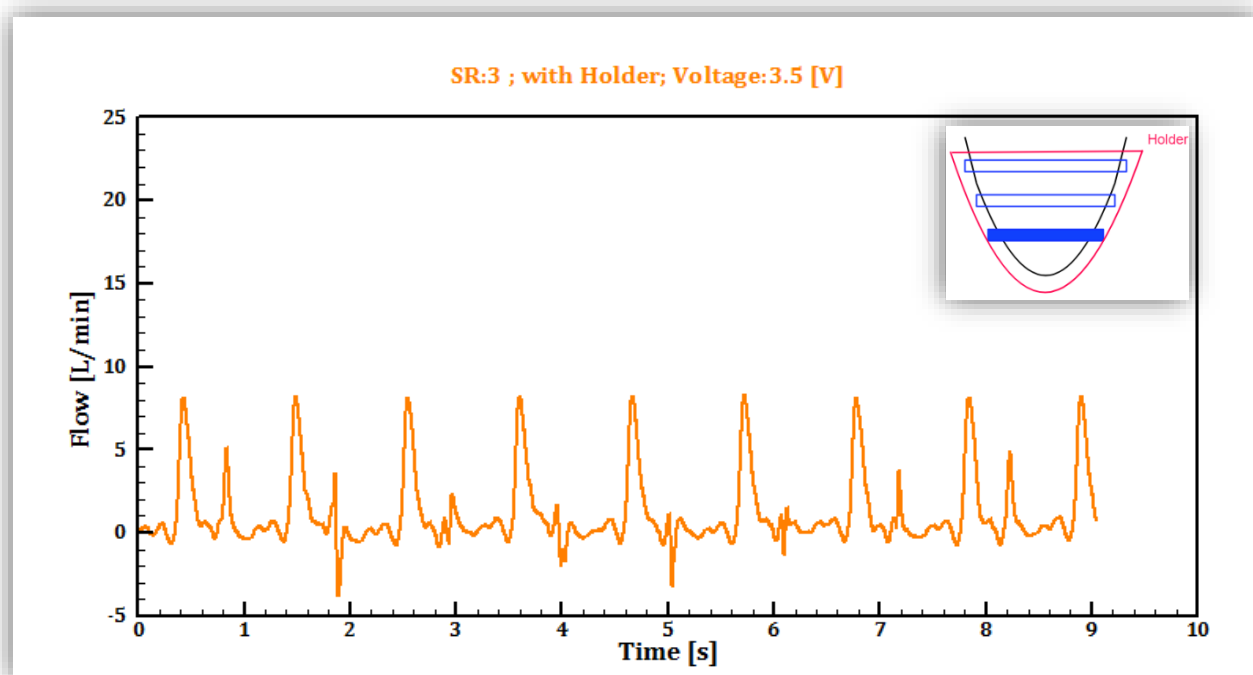
Figure 33 Flow waveform with active actuator: #3, Voltage: 1 V, with holder

Figure 34 Flow waveform with active actuator: #3, Voltage: 2 V, with holder

Figure 35 Flow waveform with active actuator: #3, Voltage: 3 V, with holder

Figure 36 Flow waveform with active actuator: #3, Voltage: 3.5 V, with holder

71

Doppler Ultrasound

Data Assessment

To observe the function of surgical valves an echocardiography machine, an E9 Logic model manufactured by GE Healthcare is used, Figure 37. The main parameters in PW Doppler measurement are:

- Aortic valve maximal velocity: AV V_{max} [m/s]
- Aortic valve mean velocity: AV V_{mean} [m/s]
- Aortic valve maximal pressure gradient: AV PG_{max} [mmHg]
- Aortic valve mean pressure gradient: AV PG_{mean} [mmHg]
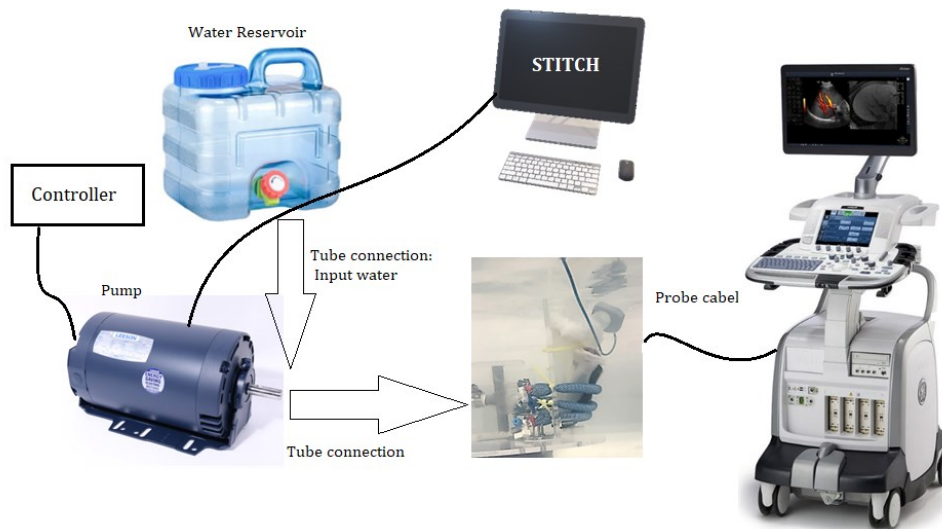- Velocity time integral: VTI [cm]

Figure 37 Experiment setup and connections for Doppler measurement

Doppler Echocardiography Results

The speed and portability of the echocardiography make it well-suited to lab research (Voorhees and Han 2015). To evaluate the performance of the valves, radiologists usually use echocardiography for diagnosis. The optimized setup is composed of three active actuators and the holder is used to observe the opening and closing of the mitral valve, Figure 38.

The pulsed wave (PW) data are reported in Table 4 The average value of VTI equals 22.8 cm, and the inner diameter of the aortic valve size is 22 mm (see section 3.3.3), based on the description provided in section 1.4.4 the CO, SV, and EF can be calculated as follow:

$$SV = VTI \times \pi \left(\frac{D}{2}\right)^2 = 86.63 \; ml$$

$$CO = SV \times HR = 86.626 \; ml \times 60 \; beats/min = 5.19 \; l/min$$

$$EF = \frac{SV}{LV \; volume \; at \; the \; end \; of \; diastole} = 64.17 \; \%$$

The results of the second-best combination of the active actuators #1 and #2 with the holder are reported in Table 5 The mean value of VTI is 16.6 cm, and the three parameters are as follows:

$$SV = 63.07 \; ml$$
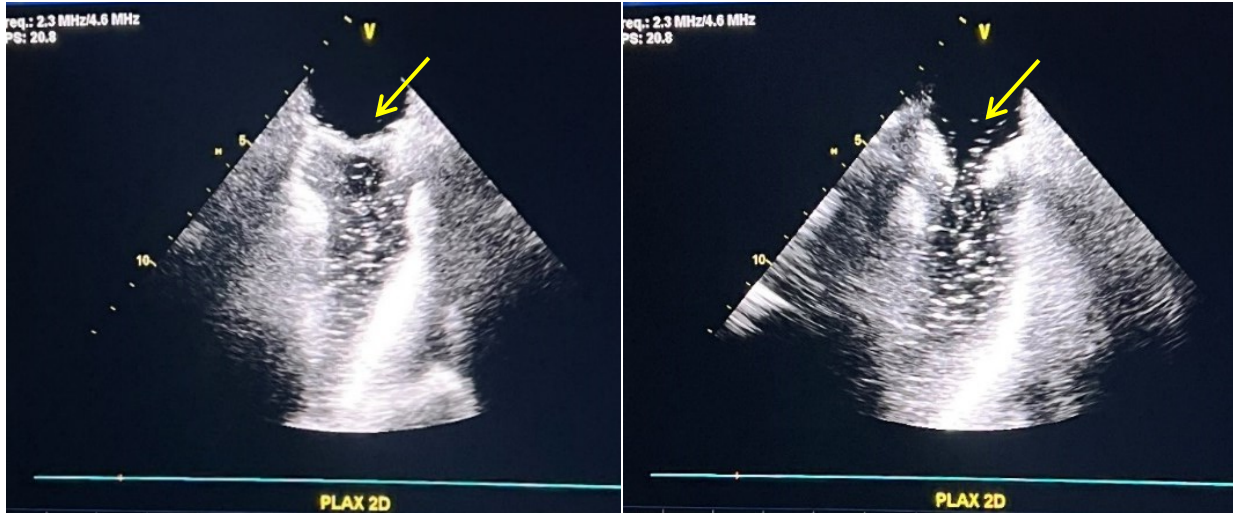
$$CO = 3.78 \; l/min$$

$$EF = 46.72 \; \%$$

Figure 38 Mitral valve: close (left) and open (right)

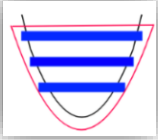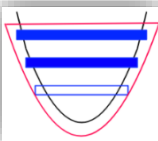**Table 4 Doppler results of the aortic valve, pulsed wave, actuators: #1, #2, & #3, with holder, Voltage: 3.5 V**

Voltage (V)	AV max (m/s)	AV V_{mean} (m/s)	AV PG_{max} (mmHg)	AV PG_{mean} (mmHg)	VTI (cm)
3.5	0.83	0.44	3	1	21
	0.87	0.44	3	1	22
	0.92	0.44	3	1	24
	0.90	0.46	3	1	23
	0.91	0.47	3	1	24

Table 5 Doppler results of the aortic valve, pulsed wave, actuators: #1 & #2, with holder, Voltage: 3.5 V

Voltage (V)	AV max (m/s)	AV V_{mean} (m/s)	AV PG_{max} (mmHg)	AV PG_{mean} (mmHg)	VTI (cm)
3.5	0.66	0.43	2	1	16
	0.65	0.40	2	1	16
	0.67	0.43	2	1	18
	0.66	0.34	2	1	17
	0.65	0.39	2	1	16

Comparison of the Two Data Assessment Methods

Data acquired from the direct flow measurement and Doppler ultrasound are compared in this section. The calculation of the data are provided in the previous section, here we just conclude all the results to prove the feasibility of data acquisition with Doppler ultrasound. The extracted data are provided in Table 4.4 and Table 4.5 for the two best configurations.
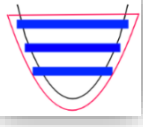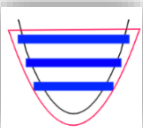
Table 6 The result comparison of the two measurement methods
for the setup with S1, S2, S3 with holder

Method	Cardiac Output [l/min]	Stroke Volume (ml)	Ejection Fraction (%)
Direct Flow Assessment	4.05	67.50	50.00
Doppler Ultrasound	5.19	86.63	64.17

Table 7 The result comparison of the measurement methods
for the setup with S1, S2 with holder

Method	Cardiac Output [l/min]	Stroke Volume (ml)	Ejection Fraction (%)
Direct Flow Assessment	3.98	66.33	49.13
Doppler Ultrasound	3.78	63.07	46.72

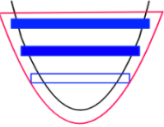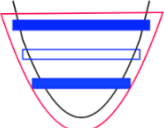**Table 8 Doppler results of the aorta, continuous wave, actuators: S2, S2, &S3, with holder**

Voltage [V]	AV V_{max} (m/s)	AV V_{mean} (m/s)	AV PG_{max} (mmHg)	AV PG_{mean} (mmHg)	VTI (cm)
1	0.55	0.39	1	1	18
	0.59	0.41	1	1	15
	0.55	0.39	1	1	16
	0.58	0.44	1	1	18
	0.57	0.43	1	1	19
2	0.71	0.42	2	1	21
	0.67	0.40	2	1	21
	0.68	0.42	2	1	21
	0.69	0.46	2	1	22
	0.68	0.45	2	1	21
3	1.02	0.65	4	2	30
	0.99	0.63	4	2	29
	0.99	0.67	4	2	28
	0.99	0.58	4	2	27
	1.00	0.73	4	2	30
3.5	1.31	0.80	7	3	36
	1.40	0.83	7	3	37
	1.31	0.80	7	3	34
	1.32	0.82	7	3	35
	1.29	0.84	7	3	34

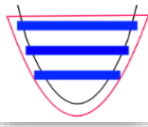**Table 9 Doppler results of the aorta, continuous wave, actuators: S2, S2, &S3, without holder**
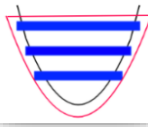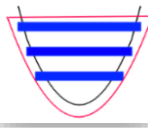
Voltage (V)	AV V_{max} (m/s)	AV V_{mean} (m/s)	AV PG_{max} (mmHg)	AV PG_{mean} (mmHg)	VTI (cm)
3.5	0.85	0.48	3	1	19
	0.91	0.54	3	1	20
	0.87	0.48	3	1	19
	0.86	0.51	3	1	22
	0.84	0.51	3	1	17

Table 10 Doppler results of the aorta, continuous wave, two activated actuators, with holder

Voltage (V)	AV max (m/s)	AV V_mean (m/s)	AV PG_max (mmHg)	AV PG_mean (mmHg)	VTI (cm)
3.5	0.81	0.53	3	1	22
	0.75	0.48	2	1	20
	0.75	0.52	2	1	20
	0.73	0.45	2	1	20
	0.73	0.48	2	1	19
	0.69	0.42	2	1	25
	0.70	0.49	2	1	25
	0.68	0.51	2	1	23
	0.66	0.46	2	1	24
	0.72	0.47	2	1	23
3.5	0.64	0.41	2	1	18
	0.67	0.45	2	1	20
	0.65	0.45	2	1	19
	0.70	0.39	2	1	18
	0.69	0.46	2	1	19

Table 11 Doppler results of the mitral valve, continuous wave, three activated actuators, with holder

Voltage (V)	AV max (m/s)	AV V_{mean} (m/s)	AV PG_{max} (mmHg)	AV PG_{mean} (mmHg)	VTI (cm)
2	0.61	0.42	2	1	24
	0.65	0.43	2	1	30
	0.65	0.44	2	1	31
	0.68	0.4	2	1	32
	0.63	0.43	2	1	29
3	0.88	0.51	3	1	37
	0.85	0.54	3	1	38
	0.85	0.68	3	1	37
	0.82	0.51	3	1	37
	0.84	0.58	3	1	35
3.5	0.86	0.56	3	1	34
	0.87	0.49	3	1	36
	0.89	0.54	3	1	31
	0.82	0.51	3	1	33
	0.91	0.56	3	1	34

Table 12 Doppler results of the mitral valve, continuous wave, three active actuators, without holder

Voltage (V)	AV max (m/s)	AV V_{mean} (m/s)	AV PG_{max} (mmHg)	AV PG_{mean} (mmHg)	VTI (cm)
3.5	0.73	0.54	2	1	25
	0.68	0.47	2	1	23
	0.71	0.43	2	1	23
	0.70	0.47	2	1	24
	0.73	0.46	2	1	25